THE EFFECT OF PHOSPHOROTHIOATE-MODIFIED DNA AND NANOPARTICLE SIZE ON QUANTITATIVE ENHANCED RAMAN SCATTERING

RICHARD NICHOLAS CASSAR

Department of Pure and Applied Chemistry

The Effect of Phosphorothioate-Modified DNA and Nanoparticle Size on Quantitative Enhanced Raman Scattering

Richard Nicholas Cassar

2013

A thesis presented, in fulfillment of the requirements for the degree of Doctor of Philosophy.

This thesis is the result of the author's original research. It has been composed by the author and has not been previously submitted for examination which has led to the award of a degree.

The research work disclosed in this publication is partially funded by the Strategic Educational Pathways Scholarship (Malta). This scholarship is part-financed by the European Union - European Social Fund (ESF) under Operational Programme II - Cohesion Policy 2007-2013, "Empowering People for More Jobs and a Better Quality of Life".

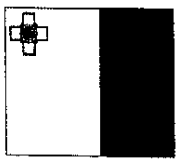

Operational Programme II – Cohesion Policy 2007-2013
Empowering People for More Jobs and a Better Quality of Life
Scholarship part-financed by the European Union
European Social Fund (ESF)
Co-financing rate: 85% EU Funds; 15% National Funds

Investing in your future

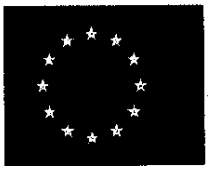

Contents

Acknowledgements

I would like to express deepest thanks to my tutor Professor Duncan Graham, for his constant help, support, advice and interest with which he has guided my Ph.D.. My sincere gratitude goes also to Dr. Karen Faulds, Dr. Jennifer Dougan, Dr. Iain Larmour and Dr. Colette Dalton for their invaluable support and continuous technical advice.

Also, a great thanks goes to my fellow students, especially to Danny van Lierop and Hainan Xie for their invaluable help and company.

This work is affectionately dedicated to my family and my girlfriend Renée, for their support and encouragement, and which I am proud of.

Abstract

Surface-enhanced Raman scattering (SERS) has been used successfully as an ultrasensitive technique for the direct analysis of dye-labelled oligonucleotides using aggregated silver nanoparticles. Key to this technique are the SERS probe and SERS substrate. Initial studies were made on the detection of phosphorothioate modified TAMRA-labelled oligonucleotides whereby a non-bridging oxygen atom in the phosphodiester backbone is replaced by sulfur. TAMRA-labelled phosphorothioate oligonucleotides with the same base pair sequence but different number of modified phosphate unites were compared to unmodified TAMRA-labelled oligonucleotides using silver nanoparticles (AgNP) as SERS substrates using different aggregation agents. Furthermore the investigation was extended to study the effect of modification in the detection of double stranded DNA (dsDNA). The focus was then turned to the SERS substrate since spherical and monodispersed silver nanoparticles are ideal for fundamental research as the contribution from size and shape can be accounted for in the experimental design. Different methods to produce size tuneable AgNP's were investigated to study in detail the effect of modified and unmodified dye-labelled oligonucleotides, thiophenol (TP), rhodamine 6G (R6G) and malachite green oxalate (MGO) on the SERS response.

The results obtained reflect the importance of each component of SERS. The phosphorothioate modifications, although their affinity towards silver surfaces can improve the DNA limit of detection (LOD), it also depends on the position and number of modifications and on the aggregating agent used which in itself also effects the LOD of DNA. The same applies for the SERS substrate where an increase in particle size results in an increased enhancement of the analyte's Raman signal but further size increments leads to a decrease in SERS intensity due to other factors such as scattering. This demonstrates the importance of choosing the right experimental setups for DNA SERS analysis, as to obtain the right balance where all factors work synergistically with each other.

Abbreviations

A	Adenine
AFM	Atomic force microscope
AgNP	Silver nanoparticle
C	Cytosine
CPG	Controlled pore glass
DCM	Dichloromethane
DCS	Differential centrifugal sedimentation
DLS	Dynamic light scattering
DMT	Dimethoxytrityl
DNA	Deoxyribonucleic acid
dsDNA	Double-stranded deoxyribonucleic acid
EDITH	3-ethoxy-1,2,4-dithiazoline-5-one
EDTA	Ethylenediaminetetraacetic acid
G	Guanine
GC	Gas chromatography
HQ	Hydroquinone
IR	Infrared
LC	Liquid chromatography
LNA	Locked nucleic acid

LOD	Limit of detection
MGO	Malachite green oxalate
mRNA	Messenger ribonucleic acid
MS	Mass spectrometry
NMR	Nuclear magnetic resonance
NHS	*N*-hydroxy-succinimide
NTA	Nanoparticle tracking analysis
PEG	Poly(ethylene glycol)
PCR	Polymerase chain reaction
PDI	Polydispersity index
R6G	Rhodamine 6G
RNA	Ribonucleic acid
SEM	Scanning electron microscopy
SERRS	Surface-enhanced resonance Raman scattering
SERS	Surface-enhanced Raman scattering
SPR	Surface plasmon resonance
ssDNA	Single stranded deoxyribonucleic acid
T	Thymine
THF	Tetrahydrofuran
TP	Thiophenol

tRNA	Transfer ribonucleic acid
U	Uracil
UV	Ultraviolet
Vis	Visible

Chapter 1: Introduction

For over a decade the use of metallic nanoparticles for the ultrasensitive detection of biomolecules has been the centre of many studies and technologies. Various types of reporting moieties have been used ranging from oligonucleotides and proteins to fluorescent dyes. Nanoparticles, especially metallic nanoparticles are taking centre stage in optical biodiagnostic methods[1] and hence this study focuses on the use of silver nanoparticles which have surface plasmon resonance energies that coincide with that of visible light hence they can be used in various sensor applications such as surface enhanced Raman scattering (SERS)[2].

In this chapter we are going to introduce the main concepts that are relevant to this thesis with particular emphasises on deoxyribonucleic acid (DNA), the principles of surface-enhanced Raman scattering and the synthesis and optical properties of inorganic colloidal nanoparticles.

1.1 Nucleic acids

There are two classes of nucleic acids; DNA, and ribonucleic acid (RNA). These nucleic acids are made up of three components; nucleobase, sugar and phosphoric acid[3]. The nucleobases are adenine (A) and guanine (G), which are purine derivatives (see figure 1-1) and thymine (T), uracil (U) and cytosine (C), which are pyrimidine derivatives (see figure 1-2).

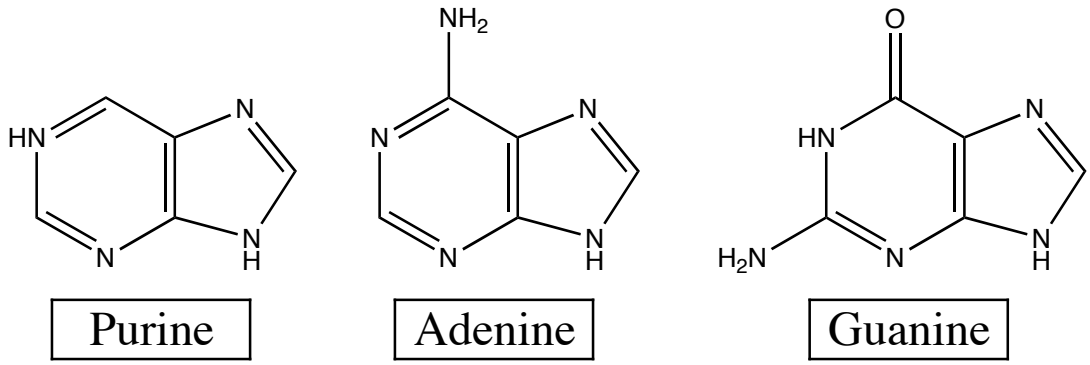

Figure 1-1 Purine and its derivatives, adenine and guanine that are bases in both DNA and RNA.

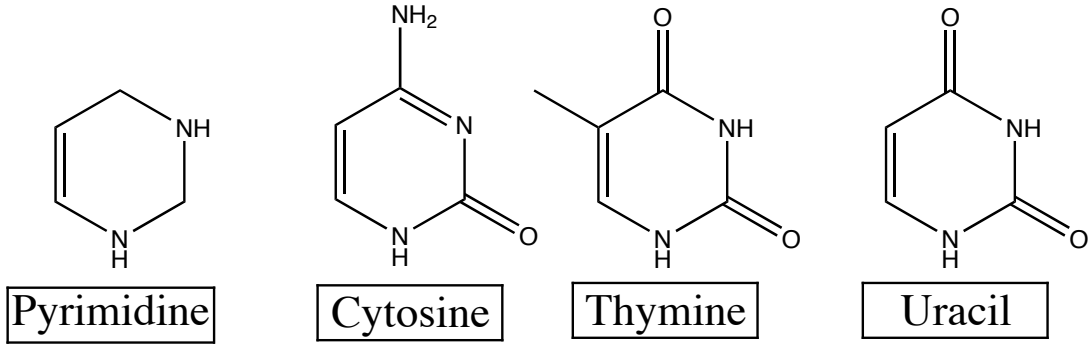

Figure 1-2 Pyrimidine and its derivatives, cytosine which is found in both RNA and DNA, thymine which is found only in DNA and uracil which is found only in RNA.

The sugar component for DNA is ß-*D*-deoxyribose and for RNA it is ß-*D*-ribose, their structure is depicted in figure 1-3.

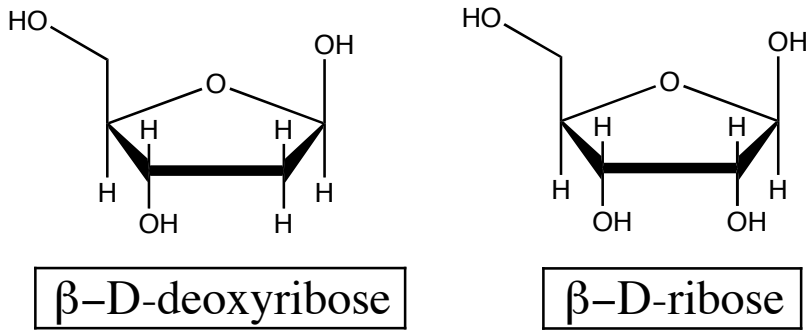

Figure 1-3 ß-D-deoxyribose is the pentose sugar in DNA and ß-D-ribose is the pentose sugar in RNA.

The sugars are covalently bound to a nucleobase by a *N*-glycosidic bond *i.e.* between a *C1'* atom of the sugar and either the *N1* atom of the pyrimidine base or the *N9* atom of a purine base, thus forming what is better known as a nucleoside. In turn the phosphate group is covalently bound to the nucleoside through the *5'*-hydroxylic group of the sugar, forming what is know as a nucleotide which can be seen as the building block of nucleic acids. The nucleotide can form polynucleotide chains by bonding of the phosphate residue at the *5'* position of one sugar to the *3'*-hydoxyl group of another sugar, as demonstrated in figure 1-4.

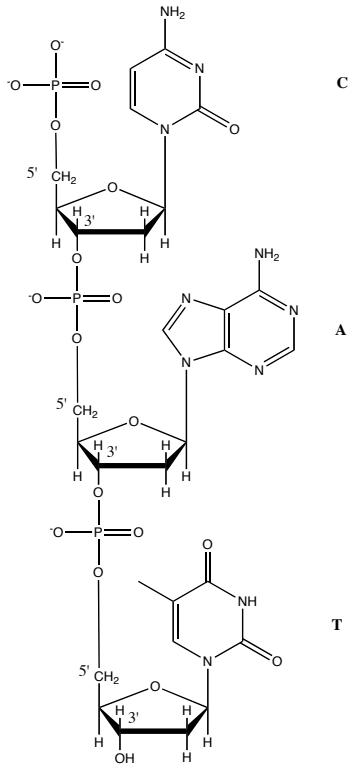

Figure 1-4 Polynucleotide structure with the bases cytosine, adenine and thymine

The sugar and phosphate units form the backbone of the chain while the nucleobases 'stick out' forming the side groups.

1.1.1 DNA

DNA is composed of two polynucleotide strands twisted around each other forming a right twisted double helix. The structure of DNA (see figure 1-5) was discovered by Francis Crick and James Watson in 1953[4].

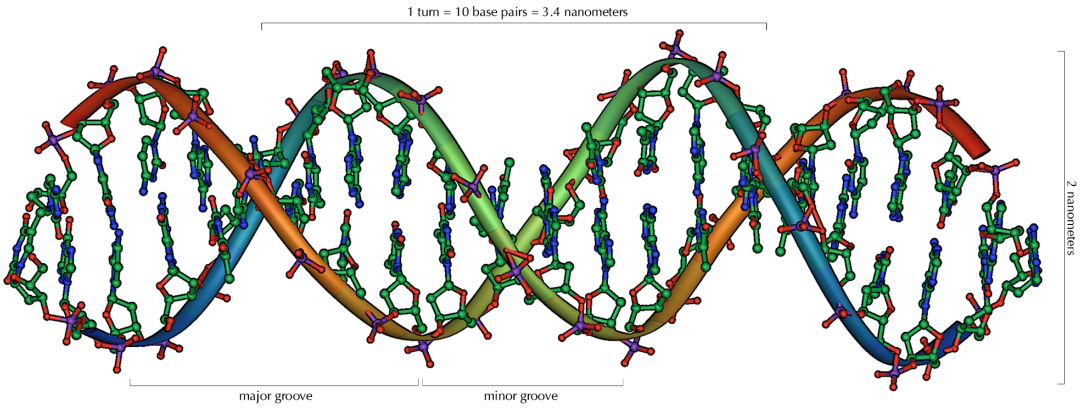

Figure 1-5 Schematic diagram of a DNA double helix[5]

The backbone of the polynucleotide is hydrophilic and has a negative charge at physiological *pH* due to the phosphate groups present which are found on the outside of the helix. The hydrophobic bases then align themselves on the inside of the helix structure. The polynucleotide strands in the helix run in opposite direction to each other, that is the *3'* end of one strand is linked to the *5'* end of the other. The strands are connected to each other by weak hydrogen bonding that forms between the base pairs. However due to steric constraints only a certain combination of base pairs allows hydrogen bonding, that is adenine only forms hydrogen bonding with thymine and vice versa, and guanine only forms hydrogen bonding with cytosine and vice versa (see figure 1-6).

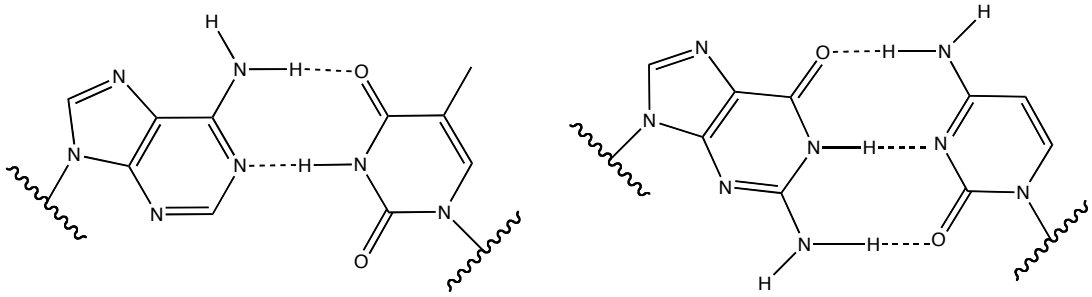

Figure 1-6 (Left) Hydrogen bonding between adenine and thymine (A-T). (Right) Hydrogen bonding between guanine and cytosine (G-C).

As the aromatic rings of the base pairs are parallel to each other, this gives DNA the twisted ladder like structure. The strands must be therefore complementary to each other hence one strand dictates the sequence of the other strand.

The structure of DNA is classified into organisational levels. The primary structure is the sequence of nucleotides, which are labelled according to the base composition. The secondary structure is the shape of the DNA; basically the double helix. There have been three different conformations of the DNA double helix identified. The one found in normal physiological circumstances and proposed by Watson and Crick is known as the B-DNA. A shorter and wider form is the A-DNA, which was found in dehydrated samples. Both of these DNA have a right-handed conformation, while the third known conformation the Z-DNA has a left-handed conformation. Studies suggest that the Z-DNA plays an important role in protection against viral disease[6] [7]. The tertiary structure of DNA is the shape taken by the coiling of the helix on itself.

The integrity of the DNA structure, is compromised when moving away from physiological *pH* and temperature. When the double stranded DNA is for example

heated above 95ºC, the hydrogen bonding between bases is disrupted and the strands are cleaved forming single stranded DNA (ssDNA). The denaturation of DNA is usually a reversible process and plays an important role in DNA replication.

1.1.2 RNA

RNA like DNA is a polynucleotide, which differs from the latter by having ribose as the sugar component, and uracil instead of thymine as a base. The different sugar component is a key factor in the structure of RNA. Due to the additional *OH* group on ribose it hinders the formation of double stranded RNA. As a result of steric hindrance, RNA is found only as a single stranded molecule, however it still can form folds and loops on itself as it forms hydrogen bonds between base pairs with itself.

1.1.3 Biological role of DNA and RNA

The main role of nucleic acids is that they encode in the base pairs sequence the genetic code that is decoded to synthesise proteins. There are three major steps for such synthesis (see figure 1-7) and these are:

1. Transcription – DNA helix unfolds and a complementary strand of RNA is synthesised along a crucial part of one of the ssDNA. This RNA strand is now referred to as messenger RNA (mRNA) and leaves the cell nucleus to be transferred to the ribosomes.

2. Translation – In the ribosome transfer RNA (tRNA), delivers amino acids according to the three base sequence on the mRNA.

Post-translation modification – After the ribosome fabricates the protein, the latter must undergo modification to become biologically active. Common modifications that occur are cleavage of amino acids and chemical modifications of side chains such as phosphorylation, acetylation and methylation.

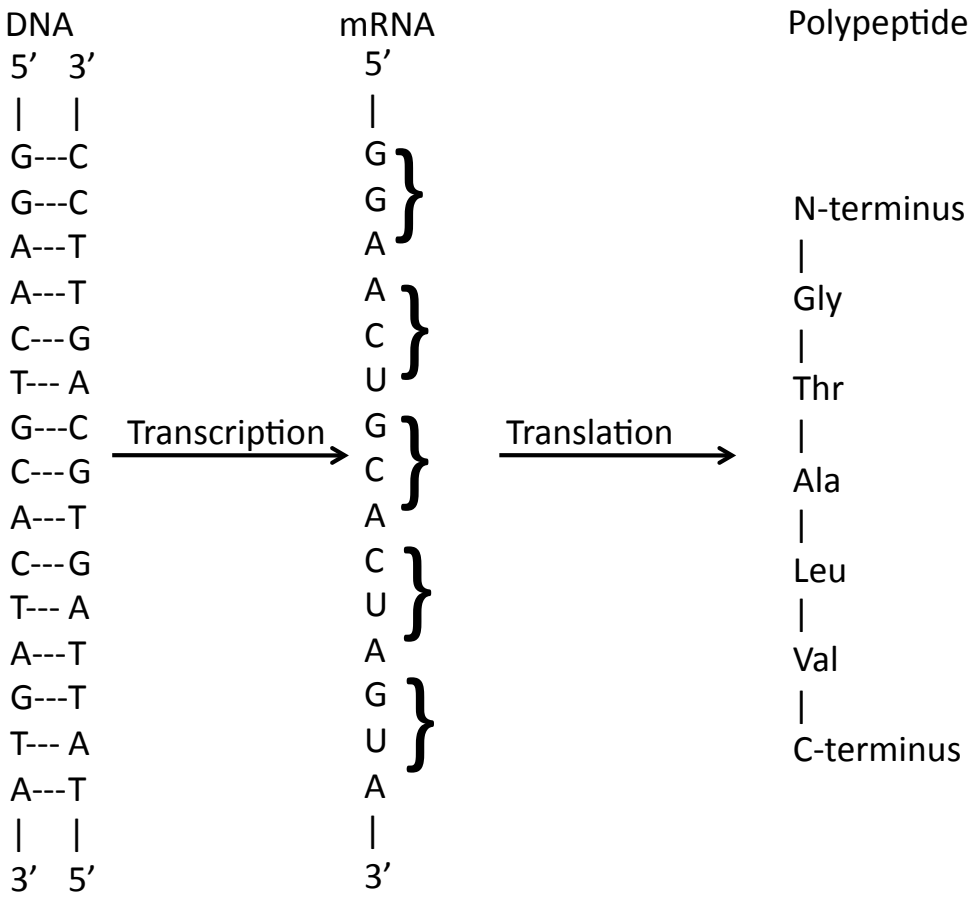

Figure 1-7 Schematic summary of the synthesis of protein

1.1.4 Analysis of nucleic acids

As more and more research occurs in the field of genomics and proteomics, analytical tools have to be developed to conduct faster, cheaper and reliable techniques for analysis. Analytical chemists in whatever field of science they work will encounter analysis that demands:

- qualitative analysis of a mixture of compounds,
- qualitative analysis of a pure compound,
- quantitative analysis of a compound in a mixture, and
- structure elucidation of a compound.

There are various methods that can be used to analyse small organic molecules. For example mixtures can be separated and quantitatively analysed by gas chromatography (GC) and liquid chromatography (LC). For identification purposes there are a variety of techniques such as the 'classical' methods of nuclear magnetic resonance (NMR), mass spectroscopy (MS), infrared (IR) spectroscopy, Ultraviolet/visible (UV/Vis) spectroscopy and X-Ray crystallography. Great development in the use of biosensors and chemosensors has been achieved especially for diagnostic medicine for the analytes such as glucose, urea, cholesterol, hepatitis B, *etc* [8]. The aforementioned methods however are not entirely suitable when it comes to analyse proteins and nucleic acids. Difficulties arise due to the physical and chemical properties of these biomolecules.

Most biomolecules have a high molecular weight, they are non-volatile, not thermally stable and furthermore have a large number of functional groups and chromophores, making analysis more complicated. All these biomolecule characteristics make them unsuitable to be analysed by conventional methods such as GC, MS, Uv/Vis and IR spectroscopy. Advances in these techniques and new techniques have been developed throughout the last two decades that helped produce large advances in proteomics and genomics. These bioanalytical techniques main goals is to have great accuracy and reliability in determining *e.g.* the peptide or nucleotide sequence, and a great sensitivity as the analytes in question are usually present in very small amounts.

The analysis of nucleic acids can be divided into three distinctive steps; isolation and purification, quantification and amplification, and sequencing. In the first step the DNA or RNA is isolated from the cell by simple straightforward methods such as centrifugation, precipitation and liquid-liquid extractions. Following its isolation, nucleic acids can be quantified by measuring with a UV/Vis spectrometer, since the aromatic groups present in the bases absorb at a maximum of around 260 nm. Other methods used to quantitatively detect DNA are by fluorescent or radioactive markers. Mixtures of DNA can be also quantified using electrophoretic methods.

The polymerase chain reaction (PCR), revolutionised genomics, as one DNA molecule can be amplified exponentially, if a part of its sequence is known[9]. Improvement in the PCR technique, now allows DNA quantification to be measured during the amplification process, this method is better known as real-time PCR. Other methods of quantification are available such as the use of biosensors that

recognise the DNA/RNA target analyte and send a signal that can be measured. A variety of sequencing methods for DNA are available and the most common ones used are the Maxam Gilbert method[10], the Sanger method[11], DNA arrays and pyrosequencing[12].

1.1.5 Synthesis and modification

1.1.5.1 Synthesis

Chemical synthesis of DNA is important for biotechnology as it allows the production of tailor made oligonucleotide sequences that can comprise synthesis of natural, non-natural sequences and various additional modifications. Manual synthesis of oligonucleotides is time consuming and is limited to experienced synthetic chemists[6]. However with the advent of the phosphoramidite approach[13-15] in the early 1980s and automated synthesisers, the synthesis of DNA is now available to anyone with basic laboratory skills. Automated synthesis not only made it to research laboratory but also to companies that specialise in the production of DNA thus drastically reducing the cost of synthesis.

The chemical synthesis of DNA consists of a four step synthesis cycle; 1) deprotection 2) coupling, 3) capping and 4) oxidation as shown in figure 1-8 on the next page.

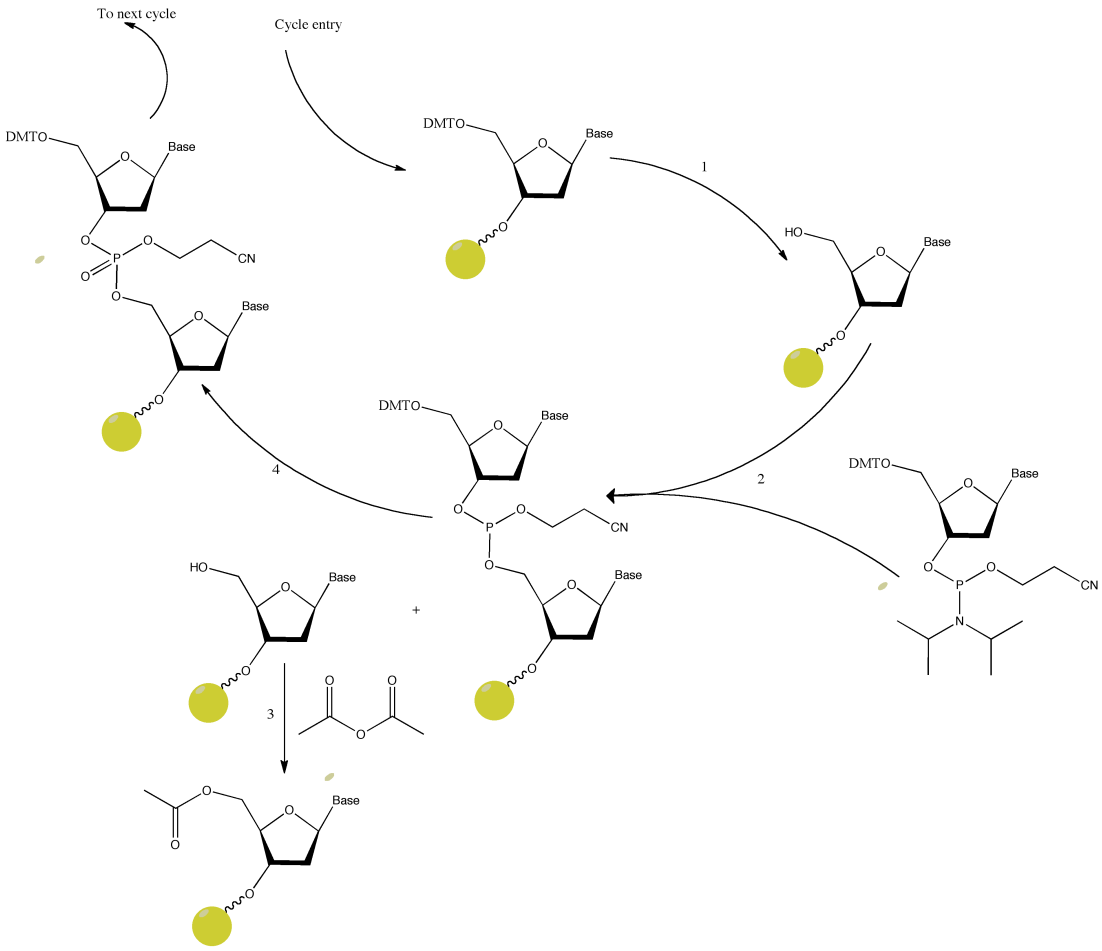

Figure 1-8 The four steps of oligonucleotide synthesis cycle: 1) Deprotection; 2) Coupling; 3) Capping; 4) Oxidation.

The synthesis in most automated synthesisers occurs on controlled pore glass (CPG)[16] solid support that is usually functionalised with one of the 4 different DNA bases, although universal supports i.e. non-base functionalised CPG are also available. Unlike enzymatic DNA synthesis[17,18], chemical DNA synthesis progresses in the 3' to 5' direction[19]. The bases are attached to the CPG via a 3'-ester linkage and the 5'-hydroxyl is protected with a dimethoxytrityl (DMT) moiety, which can be cleaved under acidic conditions. The bases are protected by isobutyryl for guanine, benzoyl for adenosine and acetyl for cytidine[20]. No protection is needed for thymine.

Other protecting groups are now available for exocyclic amine protection such as phenoxyacetyl dA[21] and dimethylformamidine dG[22]. The phosphate backbone is protected by a cyanoethyl ester[23,24].

The CPG is usually filled in columns where the reagents are automatically supplied to it in sequence with acetonitrile washing steps in between each cycle.

1.1.5.1.1 Deprotection

The first step of the cycle starts with the hydrolization of the DMT group found on the pre-attached protected nucleoside using 3% trichloroacetic acid in dichloromethane (DCM) (see figure 1-9). The DMT protecting group prevents polymerisation during resin functionalization.

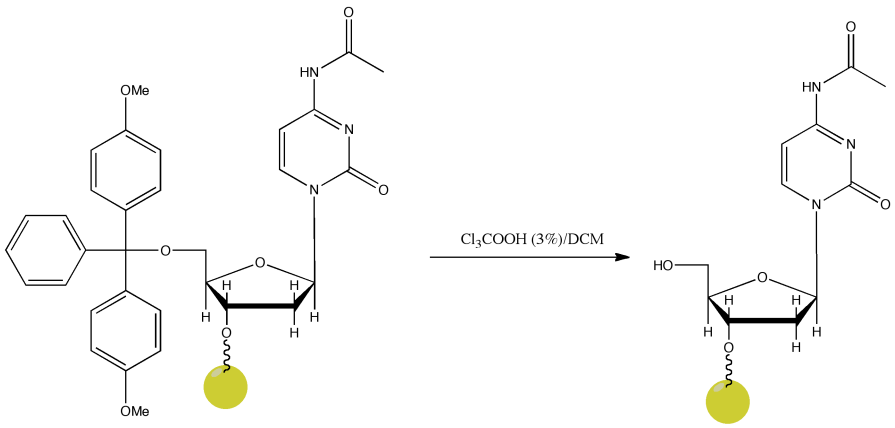

Figure 1-9 Deprotection of dimethoxytrityl cation to give free 5'-hydroxyl group for coupling.

The resulting by-product is a DMT cation which is bright orange allowing in-line monitoring of the reaction process and the coupling efficiency. After the deprotection the 5' hydroxyl group is available to react in the second step of the sequence.

1.1.5.1.2 Coupling

After the first base on the CPG is deprotected and activated the second base is introduced as an anhydrous solution of phosphoramidite.

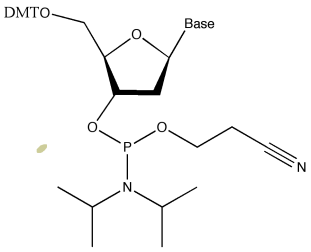

Figure 1-10 Alkyl phosphoramidite routinely employed as monomer in the synthesis.

The 5' alcohol is protected as a dimethoxytrityl ether. The phosphoramidite is activated by a weak acid such as tetrazole or other tetrazole derivatives (5-benzylthiotetrazol). The activated phosphoramidite couples with the 5'-hydroxyl of the CPG attached nucleotide producing a dinucleotide. The 5'-hydroxyl of the first nucleotide is linked to the 3'-hydroxyl of the second nucleotide by a phosphite link as shown in figure 1-11 below.

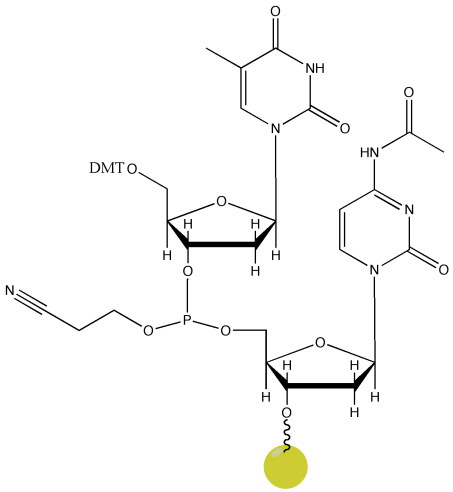

Figure 1-11 Phosphite triester linked dinucleotide after coupling step.

This step is more than 98% efficient[25] and any side reactions are reversed during the capping step of synthesis[26].

1.1.5.1.3 Capping

Even if the coupling chemistry is highly efficient it is not possible to achieve 100% reaction efficiency of the CPG attached nucleoside with the incoming phosphoramidite, therefore the few unreacted 5'-hydroxyl groups on the CPG attached nucleotide need to be capped. This prevents from taking part in the next coupling step. The capping is done by the acetylation of the 5'-hydroxyl group (see figure 1-12) with acetic anhydride in tetrahydrofuran (THF)/pyridine solution catalysed by N-methylimidazole.

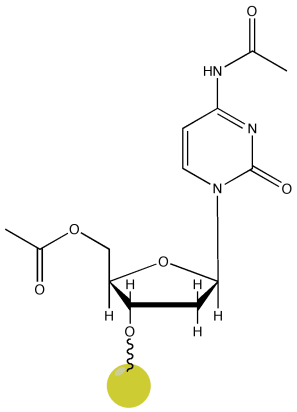

Figure 1-12 The uncoupled nucleotide is acetylated to prevent further reaction during the next synthesis cycle.

This step also reverses any phosphitylation of the O6 position of guanosine[26].

1.1.5.1.4 Oxidation

The last step of the cycle is the oxidation of the acid unstable phosphite triesters (P(III)) formed in the coupling step to the more stable pentavalent phosphotriester

(see figure 1-13). The oxidation is achieved by iodine in the presence of water and pyridine[27,28]. The phosphotriester produced is effectively a DNA backbone, protected with a 2-cyanoethyl group that prevents undesirable reactions at the phosphorus during subsequent synthesis cycles.

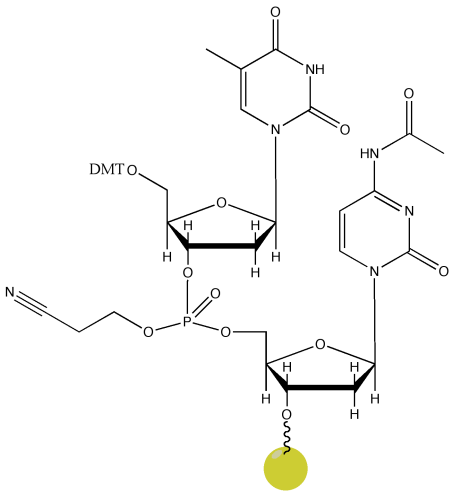

Figure 1-13 Dinucleotide as produced after the first cycle, with DMT protected 5'-hydroxyl ready for next cycle.

1.1.5.1.5 Cleavage and deprotection

The cycle is then repeated until the sequence of the desired length is obtained. The final DMT is left at the 5'-end of the oligonucleotide at the discretion of the operator, usually the purification method is the main factor of the decision. The sequence obtained on the CPG column is removed from the synthesiser and the oligonucleotide is cleaved from the solid support by treatment with concentrated ammonium hydroxide for one hour at room temperature. The cyanoethyl groups and the protecting groups of the exocyclic primary amino groups on the heterocyclic bases are removed with ammonium hydroxide at 55 ºC for sixteen hours.

1.1.5.2 Modification

Applications based on DNA such as PCR[17], DNA microarrays[29] and molecular beacons[30] require modified synthetic DNA. These modifications can range from fluorescent tags to linkers and spacers. The modifications can be done at the 5'- ,3'- ends as well as in mid-sequence sites. Furthermore sugar and backbone modifications can be done to confer extra stability to the molecule.

1.1.5.2.1 5'- and 3'- modification

Some common terminal modifications that are commercially available are fluorescent dyes, non-fluorescent modification such as thiol- and amino- handles, biotin and various spacer molecules. Since solid-phase synthesis goes in a 3'- to 5'- direction, 5'-modifications are the most common. Using a modified phosphoramidite the modification can be incorporated at the end of the sequence. In solid-phase synthesis the 3'-terminus is attached to the CPG therefore any modification at the 3'- end must leave a DMT-protected alcohol for subsequent coupling. There are also commercially available columns where the CPG beads have both DMT protected hydroxyl and fluorenylmethyloxycarbonyl (Fmoc) protected amino groups on the same carbon chain, which permit easy functionalization (see figure 1-14).

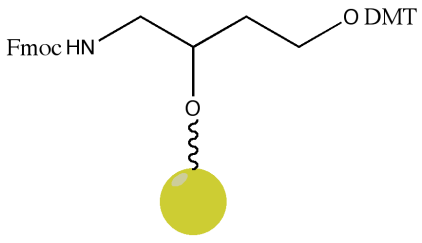

Figure 1-14 CPG functionalised for 3'-modification.

Other commercially available universal columns have pre-functionalised fluorescent probes or non-fluorescent modifications whereby the first base of the DNA must be added.

1.1.5.2.2 Mid-sequence modification

The most common and popular method used for mid-sequence modification is through the Sonogashira reaction[31] whereby a 5'-iodouridine nucleoside can react with an alkyne modified group (fluorescent tag, protected amino group) yielding a modified base.

1.1.5.2.3 Sugar and backbone modification

Sugar and backbone modifications are used mainly to confer thermal stability and resistance to nucleases. An example of sugar-modified oligonucleotides is the locked nucleic acid (LNA) where the 2'OH is bridged through a methylene unit to the C-4' (see figure 1-15). These LNA can be introduced into the sequence by replacing the DNA phosphoramidites with LNA analogues in the synthesis cycle. LNA oligonucleotides have a high binding affinities to complementary nucleic acids[32].

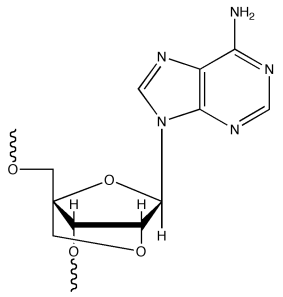

Figure 1-15 Locked nucleic acid (LNA) where the 2'-hydroxyl of the ribose sugar is bridged to the C-4' by a methylene group.

Backbone modification usually consists of the replacement of the charged oxygen of the backbone with a sulfur atom (see figure 1-16), producing phosphorothioates[33]. Phosphorothioate-containing oligonucleotides have found wide spread use in molecular biology due to their increased resistance to nuclease digestion and as antisense oligos for *in vitro* and *in vivo* inhibitors of gene expression[34]. Using solid-phase synthesis there are two ways of preparing phosphorothioates. The first option is to use H-phosphonates monomers which are useful for the preparation of internucleotide linkages not attainable by standard phosphoramidite chemistry[35]. The second option is using a sulfurizing reagent in conjunction with phosphoramidite chemistry. This method gives better control on the state of each linkage in a site-specific manner. Although there are various sulfurization agents that can be used[36-40], 3-ethoxy-1,2,4-dithiazolidine-5-one (EDITH) is nowadays widely used[41-44] as it is soluble in the acetonitrile standard solvent for phosphoramidite dilution and stable in solution for several months.

These DNA modifications are important tools for the development and enhancement of SERS based bio-diagnostics as shown in the following section.

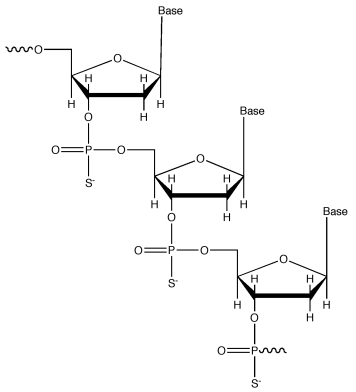

Figure 1-16 An oligonucleotide with a phosphorothioate linkage, in which a non-bridging oxygen is replaced by a sulfur.

1.2 Surface-enhanced Raman scattering

1.2.1 Basic principles

As biodiagnostics is pushing towards goals of high throughput, multiple analysis capacities and inexpensive miniaturised platforms, SERS is gaining good momentum as a platform for future development of bioanalytical tools. Understanding the basic principles of SERS gives an insight of its potential.

SERS amplifies the Raman signals from molecules by several orders of magnitude. The amplification of the signals is attributed to the electromagnetic interaction of light with metals. Such interactions cause the large amplification of the laser field through excitations generally known as plasmon resonances. Molecules can thus be analysed by profiting from this phenomenon, by being adsorbed or in close proximity of a metal surface. Raman signals come from the inelastic light scattering. Such signals can be analysed and used to give useful information on the vibrational structure of a molecule[45].

SERS great potential cannot be fully appreciated if the Raman process is not understood. The Raman process/effect is a scattering process of light, it was first discovered by Sir Chandrasekhara Venkata Raman[46] in 1921 in India using very simple colour filters, the sun as a light source and his eyes as detectors. The observation of this new optical scattering phenomenon earned Raman a Nobel Prize in physics in 1930. It was officially awarded to him "for his work on the scattering of light and for the discovery of the effect named after him"[47].

Raman scattering is one of many physical processes (such as absorption, luminescence and other scattering processes) that occur when light interacts with matter. The outcome of the interaction of light with molecules is determined by the energy levels of the degrees of freedom of the molecule in question. Energy levels can be represented schematically as Jablonski diagrams[48-50] (see figure 1-17) in which molecular electronic states are represented as bold curves (see figure 1-17) that show the energy state as a function of the atomic coordinates. The minima of such curves correspond to the equilibrium position of the atoms. Motional states, which are usually vibrational states, for each electronic state, are depicted as thin lines while transition between states are represented by arrows (see figure 1-17).

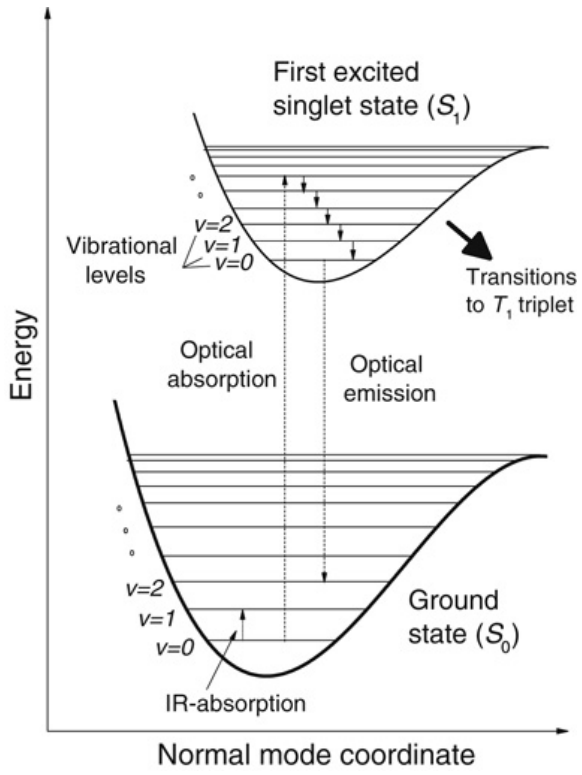

Figure 1-17 Jablonski diagram. The electronic energy levels are represented as bold lines and the vibrational/rotational levels represented as thin lines. Possible transitions between states are indicated by arrows (dotted lines for radiative transitions and solid lines for non-radiative transitions). Adapted from Le Ru[45].

In the ground state the electrons occupy the lowest energy state possible, hence following the Pauli exclusion principle, electrons of opposite spins are paired up together, having a total spin of zero. This ground state is then called a singlet state (S_0). When an electron is excited to a new state, the total spin may not be zero, as nothing prevents it from having a different spin value, hence the electronic excited state is four times degenerate, as four different spin states can be assumed: a singlet state (S_1) corresponding to the only excited state configuration of a total spin of zero and a triplet state (T_1) corresponding to a triply degenerate excited state with a total spin of one.

There are a lot of transitions that can occur between molecular states. Each transition would correspond to either an absorption or loss of energy, thus conservation of energy is upheld. Transitions between electronic states are known as electronic transitions while transitions between two states in the same electronic state are called internal or vibrational transitions. These transitions can be further classified in to two groups:

- Radiative transitions; which involve interaction with a photon. Such transition is depicted by a straight vertical dotted arrow as depicted in figure 1-17. It involves absorption of a photon *i.e.* transition to a higher energy or the reverse emission of a photon. Transitions between singlet and triplet state are forbidden, however may occur if a spin relaxation mechanism occur as a photon cannot introduce a change in total spin.

- Non-radiative transitions; are a result of interaction with the environment (solvent, other molecules) or of internal interactions (internal conversion, intra-molecular vibrational redistribution).

From all the radiative transitions, Raman scattering is part of an important family of processes that involve scattering. These scattering processes, unlike other optical processes such as absorption and emission, involve the instantaneous absorption of an incident photon and emission of another photon, known as the scattered photon. Scattering processes are classified into two:

- Elastic scattering, whereby both incident and scattered photons have the same energy, however can have different direction and/or polarisation. It is known as Rayleigh scattering in molecules and for large objects such as nanoparticles it is called Mie scattering. Such scattering process involves no transfer of energy between molecule and photon hence not much is revealed on the internal molecular structure.

- Inelastic scattering, whereby the scattered photon is at a different energy from the incident photon. The energy difference is essentially the transition between two states in the molecule. Raman scattering is in fact an inelastic scattering process involving transition between vibrational/rotational levels. When scattered photons have less energy than the incident photon ($E_S < E_L$), the process is called Stokes process. It usually corresponds to a transition from the vibrational ground state $v = 0$ to a first excited state $v = 1$, with energy $\hbar_{wv}=E_L - E_S$, where $\hbar_{wv}$ is the energy of vibration (see figure 1-18). Opposite to this process is the anti-Stokes process when a scattered photon

has more energy than the incident photon ($E_S > E_L$), hence the molecule relaxes from a vibrational mode $v = 1$ to the vibrational ground state $v = 0$. The energy of the vibration is now $\hbar_{wv}=E_S - E_L$ (see figure 1-18). As an excited vibrational state is needed for the anti-Stokes process (usually through thermal excitation), it is a weaker phenomenon than the Stokes process.

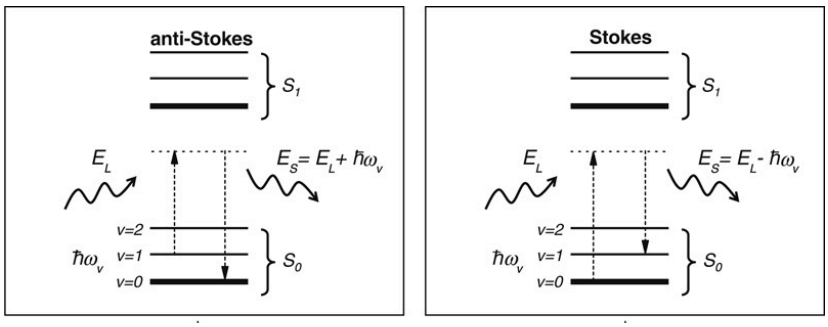

Figure 1-18 Simplified Jablonski diagrams of the anti-Stokes (left) and Stokes (right) Raman processes. Figure adapted from Le Ru[45].

One of the great advantages of Raman scattering unlike fluorescence is that it is an instantaneous process that can happen without a direct absorption of the photon. This allows the process to happen even when no electronic transition is present at the incident wavelength, hence incident light where no molecular absorption (no fluorescence) occurs can be used. However a disadvantage of scattering is that they are usually a weak phenomenon especially when compared to absorption and fluorescence processes. When the incident light (energy) corresponds to one of the real electronic levels in the molecule, resonant scattering occurs. Resonance Raman scattering has an important application in both normal Raman and SERS conditions, as it increases by several orders of magnitude the scattering effect. When resonance

Raman scattering is used in SERS conditions, the technique is better know by the acronym SERRS *i.e.* surface-enhanced resonance Raman scattering.

1.2.2 SERS substrates

A substrates main role in SERS is to provide a surface to support a plasmon resonance, which enhances the Raman signal. The plasmon resonance of the substrate is wavelength dependent therefore substrates usually exhibit a good enhancement in a limited wavelength range. Raman spectroscopy usually operates in the 400 -1000 nm region hence ideal SERS substrates should have a good plasmon resonance in this particular region.

Substrates that have suitable enhancements in such a region are usually:

- substrates made of gold and silver,
- substrates with dimensions less than 100nm.

The noble metals gold and silver along with the others, are well known to have special properties, both physical and optical which all arise from the availability of free conduction electrons. The 'sea' of electrons form what is known as a plasma or solid state plasma[51]. The plasma response to light governs the optical properties of metals especially in the visible part of the spectrum. SERS substrates are usually used in the form of metallic colloids whereby they are used in solution or else attached to a substrate forming planar metallic structures. Other types of substrates used are in the form of electrodes. Electrodes played an important role in the

discovery and development of SERS, however their use has decreased lately mainly because of their low enhancement factor.

1.2.3 SERS probes

A wide range of molecules/analytes can be measured by SERS, as in principle any molecule that produces a Raman signal, can interact with the plasmon resonance of the metallic substrate and in turn be amplified. A molecule that satisfies the two prerequisites of having intense Raman scattering, and good metal interaction can be used as a tagging/probe for target analytes, that do not have a satisfactory amplification in normal experimental procedures.

Raman scattering intensities are characterised by the Raman cross-section *i.e.* the cross-section σ [m^2] of a molecule in relation to the signal produced by Raman scattering which is made up by the intensity/power P [W](proportional to the number of photons per unit time involved in the process) to the incident power density S_{Inc} [Wm^{-2}] at the molecule position as in equation 1-1.

$$\boldsymbol{P = \sigma S_{Inc}}$$

Equation 1-1

The intensity varies by several orders of magnitude depending on both the analyte/probe under study and the incident wavelength used. Molecules, which have electronic energies close to the exciting laser energy, have a high intensity and are called resonant Raman scatterers. Examples of such molecules are dyes (*e.g.* R6G) for which resonance Raman scattering intensities can be $\approx 10^6$ larger than normal Raman intensities. It is important to note that when a resonant Raman scattering

probe is used in SERS conditions, the technique can be referred to as SERRS, however enhancement mechanisms still operate the same way.

As stated before a good Raman scatterer or a resonant Raman scatter is not sufficient for being used in SERS conditions. The molecule must also be able to chemically or physically adsorb to the SERS substrate. Since substrates are usually made of gold or silver, it is easier to work with probes/analytes that have thiol or triazole groups as they show a high chemical affinity to such metal surfaces. Other ways to attach such molecules is through electrostatic interactions or surface functionalization of the substrates.

1.2.4 SERS enhancement

1.2.4.1 Electromagnetic and chemical enhancements

Central point to the SERS technique is the ability to quantify the magnitude of the enhancement and to understand the physical origins of the enhancement. As stated before in section 1.2.3 the average Raman intensity of a molecule is directly proportional to the laser power density and the Raman cross-section of the molecule. This can also be generalised to SERS, however the SERS intensity is affected by an enhancement factor (EF). The physical origins of SERS EF are usually separated into two multiplicative contributions:

- The electromagnetic (EM) enhancement factor F_{EM} which is thought to be the major contributor of SERS enhancement. It arises from the coupling of the incident and Raman electromagnetic fields with the SERS substrate. The EM enhancement relies on the large local field enhancement that occurs close to metallic surfaces when localised surface plasmon (LSP) resonances

are excited. The molecule must be in close proximity to the metal surface (~ 10 nm) to profit from them.

- The second contribution to the EF is called the chemical enhancement (CE) factor F_{chem}. The existence and the definition of the CE factor is still a subject of controversy (7) nonetheless it is believed that its contribution to the SERS enhancement is much smaller than by the EM factor. One view of the CE factor is that the modification of the electronic polarizability of the probe molecule can induce resonant Raman scattering at wavelengths where the non-absorbed molecules would not be resonant (7). However the more accepted explanation is through a charge transfer (CT) mechanism (161), where the probe must be chemisorbed to the metal surface.

SERS substrates are highly non-uniform even at the nanometre scale and since local field enhancement depends strongly on the exact position of the molecule on the surface, points of very large enhancement (hot spots) can be very localised. Single molecule (SM) SERS detection applications can profit from such hotspots, however many applications in analytical chemistry are more interested in the average enhancement factor i.e. for molecules with random position on the substrate. Most SERS EF definitions will therefore fall into one of the two categories :

1. Maximum SERS enhancement factor. They occur on specific positions on the surface of the substrate and are known as hot spots. Only molecules in the hot spot may profit from it. These hot spots can give enhancement factors up to 10^6 in spherical nanoparticles and up to 10^{10}-10^{11} at nanometre gaps between two nanoparticles. Such high enhancement factors are sufficient to detect

SERS signal of a single molecule, however the hot spots cannot yet be made in a controlled manner or bring analytes specifically to their location. Single molecule detection can still be achieved when using resonant Raman dyes[52].

2. SERS average enhancement factor. It assumes a molecule is randomly adsorbed on the surface of a SERS substrate; hence it is an average of all the possible positions the molecule in question might take on the metallic surface. Typical values of SERS enhancement factors are in the range of 10^5-10^6.

1.2.5 SERS applications

The main advantage of Raman spectroscopy is that it gives a distinct and unique spectrum of a molecule and hence provides a spectroscopic fingerprint. Raman spectroscopy is more specific than IR spectroscopy; only NMR is better when it comes down to specificity. This allows Raman spectroscopy to be exploited in a variety of applications.

SERS is being implemented for applications, as it combines the advantage of the high specificity of the Raman effect and the high sensitivity which is equivalent or even better than that of fluorescence[53]. These advantages open up other niches of application that would be impossible to implement with normal Raman spectroscopy. Examples of such applications is the use of SERS in trace analysis especially in the detection, identification and quantification of dyestuff in old paintings, medieval manuscripts[54-56], medicines[57-59], explosives[60], drugs and bio-fluids such as glucose[61]. Recently trace detection of biomolecules have been the main driving

force in providing new SERS applications, specifically for analysis of DNA[62] and proteins[63]. A great benefit of SERS in trace analysis is that SERS conditions such as substrate, probe and laser excitation are optimised according to the analyte under investigation as to have the optimum signals and the detection limit.

The SERS probes usually used in applications involving biomolecules, are ideal in substituting fluorophores in fluorescence based applications[53]. The apparent competition between the two techniques is artificial as each one fills the gaps where the other cannot cover. Table 1-1 below summarises the advantages of each technique over each other.

Table 1-1 Advantages of fluorescence and SERS.

Fluorescence	**SERS**
Single molecule detection more practical and straightforward than SERS.	High specificity, thus SERS signature easily distinguished from background signal and allows multiplexing (*i.e.* monitoring of different probes/tags).
Well-established, readily available instruments, probes and conjugates.	Applied to any molecule without the need of tagging
Quantitative.	Works with any excitation wavelength with the appropriate substrate unlike fluorescence.
	Photo-bleaching not as problematic in SERS than in fluorescence.

1.3 Inorganic colloidal nanoparticles

1.3.1 Introduction

Inorganic colloidal nanoparticles are ideal SERS substrates and are defined as small nanoscale objects that have an inorganic core and are dispersed in a solvent. There are large selections of inorganic nanoparticles that have different properties according to their inorganic core, such as photoluminescence in the form of fluorescence (semiconductor quantum dots *e.g.* CdSe or CdTe) or phosphorescence (doped oxide materials *e.g.* Y_2O_3) or magnetic moment (*e.g.* iron oxide or cobalt). The most interesting nanoparticles for SERS as described in section 1.2.2 are silver and gold nanoparticles, which have high electron density and strong optical absorption, making them ideal for the use as a substrate in SERS. In fact they were used in the first claims of single molecule detection both in water[64] and as deposits on a planar substrates[65].

1.3.2 Metallic colloids for SERS

1.3.2.1 Introduction

There are several chemical routes by which silver and gold colloids can be synthesised in solution[66]. Most of these synthesis routes involve a reduction mechanism. Since colloids are dispersed in a solvent and most of the time it is water, they are stable only because of coulombic and steric repulsions among the particles and this is brought about by the use of a stabilising agent that covers the colloid surface and prevents aggregation. One of the most used methods of synthesis for

SERS colloid is the sodium-citrate reduction method[67] by Lee &Meisel whereby the citrate acts as both reducing and stabilisation agent.

Gold nanoparticles are the most well studied colloids for SERS, since they are easily stabilised, less susceptible to oxidation and usually have a longer shelf life than silver nanoparticles. Due to such properties gold nanoparticles have been widely used in biological applications[68-72] for many years now. This gives a wide understanding on the synthesis[73,74] properties and the chemistry of molecular binding.

In spite of all gold's advantages, silver nanoparticles are being widely used in SERS mostly because of the high electromagnetic enhancement in the visible region (500-650nm), hence more emphasis on silver nanoparticle synthesis, properties, characterisation and uses, as a SERS substrate shall follow. Still most of the points made on silver can equally apply to gold colloids.

1.3.2.2 Synthesis

The synthesis of colloids is not yet fully understood, however there are many processes that have been studied in great detail[75-77]. Colloids are usually fabricated by first having a nucleation process that will create the nanoparticles to a certain shape and size, after which the growth of the particles will continue until the metal or reducing agent has finished. There are a lot of chemical and physical factors that affect the synthesis mechanism, which in turn give different size, shape and polydispersity (size distribution) to the nanoparticles.

The most common cited methods for the preparation of silver colloids is the one described by Lee and Meisel[67]. From the three different methods for silver sols

production described by Lee and Meisel[67], the citrate reduction route is the one which is easiest to prepare and which gives stable particles, in fact it was further investigated and optimised by Munro *et al.*[75]. The three basic steps of silver colloids by the citrate-reduction method involve:

1. Dissolve silver nitrate ($AgNO_3$) in water and boil
2. Reduce the former with sodium citrate (trisodium citrate $Na_3C_6H_5O_7$) while boiling
3. Boil under reflux for one hour

Gold colloids can be prepared in a similar fashion using citrate as a reducing agent, following these general guidelines:

1. Dissolve chloroauric acid ($HAuCl_4$) in water and boil
2. Reduce the former with sodium citrate (trisodium citrate $Na_3C_6H_5O_7$) while boiling
3. Boil under reflux for one hour

There are various other methods that can be found in scientific literature involving different reducing and stabilizing agents for the synthesis of inorganic metallic colloids. Each method give different sizes, and shapes, hence also different extinction spectra.

Examples of well-known alternatives for production of silver colloids (can be adapted for gold) are:

- Reduction with sodium borohydride ($NaBH_4$) of $AgNO_3$, however the BO_3^{3-} ion does not act as a good stabilizing agent[2].

- Reduction of silver perchlorate ($AgClO_2$) with sodium borohydride ($NaBH_4$) with the perchlorate ion acting as a stabilizing agent[77].

- A two step synthesis; 'small' nanoparticles are first produced by borohydride reduction and used a seed for the second step, whereby ascorbic acid is used for a slower and more controlled reduction[78]. This gives colloids with better size uniformity and better size control. A similar approach was taken for the fabrication of silver sol by reaction of $AgNO_3$ with hydrazine hydrate[79] and HQ[80].

- Another two step process for the production of spherical monodispersed silver nanoparticles with controlled size range was reported by Lundahl *et al.*[81], whereby ethylenediaminetetraacetic acid (EDTA) reduced silver nanoparticles[82] are used as seeds to eventually grow controlled sizes of nanoparticles by reduction of silver nitrate with hydroxylamine hydrochloride ($HONH_2 \cdot HCl$).By this method, different sizes can be grown according to how much silver nitrate is available for reduction.

Other possible synthesis routes can also involve formation of silver colloids in non-aqueous environment such as that reported by Kim *et al.* [83].

1.3.2.3 Properties

Silver colloids prepared by the Lee and Meisel method[67], result in a grey-yellow solution with the extinction spectrum maximum in between 400-430nm. Gold nanoparticles produced by the citrate reduction method give a ruby red solution with an extinction spectrum at a maximum in the range of 520-530nm. The citrate reduction method usually give a wide size distribution range, with a mean of about 60nm and various shapes, however with optimisation work done on the Lee and Meisel method by Munro *et al.*[75] provided less polydispersed colloids with smaller particle size average of around 27nm. Silver colloids display aging over time, they can be stored up to one year in a fridge at 4ºC. The stabilizing agent, the citrate ion ($C_6H_5O_7^{3-}$) is a weak base, whose triple acid form is citric acid ($C_6H_8O_7$) (pK_a 6.4/3.76/3.13), hence this has to be taken into account when doing *pH* dependant SERS experiments.

1.3.2.4 Characterisation

Inorganic metallic colloids need to be fully characterised since knowing their size distribution and shape, allows one to know the plasmon resonance and electromagnetic enhancements when used as SERS substrates.

The most direct method to characterise colloids is by electron microscopy. The commonest microscopic technique used is scanning electron microscopy (SEM). From SEM images the accurate size and shape can be obtained. The colloid samples cannot be used directly in SEM but they need to be dried in an appropriate substrate, which can lead to clustering between particles (see Figure 1-19). Such a problem can be avoided (in this case for negatively charged nanoparticles) by either treating the

silicon wafer to give it a positive surface charge or by grafting on a positively charged poly-lysine glass slide. Unfortunately SEM is a time consuming and costly technique, however an alternative to SEM is atomic force microscopy (AFM), which can measure accurately the height of the particles, however the in-plane measurements are not as accurate as with SEM.

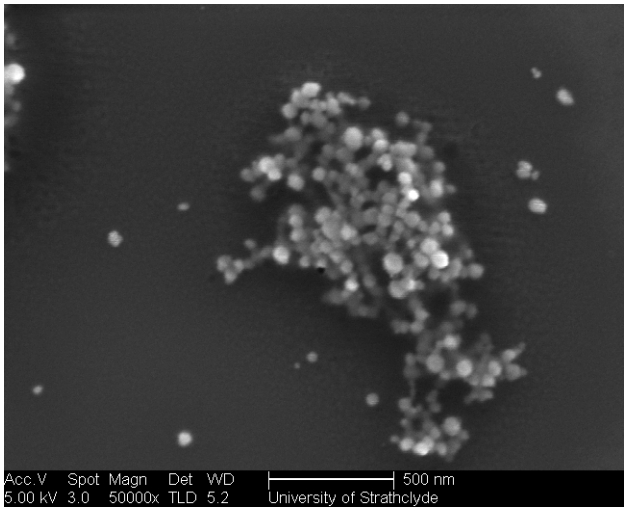

Figure 1-19 Clustering of silver nanoparticles after drying on a silicon wafer for SEM analysis.

A relative simple and cheap technique for the optical characterisation of inorganic metallic colloids is UV/Vis spectroscopy whereby the absorption and transition (extinction) can be measured. The peaks observed in the extinction spectra are directly associated with the resonant optical response at the wavelength corresponding to the localised surface plasmon resonance of the substrate. If the peak is broad it reflects polydispersity of the colloid. The resonance wavelength obtained from the extinction spectra of the colloid is important for SERS, as the largest enhancement for the substrate is when both incident laser and/or Stokes shifted SERS photons are close to the resonance wavelength. It is to note that although the wavelength dependence of the extinction spectrum and the SERS enhancement are

related, the extinction spectrum and the magnitude of the SERS enhancement are indirect. To better illustrate this, it is known that resonances associated with gap-plasmons do not have more intense extinction spectra despite their much bigger SERS enhancements[84]. Another example is when using aggregated colloid from which the SERS signal is mostly due to hot spots, the extinction spectrum is not a good indicator where in the wavelength the maximum SERS enhancements occur. UV/Vis spectroscopy is ideal for quality control of the colloid solution prepared rather than accurate measurement for shape and size, however recent studies tried to relate the size and shape of silver nanoparticles to their plasmon resonance[85].

From UV/Vis measurements one can also deduce the concentration of the colloids in solution, the same way dye concentrations are obtained by the use of the Beer-Lambert law (see equation 1-2):

$$A = log_{10}(T) = c_m \varepsilon l$$

Equation 1-2

where for monodispersed colloid solutions c_m [M] is the colloid concentration and ε [$M^{-1}cm^{-1}$] is the extinction coefficient and l is the light path length. The extinction coefficient depends on the material. Gold nanoparticles of approximately 40 nm have an ε corresponding to 1.63 x 10^{10} $M^{-1}cm^{-1}$while silver nanoparticles of the same size has a ε of 2.8 x 10^{10} $M^{-1}cm^{-1}$. The extinction coefficient also increases with an incrimination of particle size.

Another interesting technique that is commonly used for colloid characterisation is dynamic light scattering (DLS). DLS relies on the principles[86] of measurement of

intensity fluctuations in the light scattered by a monochromatic source. Assuming that the particles are spherical, DLS can give the radius of the particles, as it is directly related to the diffusion coefficient *D*, as shown in equation 1-3 the Stokes Einstein equation[86]:

$$D = \frac{k_B T}{6\pi\eta R_h}$$

Equation 1-3

where *h* [kg $m^{-1}s^{-1}$] is the solvent viscosity, R_h is the hydrodynamic radius of the particle. DLS is an important tool for characterisation alongside other techniques as the average properties of the particles can be easily obtained.

Another method for particle size characterisation is by differential centrifugal sedimentation (DCS), which allows extremely high-resolution size distribution that can range from 0.01μm to 50μm. The theory behind particle size analysis of an unknown distribution of spherical particles by sedimentation is the Stokes' law[87] whereby the time taken by particles to settle a known distance in a fluid of known viscosity and density is measured. If sedimentation is done under gravity alone, it is not very practical as it would be limited to particles of a relatively large size. Small particles would take a long time to settle and settling itself would be hampered by Brownian motion. Using centrifugal forces for sedimentation through the use of a centrifuge allows sedimentation analysis of smaller particles. This is due to the high *g* forces, which make sedimentation of small particles much faster than Brownian diffusion. The stokes law has to be modified (see equation 1-4) to take in account the variation in *g* force with distance from the centre of rotation:

$$D = \left\{ \frac{\left(18\eta \ln\left(R_f / R_0\right)\right)}{\left(\left(\rho_p - \rho_f\right)\omega^2 t\right)} \right\}^{0.5}$$

Equation 1-4

where D is the particle diameter [cm], h is the final viscosity [poise], R_f is the final radius of rotation [cm], R_0 is the initial radius of rotation [cm], r_p is the particle density [g ml^{-1}], w is the rotational velocity [rad s^{-1}] and t is the time required to sediment from R_0 to R_f [s]. All parameters are kept constant except for time during analysis, so that the diameter of spherical particles are measured based on arrival time at the detector. The common designs for DCS instruments usually consist of a hollow optically clear disc that is driven by a variable speed motor, with a monochromatic detector beam (see figure 1-20). The wavelength for the beam is usually in the range of 400 to 500nm as short wavelengths give better detector sensitivity for particles smaller than 100nm.

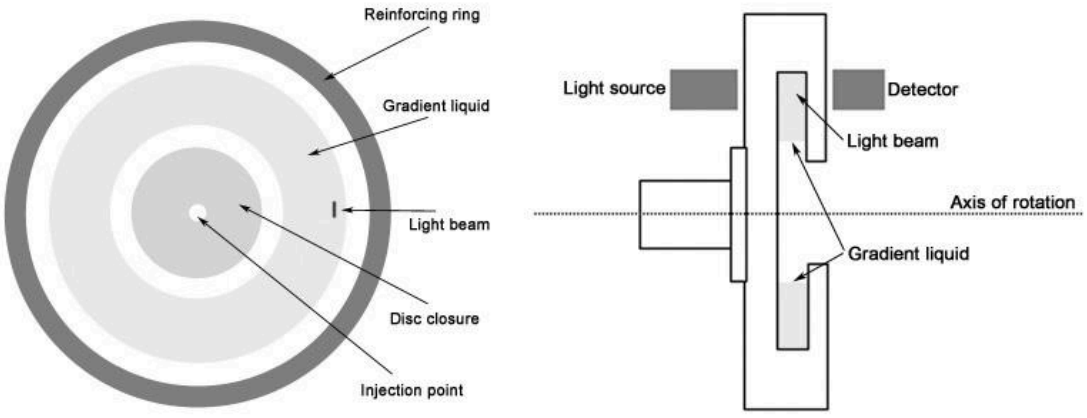

Figure 1-20 Hollow disc centrifuge design. Taken from Laidlaw[88]

The overall advantages of the DCS method are accuracy, repeatability of the size distribution reported and an overall better resolution.

1.3.2.5 Functionalization

Inorganic colloidal nanoparticles can be functionalised with a variety of moieties that can range from simple molecules such as *N*-hydroxy-succinimide (NHS) to polymers such as poly(ethylene glycol) (PEG) and biomolecules from the smaller ones such as lipids and peptides to larger molecules such as DNA and proteins.

When inorganic nanoparticles are conjugated with biomolecules, hybrids are generated. These hybrids can then interact specifically with a biological system. The greatest advantage that these conjugations offer is that they bring together the unique properties of both materials. For example inorganic nanoparticles such as silver bring the optical properties together with the property of an aptamer of high specific binding by molecular recognition. Such systems would be an ideal candidate for SERS sensing applications or with addition of a dye for SERRS sensing applications.

Conjugation of biomolecules to nanoparticles fall generally into four classes:

1. Chemisorption, whereby the biomolecule binds to the surface of the inorganic particle core *e.g.* thiol groups.

2. Electrostatic adsorption, whereby a charged biomolecule adsorbs to an oppositely charged nanoparticle.

3. Covalent binding by conjugation chemistry, whereby already present functional groups present on particle and biomolecule are exploited.

4. Non-covalent, affinity-based receptor-ligand systems *e.g.* an avidin (protein) –biotin (vitamin H) system.

Nucleic acids, apart from containing genetic information of organisms can be employed as a very specific polymeric molecule for molecular recognition. This sought after property could be transferred to metallic inorganic colloids by conjugation. Oligonucleotides can be conveniently attached in an aqueous solution to both silver and gold nanoparticles[68-71,89] by a thiol-metal bond. Unlike double-stranded DNA (dsDNA), ssDNA is more flexible[90] and can take a curved or coiled formation on the nanoparticle. Studies have found that ssDNA attached to nanoparticles undergo a stretching when an increased surface coverage induces steric pressure or when it is hybridised with a complementary strand, which results in a stiffer double helix[91-93]. Aptamers have the desirable property of strongly binding to a target molecule by molecular recognition, determined by geometric matching of the surfaces of the two molecules, hence they have been attached to various nanoparticles as to exploit such characteristic. Aptamers have been attached to gold nanoparticles via a thiol functional group[72,94] and to quantum dots, and silica coated gold particles by covalent conjugation chemistry[95,96], to avidin-modified magnetic nanoparticles[97] and to biotinylated DNA aptamers to quantum dots with streptavidin[98]. Aptamer functionalised nanoparticles have been successfully used to detect the thrombin protein using both colourimetry and SERRS[99,100].

Functionalised nanoparticles are being also widely used in research to investigate nucleic acids, especially when SERS and SERRS techniques are used thus offering high enhancement factors[101]. Such techniques make it possible for handling low sample concentrations which rival and in most cases are better than fluorescence[65,102]. Detection for very low DNA concentrations can be devised using

SERRS systems, whereby a DNA probe is modified as to be able to adsorb to the metal nanoparticle surface and linked to a chromophore which will give a resonance contribution with the exciting laser wavelength (see figure 1-21).

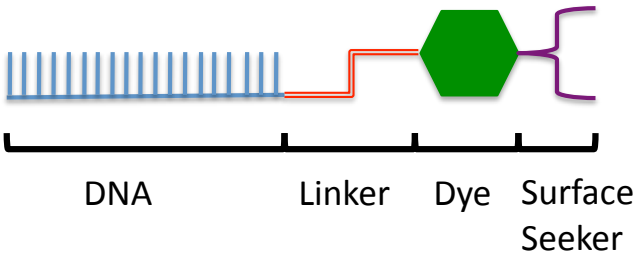

Figure 1-21 Schematic diagram of a SERRS active DNA probe. Four main components are present however it should be noted that the dye and surface-seeking group could be the same species. Figure adapted from Graham *et al.*[103].

Array based formats have been developed where the probe is immobilized as to capture the target sequence from the sample. These systems were effectively used to detect and analyse the breast cancer gene BRCA1[104] and also the detection of 6 different labelled oligonucleotide sequences[105]. Other approaches use molecular sentinels whereby the SERRS signal changes through hybridization of the probe[106].

SERRS based diagnostic systems are being also developed to detect a wider variety of target molecules by using the numerous high affinity and highly specific aptamers that are readily available as probes[107]. Aptamer-based SERRS systems characteristics are that they provide an ultrasensitive detection technique as demonstrated by Cho *et al.*[99] in the detection of thrombin protein by combining resonance Raman scattering with SERS enhancement in the presence of a metallic nanoparticle.

1.4 Aims

In the following chapters two fundamental aspects of SERS are examined, the SERS probe and the SERS substrate. In chapters two and three the effect on SERS with the modification of the oligonucleotide SERS probe is investigated. The aims of chapter two were to determine the effects of phosphorothioate modified DNA on SERS when:

- The concentration of the aggregating agent spermine are changed
- The number of phosphorothioate modifications in the TAMRA-labelled oligonucleotide are changed
- Inorganic salts are used as aggregating agents

The results obtained in this chapter were further backed up with a study on the interaction of phosphorothioate modified DNA with the silver nanoparticle surface using un-labelled polyadenine oligonucleotides. While in chapter two the focus was on single stranded DNA the aim of chapter three was extended to double stranded DNA. The different electrostatic properties of single-stranded and double stranded DNA favours the single-stranded DNA to give higher SERS intensities, when negatively charged silver nanoparticles are used. The aim of chapter 3 was to:

- Determine the effects of DNA melting curves with phosphorothioate modification
- investigate the effect of different combination of unmodified and phosphorothioate modified DNA with complimentary unmodified and phosphorothioate modified DNA on SERS intensities.

- Find a relation between melting curves and change in SERS intensities

In the following chapters four and five the focus turns to the SERS substrate. The aims of chapter four were:

- To produce different monodispersed silver nanoparticle size.
- to understand the effect of nanoparticle size on SERS enhancement, using three different dye-labelled oligonucleotides with different absorption maximum wavelength.

In chapter five the aim was to:

- improve on the synthesis of monodispersed size tuneable silver nanoparticles using hydroquinone which is a selectively reduces Ag ions when nanoparticle seeds are present.
- to determine the analytical enhancement factor for each size using rhodamine 6G, malachite green oxalate and thiophenol as probes.

The aim of chapter six was to:

- bring together the work of the previous chapters together evaluating the effect of combining nanoparticle size and phosphorothioate modification on SERS analysis and
- comparing different methods of nanoparticle characterisations

Chapter 2: Quantitative Enhanced Raman Scattering of Dye-Labelled Phosphorothioate Oligonucleotides

2.1 Introduction

Molecular biodiagnostics are evermore relying on nanotechnology to improve sensitivity capabilities and the ability to multiplex *i.e.* to identify more than one analyte simultaneously. Gold nanoparticles have become a general tool for such biodiagnostic techniques whether monitoring their colorimetric[108], scattering[109] or electrical properties[110].

A point in case of improvement in diagnostics by nanomaterials is the detection of DNA. Routinely this is done by fluorescence labelling of DNA whereby the common disadvantage encountered apart from photostability issues is having a broad spectral response making it an inefficient multiplexing technique. Photostability and sensitivity for the detection of DNA was greatly increased with the use of quantum dots[111,112] whereby the excitation occurs at a single wavelength, however the emissions from such systems are still broad (25 nm). The solution for multiplexing lies in the use of spectroscopic techniques, especially in conjunction with metal nanoparticles in SERS as it gives narrow spectral lines[101]. The sensitivity is further enhanced by labelling the DNA with chromophores (the same used in fluorescence) as to have resonance Raman scattering[113] which as reported enables single-molecule detection[64,65]. SERRS has been effectively used as a quantitative technique for the direct analysis of dye-labelled oligonucleotides[114-122]. It has been shown that SERRS can have limits of detection of at least three orders of magnitudes lower than

those obtained by a fluorescent technique[115]. For SERRS analysis of dye-labelled oligonucleotides it is important not only for the biomolecule to adsorb onto a suitable metal surface[123] but also that the chromophore attached coincides with the laser excitation wavelength. The metal substrate used was a silver colloidal solution, which gives high electromagnetic enhancement in the visible region. In direct SERRS analysis of dye-labelled oligonucleotides using negatively charged silver nanoparticles, spermine a tetramine molecule is used which in turn reduces the negative charge of the DNA backbone and induces formation of silver nanoparticle aggregates creating appropriate SERRS conditions in solution. Furthermore if a dye that has a net negative charge in solution is used the oligonucleotide can be modified using propargylamine[124] which will provide a positive charge facilitating adsorption to the silver surface. Backbone and sugar modifications of DNA are becoming cheaper and easier to make. A modification that is gaining interest due to its properties are phosphorothioates linkages whereby a non-bridging oxygen atom of a phosphodiester is replaced by a sulfur atom[125]. Phosphorothioate oligonucleotides can be easily prepared through solid phase phosphoramidite synthesis where the oxidation step is replaced with a sulfurization step. Phosphorothioates modified oligonucleotides have been used in antisense applications[126] as the backbone modification infers to the strand resistance to both exo- and endonucleases. This is particularly useful for clinical applications whereby the enhanced stability is ideal when used in cells and sera. Another useful property that such modification brings about is its affinity towards silver and gold surfaces. As thiol modified molecules[127-129] and thioctic acid modified DNA[130], phosphorothioate modified DNA are being used to functionalize quantum dots[131], gold nanoparticles[132], as a cross-linking

agent for gold nanoparticles to form rigid structures[133] and fabrication of bimetallic core-satellite nanoclusters[134]. In this study the limit of detection of phosphorothioate modified dye-labelled oligonucleotides is compared to an unmodified dye-labelled oligonucleotide using SERRS. The mechanism by which the phosphorothioate-modified DNA attaches to the nanoparticle surface was explored using poly-adenine oligonucleotides.

2.2 Experimental

2.2.1 Chemicals and materials

Oligonucleotides were purchased from Eurofins (Germany) and purified by HPLC. All other materials were purchased from Sigma-Aldrich and used without further purification. All water used was doubly distilled (18.2 mΩ cm).

2.2.2 Nanoparticle preparation

The citrate reduced silver colloid was prepared using a modified version of the Lee and Meisel method[67] Water (500 mL) was heated up to 45 ºC in a three parallel-necked round bottom flask (1 L) and silver nitrate (90 mg in 10 mL H_2O) was added. The solution was heated up to 98 ºC and 1% w/v sodium citrate solution (10 mL) was added. The temperature (98 ºC) was maintained stable for 90 minutes with continuous stirring throughout the flask. The necks were covered with aluminium foil to prevent excessive water evaporation.

2.2.3 Instrumentation

Spectra recorded at 532 nm excitation wavelength an Avalon probe system Ramanstation R3was used which is equipped with an optical fibre probe with a 532 nm diode laser excitation and a power of approximately 24 mW at the sample. Spectra recorded at 633 nm used a setup consisted of a Leica DM/LM microscope equipped with an Olympus 20x/0.4 long-working distance objective that collects 180º backscattered light from a cuvette. The spectrometer system was Renishaw Ramascope System 2000 (Gloucestershire, UK) with a Renishaw diode laser with a power output of 1 mW at sample. Holographic edge filters were used to reject Rayleigh scattered light. The detector used was a deep-depletion RenCAM charge-coupled device (CCD).

2.2.4 Aggregation study

Aggregation studies were carried out on the modified and unmodified TAMRA-labelled oligonucleotides. The samples were prepared for SERRS analysis using 7 µL of TAMRA-labelled oligonucleotide, 10 µL of spermine, 175 µL of water and 175 µL of 0.3 nM silver nanoparticles. The following initial concentrations of spermine tetrahydrochloride diluted in water were used: 0.1, 0.01, 0.001, 0.0001, and 0.00001 mol dm^{-3}, followed by an analysis with no spermine present. The aggregation was monitored using the Avalon probe by taking a spectrum of the colloid solution every 30 s for 30min with 1s exposure time and 5 accumulations. The order of addition of analyte, spermine, water and nanoparticles was found to give the highest peak counts.

2.2.5 Limit of detection studies

Concentration studies were carried out on the modified and unmodified oligonucleotides by diluting them with water to various concentrations. The samples were prepared for SERRS analysis as before by adding 7 μL of TAMRA-labelled oligonucleotide, 10 μL of 0.1 mol dm^{-3} spermine, 175 μL of water and 175 μL of 0.3 nM silver colloid. The samples were analysed 10 minutes after the addition of the silver colloid. Using the Avalon probe each concentration was analysed 5 times, with a 2 s exposure and 5 accumulations. The average peak height of the TAMRA dye which gives the strongest peak (1650 cm^{-1}) in the spectrum was plotted against the concentration of the dye-labelled oligonucleotide after being normalised to a hexane standard. This was repeated with 0.01 M initial spermine concentration and 2M initial concentrations of NaCl, KNO_3 and $MgSO_4$ as aggregating agents. The LOD was calculated using equation 2-1

$$LOD = \frac{\chi_{BL} + 3\sigma_{BL}}{m}$$

Equation 2-1

where χ_{BL} is the mean of the blank sample measurements, σ_{BL} is the standard deviation of the blank sample baseline and *m* is the gradient of the calibration line.

2.2.6 Poly-adenine study

SERS spectra were obtained for modified and unmodified poly-adenine oligonucleotides (PA1, PA2 & PA3). The DNA was prepared for SERS analysis by heating them up to 95 ºC for 15 minutes after which they were immediately cooled

down in an ice bath. Following this 7 μL of the oligonucleotide was added to 10 μL of 0.1 M spermine, 175 μL of water and 175 μL of 0.3 nM AgNP solution, giving a final DNA concentration of 100 nM. The same procedure was used when 1% (w/v) NaCl solution was used as aggregating agent, however a final DNA concentration of 1.9 μM was used. The SERS spectra of three identical samples was recorded after one minute of mixing the analyte with the AgNP with an instrumental setup in a confocal arrangement at an extinction wavelength of 633 nm. The SERS spectra were obtained with an exposure time of 2 seconds and 5 accumulations.

2.3 Results and discussion

Phosphorothioate modified oligonucleotides are known to have a great affinity towards a silver surface due to the sulfur atoms availability for coordination with the metal surface. This is the first report to the best of our knowledge of phosphorothioate dye-labelled oligonucleotides used in direct DNA SERRS analysis. Increasing the affinity of the oligonucleotide towards the nanoparticle should in practice increase the Raman enhancement and give lower detection limits if affinity was the only the key factor and not taking in consideration the mechanism by which the aggregating agent works. To examine this hypothesis, three oligonucleotides with an identical 20 base pair sequence but with different backbone linkages were used as listed in table 2-1.

Table 2-1 Dye-labelled oligonucleotide sequences

	5'-dye label	oligonucleotide sequence
O1	TAMRA	5'GGTTCATATAGTTATAATAA3'
O2	TAMRA	5'*G*G*T*T*C*A*T*A*T*A*G*T*T*A*T*A*A*T*A*A3'
O3	TAMRA	5'*G*G*T*T*C*A*T*A*T*AGTTATAATAA3'

* is a phosphorothioate linkage

The first oligonucleotide (O1) has normal phosphodiester linkages, the second one (O2) has all phosphorothioate linkages and the last sequence (O3) was a chimeric DNA whereby the first ten linkages starting from the 3' are normal phosphodiester bonds, while the other half, the remainder ten linkages are phosphorothioate bonds. The dye-label attached at the 5' end of the oligonucleotide used is carboxytetramethylrhodamine (TAMRA) which has an overall positive charge, facilitating the adsorption to the substrate. The absorption of the dye is at 544 nm which makes it in resonance with the laser excitation wavelength used (532 nm).

Initial experiments were conducted using spermine as to understand if the phosphorothioate modifications change the interaction of the oligonucleotide with the spermine. This is due to the fact that spermines' advantage over inorganic ions or acids as aggregating agents in DNA analysis apart from causing the aggregation of colloid by the reduction of the nanoparticle surface charge, that it also interacts with the DNA to modify its charge[122]. This was found to give a controlled aggregation of the nanoparticles. From our study it has been shown that decreasing the concentration of spermine for the three different oligonucleotides decreases SERRS

intensity from the TAMRA dye peaks (see figure 2-1) and No dye peaks could be observed at very low spermine concentrations.

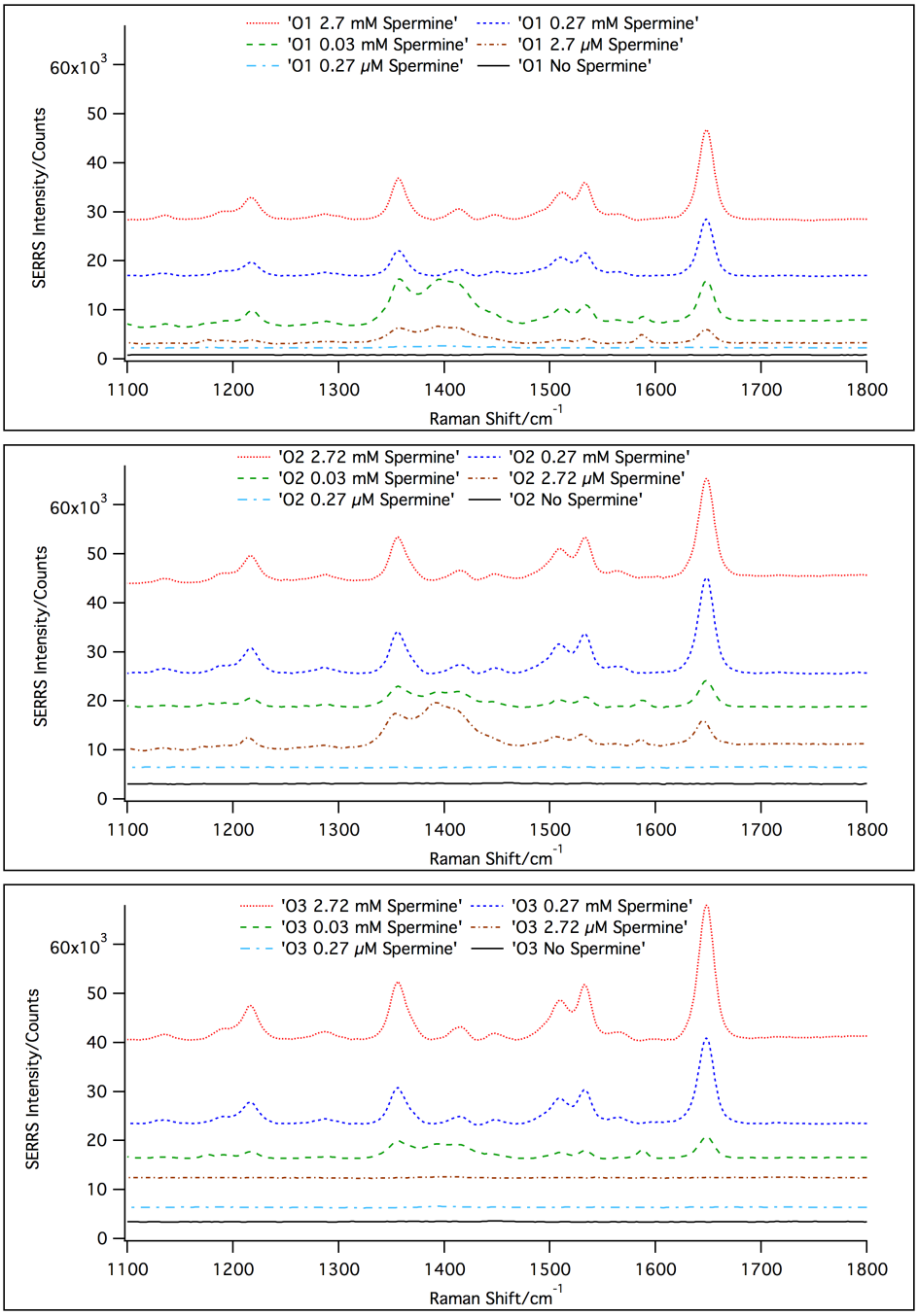

Figure 2-1 Comparison of SERRS spectra containing 1 nM TAMRA-labelled oligonucleotide (O1, O2 & O3) at different spermine concentrations and no spermine at laser excitation wavelength of 532 nm excitation wavelength with 1 seconds exposure time and 5 accumulations. For visualisation purposes the spectra have been baseline corrected and offset on the *Y*-axis.

When no aggregation agent was added no dye spectrum could be obtained, however when the oligonucleotides were left to incubate with the colloid for 24 hours the TAMRA peak at 1650 cm^{-1} could be seen for O2 (see figure 2-2). This shows that the phosphorothioate is actually seeking and interacting with the silver nanoparticle surface.

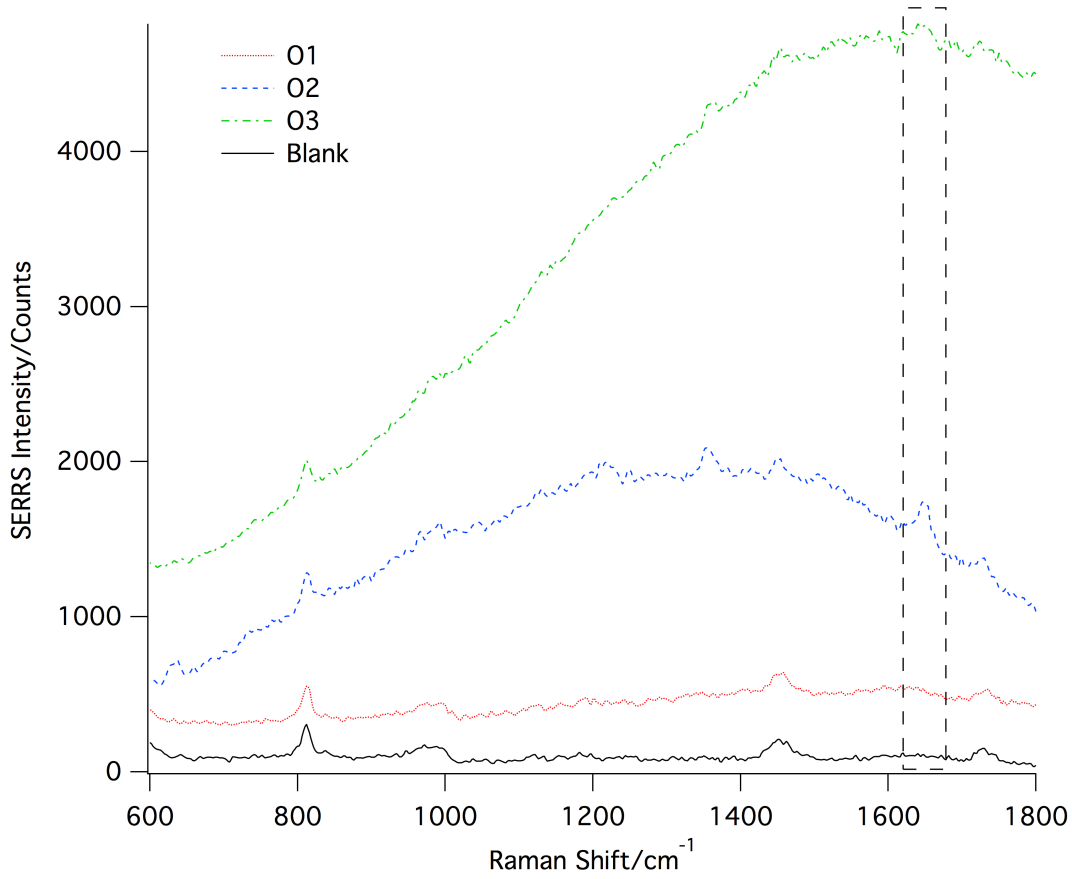

Figure 2-2 Monitoring the 1650 cm-1 peak of the three TAMRA-labelled oligonucleotide at 1 nM concentration after 24 hours of incubation with AgNP using a 532 nm excitation wavelength with 2 seconds exposure time and 5 accumulations. For visualization purposes the spectra were offset on the *Y*-axis.

When using dye-labelled oligonucleotides, the spectral features of DNA are often not observable. In an attempt to understand the interaction of the phosphorothioate-modified oligonucleotides with the AgNP label-free measurements were carried out

whereby the Raman signal originates from the nucleobases. More specifically to confirm that the phosphorothioate-modified oligonucleotides are attaching to the surface through the sulfur on the DNA backbone when spermine is used as an aggregating agent. Poly-adenine oligonucleotides modified analogously to the TAMRA-labelled oligonucleotides but without dye were used as shown below in table 2-2. Poly-adenine oligonucleotides were used as to facilitate the assignment of peaks. No dye was used, as its enhanced Raman spectra would overshadow the weaker peaks coming from the actual DNA hence the DNA itself is used directly in the analysis to understand the factors determining the observed signals.

Table 2-2 Poly-adenine oligonucleotide sequence

	oligonucleotide sequence
PA1	5'AAAAAAAAAAAAAAAAAAAA3'
PA2	5'A*A*A*A*A*A*A*A*A*A*A*A*A*A*A*A*A*A*A*A*A*A3'
PA3	5'A*A*A*A*A*A*A*A*A*A*AAAAAAAAAA3'

* is a phosphorothioate linkage

Figure 2-3 shows the SERS spectra of the thermally treated unmodified poly A and phosphorothioate modified poly A on AgNP aggregated with spermine. In all three spectra the in-plane ring breathing mode at approximately 736 cm^{-1} and the skeletal vibration modes in the 1200-1600 cm^{-1} range can be seen[135].

From the spectra obtained a 620 cm^{-1} peak which corresponds to the P-S vibration on to a metal surface[136] can be seen for the modified DNA (O2 & O3) (see figure 2-3). These preliminary results show that phosphorothioate oligonucleotides have an

affinity to the silver nanoparticle surface attaching themselves through the backbone. Therefore in theory an increase in the enhancement from the dyes is expected, as more DNA molecules would be found in SERRS hot spots. However this does not exclude strong non-specific interactions between the nucleobases and the metal surface[137]. Furthermore from the limit of detection studies carried out it is shown that oligonucleotide affinity when using spermine as aggregating agent is not the only factor that contributes to the detection but also the number and position of the modification and the interaction of the modified oligonucleotide with the aggregating agent.

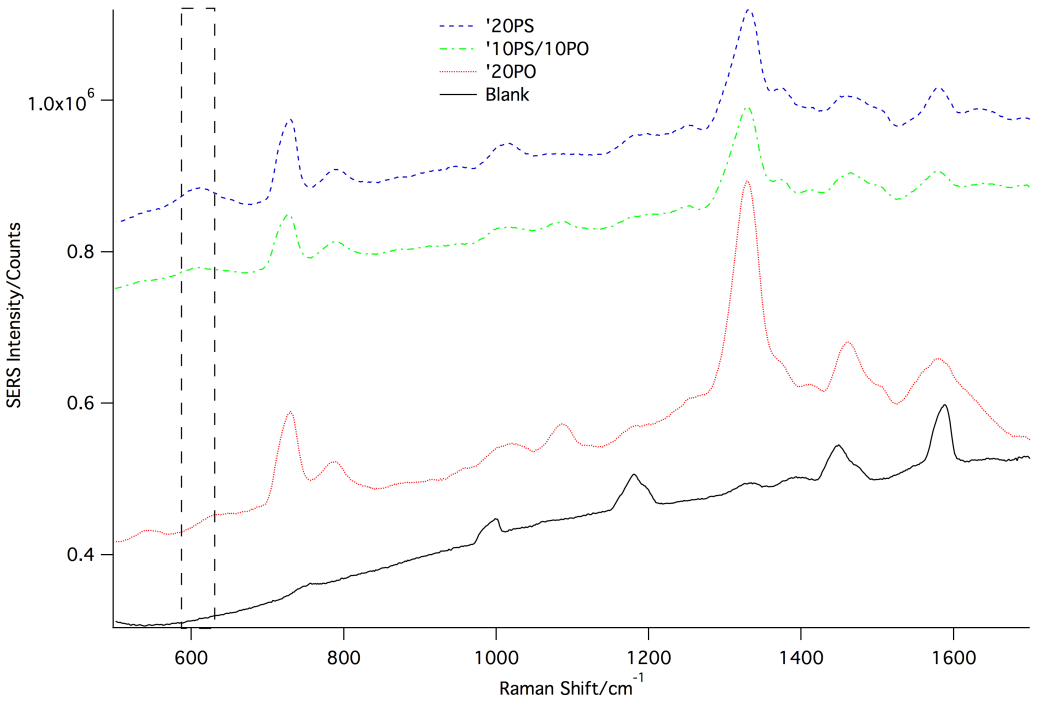

Figure 2-3 SERS spectra of 100nM poly-A oligonucleotides at 633 nm excitation wavelength (2 seconds exposure time and 5 accumulations) using 2.72 mM spermine as aggregating agent. Peaks at 620 cm^{-1} are present for poly-A phosphorothioate modified oligonucleotides (PA2 & PA3). For visualization purposes the spectra were offset on the *Y*-axis.

When using a 2.72 mM final spermine concentration the unmodified TAMRA-labelled oligonucleotide (O1) gives a limit-of-detection (LOD) of 1.1 x 10^{-12} M a whole order of magnitude lower to the modified ones (O2 & O3) (see figure 2-4 and table 2-3). This suggests that spermine interacts with the DNA to give a better detection limit when phosphodiester linkages are present since O2 gave the highest LOD and the peak intensity at 1650 cm^{-1} did not increase as concentration of DNA is increased as seen in figure 2-4.

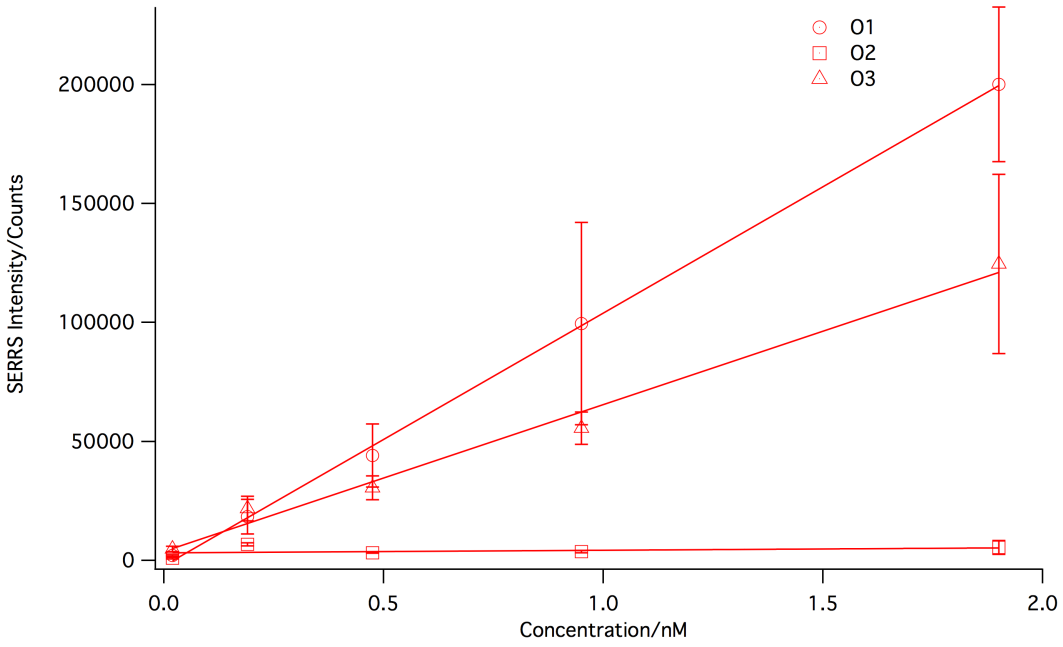

Figure 2-4 Concentration dependence of the signal graph obtained for the three different TAMRA-labelled oligonucleotides (O1, O2, & O3) using a final concentration of 2.72 mM spermine. Each point is the average of the main peak intensity (1650 cm^{-1}) of five repeat samples and the error bars are their corresponding standard deviation.

Table 2-3 Limit of detection of the 3' labelled oligonucleotides with different spermine concentrations

Oligonucleotide	2.72 mM Spermine LOD/mol dm^{-3}	0.27 mM Spermine LOD/mol dm^{-3}
O1	$1.1x10^{-12}$	$6.2x10^{-12}$
O2	$3.7x10^{-11}$	$4.1x10^{-11}$
O3	$3.0x10^{-11}$	$3.5x10^{-12}$

When the final spermine concentration is lowered to 0.27 mM the chimeric DNA (O3) now gives a better LOD of detection than the normal oligonucleotide showing that an appropriate balance between the affinity of the sulfur towards the surface and the spermine interaction with the DNA is found (figure 2-5). The fully modified DNA (O2) however still shows a high LOD of detection hence establishing that phosphodiester linkages need to be present when spermine is used as an aggregating agent (figure 2-5). Also the results show that when using spermine, modification of the DNA backbone does not give a better LOD unless spermine final concentrations lower than 2.72 mM are used.

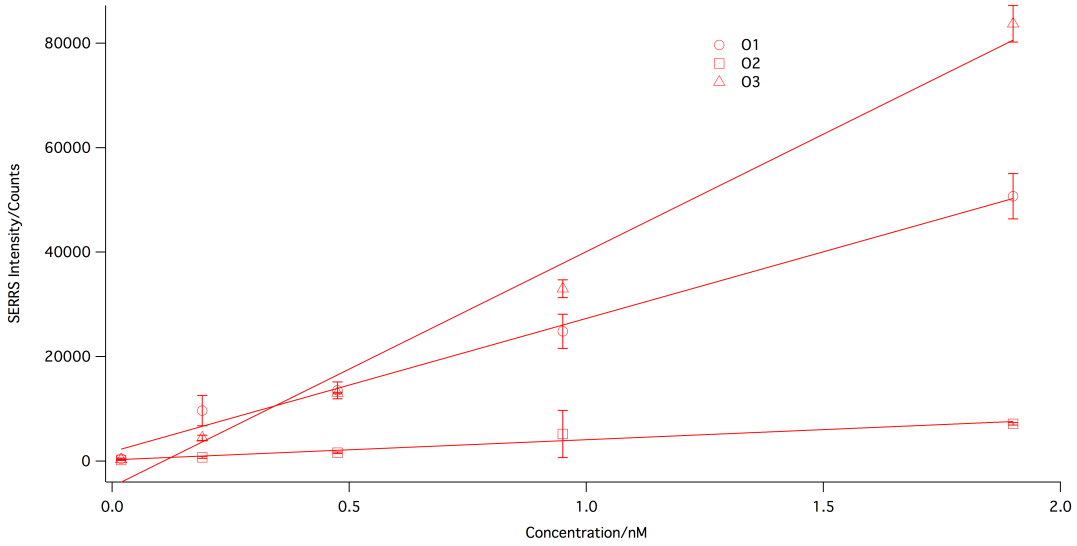

Figure 2-5 Concentration dependence of the signal graph obtained for the three different TAMRA-labelled oligonucleotides (O1, O2, & O3). An initial concentration of 0.27 mM spermine and a laser excitation wavelength of 532 nm. Each point is the average of the main peak intensity (1650 cm^{-1}) of five repeat samples and the error bars are their corresponding standard deviation.

Further experiments were carried out to show that the results obtained are due to the interaction of spermine with the modified phosphorothioate. The LOD for the three different oligonucleotides were repeated using the same procedure but instead using NaCl, KNO_3 and $MgSO_4$ as aggregating agents since they do not cause aggregation through the attachment of DNA to the silver surface but only act by reducing the surface charge on the colloid[75]. As can be seen from table 2-4 these inorganic ions give a better LOD when phosphorothioates are present, although they give a high LOD when compared to spermine.

Table 2-4 Limit of detection of the 3' labelled oligonucleotides with different inorganic salts

Oligonucleotide	NaCl LOD/mol dm^{-3}	KNO_3 LOD/mol dm^{-3}	$MgSO_4$ LOD/mol dm^{-3}
O1	$1.3x10^{-10}$	$8.9x10^{-10}$	$4.6x10^{-10}$
O2	$6.1x10^{-11}$	$4.9x10^{-10}$	$2.4x10^{-10}$
O3	$3.1x10^{-11}$	$4.4x10^{-10}$	$1.9x10^{-10}$

Any difference in LOD between the oligonucleotides can be attributed to the modification on the DNA. From the results obtained in figure 2-6 it shows that the modified DNA gives a lower LOD when compared to the unmodified DNA, showing that the affinity of phosphorothioate DNA in this case helps in the limit of detection. The chimeric DNA O3 gives a better LOD over all the three different inorganic salts. This can be attributed to the fact that its affinity (due to the presence of the phosphorothioate linkages) towards the silver surface is greater toward the 5' terminal half where the dye is. For O2 however there is no preference for the 5' or 3' terminal, unless the dye itself is directed away from the surface due to steric hindrance and/or better packing. It was also shown using poly-adenine oligonucleotides that the phosphorothioate DNA attaches via the backbone to the silver nanoparticle through the sulfur (see figure 2-7) when using NaCl as the aggregation agent, since a peak at 620 cm^{-1} was present only for the phosphorothioate-modified DNA. It is to note that a higher concentration of DNA was needed (1.9 μM) to obtain suitable spectra. When using spermine as an aggregating agent lower DNA concentrations were needed (100 nM).

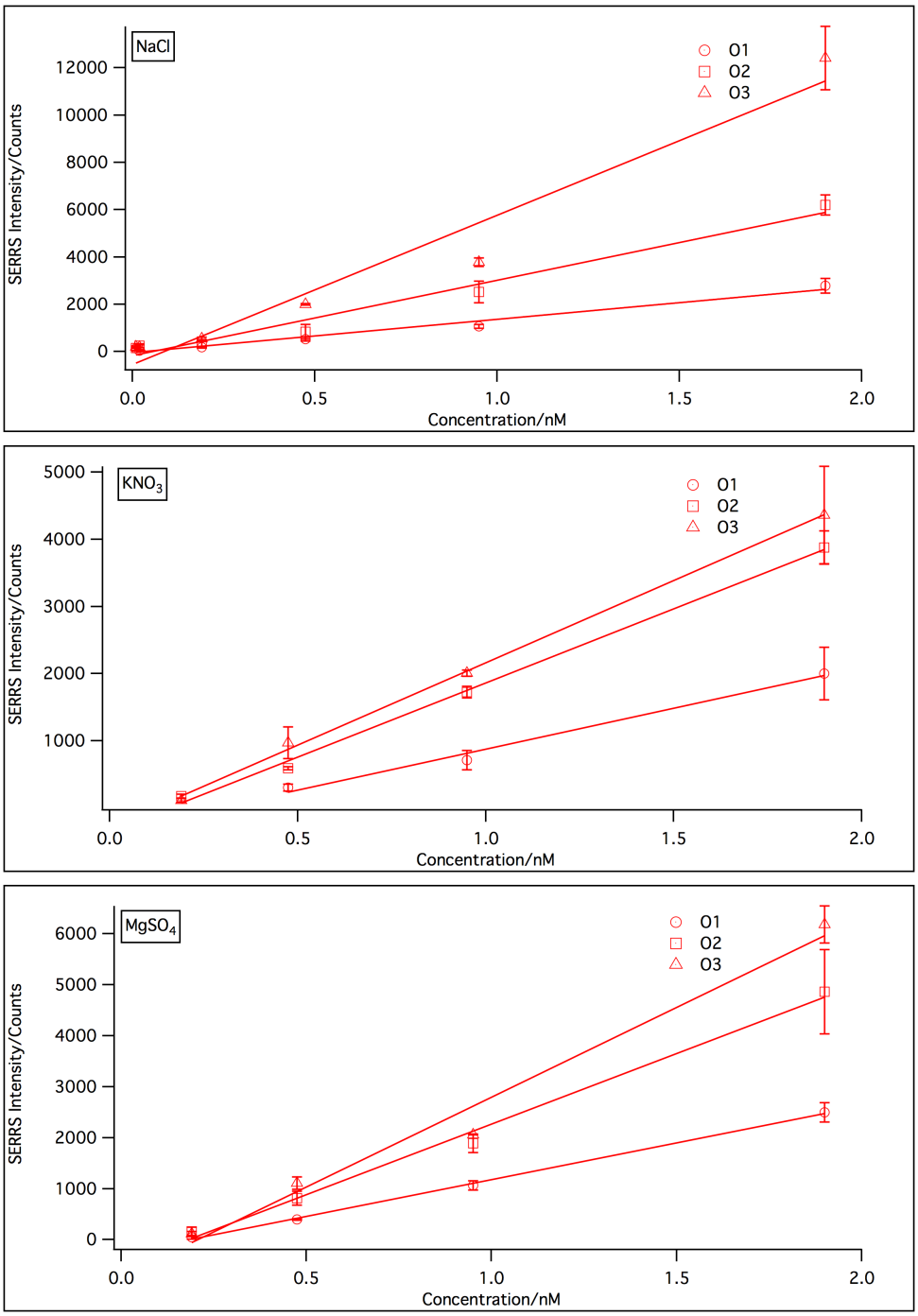

Figure 2-6 Concentration dependence of the signal graphs obtained for the three different TAMRA-labelled oligonucleotides (O1, O2, & O3). A final concentration of 54.5 mM inorganic salts (NaCl, KNO_3, & $MgSO_4$) as aggregating agent and a laser excitation wavelength of 532 nm. Each point is the average of the main peak intensity (1650 cm^{-1}) five repeat samples and the error bars are their corresponding standard deviation.

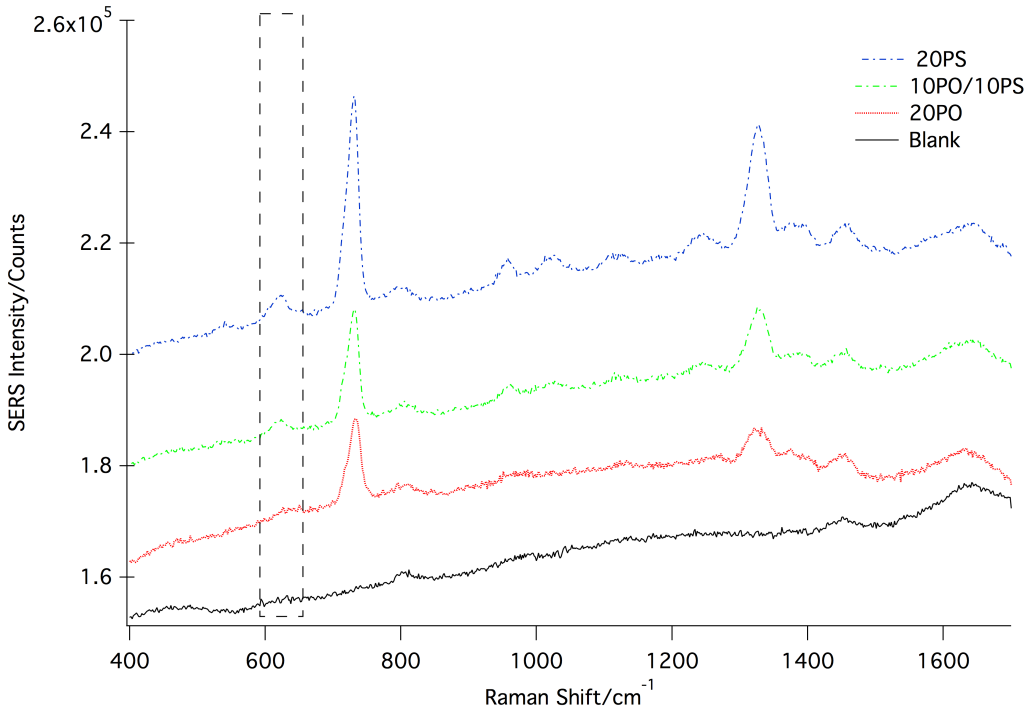

Figure 2-7 SERS spectra of 1.9µM poly-A oligonucleotides at 633 nm excitation wavelength (2 seconds exposure time and 5 accumulations) using 1% (w/v) NaCl as aggregating agent. Peaks at 620 cm^{-1} are present for poly-A phosphorothioate modified oligonucleotides (10PO/10PS & 20PS). For visualization purposes the spectra were offset on the *Y*-axis.

2.4 Conclusion

This chapter gives an insight on the effect of phosphorotioate modification on SERS intensity and limit of detection when using silver nanoparticles and different aggregating agents. From the experiments conducted, it was concluded that a decrease in spermine concentration decreases the SERS intensity for both modified and unmodified DNA. However the SERS signal (at 1650 cm^{-1}) from the oligonucleotide dye-label can still be detected for phosphorothioate modified DNA even when no aggregating agent is used, therefore confirming the increased affinity for the silver surface. SERS spectra have shown that the affinity was through the sulfur moiety present on the oligonucleotide backbone, since using poly-adenine

oligonucleotides the 620 cm^{-1} peaks characteristic of the P-S vibration on a metal surface can be seen. Furthermore it was concluded that O1 gives a better limit of detection than the modified oligonucleotides O2 and O3 (O1<O3<O2). However if the spermine concentration is decreased O3 has a lower limit of detection (O3<O1<O2). The differences in the LOD between the DNA used shows that spermine interacts differently with unmodified and phosphorothioate-modified oligonucleotides. This is in contrast to when inorganic salts were used as aggregating agent, were the modified oligonucleotides gave a better LOD (O3>O2>O1). From this one can conclude that spermine interacts with the phosphorothioate modified DNA, causing a decrease in affinity and therefore an increase in LOD. It also shows the importance of the positioning of the modifications, where a fully modified DNA has a higher LOD than that of the chimeric one. In the next chapter the study will thus be extended to modified-dsDNA as to see if it behaves in a similar fashion to ssDNA, to give a complete picture of the behaviour of phosphorothioates.

Chapter 3: SERS Response from Double Stranded Dye-Labelled Phosphorothioate Modified DNA

3.1 Introduction

Most of SERS DNA detection assays use ssDNA as the analyte. This stems from the high surface affinity for metallic surfaces[117,138]. As in the previous chapter the AgNP's are negatively charged, to which the ssDNA exposed bases facilitates absorption to its surface[139]. Other assays such as molecular beacons[30] and scorpion probes[140] will contain a mixture of both single and double stranded DNA as the detection of the target relies on a specific hybridisation event. Li and Rothberg[141] were the first to report a colourimetric method that discriminates between ssDNA and dsDNA.

ssDNA and dsDNA have different adsorptions to gold and silver nanoparticle surfaces. This difference has been implemented not only in colourimetric methods but also in fluorescence and SERS based DNA detection. The adsorption difference between the two stems from the different electrostatic properties which are intrinsic to their structure. The double-helix geometry of dsDNA has the negatively charged phosphate backbone on the outside and the bases on the inside. On the other hand ssDNA although still having a negatively charged backbone it has its bases exposed. Therefore gold and silver nanoparticles that are usually stabilised by adsorbed negative ions repel the charged phosphate backbone of dsDNA and thus won't adsorb. However the flexible ssDNA adsorbs to negatively charged nanoparticles by

attractive Van der Waals forces between the exposed bases and the nanoparticle surface.

In chapter two the qualitative and quantitative SERS detection of phosphorothioate-modified ssDNA was compared to unmodified ssDNA showing that spermine increases the LOD for phosphorothioate-modified oligonucleotides. In this chapter the study will be extend to dsDNA. ssDNA and dsDNA are compared using a combination of phosphorothioate-modified and unmodified dye-labelled oligonucleotide probes hybridized with their respective phosphorothioate and unmodified complements, in an attempt to shed light on the interaction of spermine with phosphorothioate-modified DNA.

3.2 Experimental

3.2.1 UV-Vis spectroscopy DNA melts

UV-Vis spectroscopy was used to monitor the thermodynamic and kinetic properties of the dye-labelled oligonucleotides in the presence of its complementary oligonucleotide sequence. UV-Vis spectroscopy was carried out on a Varian Cary 300 BIO spectrophotometer with a Peltier thermal control cycling between 10 ºC to 90 ºC with 1 ºC per minute increments. The UV absorbance was measured at 260 nm.

The DNA melts were prepared by adding 50 µL of dye-labelled oligonucleotide (10 µM) and 50 µL of complementary oligonucleotide (10 µM) and 400 µL of PBS (0.3 M, pH 7.3). After a baseline spectrum was gathered using blanks (100 µL H_2O and 400 µL PBS) the samples were placed in the multi-cell block Peltier and the UV

absorbance at 260 nm was measured every minute as the temperature cycled between 10 ºC and 90 ºC with 1 ºC per minute increment. Each cycle was repeated 6 times from which the average absorbance at each temperature was calculated. The absorbance at 260 nm was plotted against temperature. The 15 samples prepared comprised all combinations of dye-labelled oligonucleotides with complementary sequence. Control samples were also prepared whereby the dye-labelled oligonucleotide was added to a nonsense sequence or a diethylpyrocarbonate (DEPC) treated water.

3.2.2 Synthesis and characterisation of silver citrate reduced nanoparticles

3.2.2.1 Synthesis

All materials were purchased from Sigma-Aldrich and used without further purification unless otherwise stated. All water used was doubly distilled (18.2 *mΩ•cm*). All glassware was soaked in *aqua regia* for at leas two hours and rinsed with double distilled water.

The citrate reduced silver colloid preparation method used is a modification of the method reported by Lee and Meisel[67]. Water (500 mL) was heated up to 45 ºC in a three parallel-necked round bottom flask (1 L) and silver nitrate (90 mg in 10 mL H_2O) was added. The solution was heated up to 98 ºC and 1% w/v sodium citrate solution (10 mL) was added. The temperature was maintained at 98 ºC for 90 minutes with continuous stirring throughout the flask. The necks were covered with aluminium foil to prevent excessive water evaporation.

3.2.2.2 Characterisation

3.2.2.2.1 UV-Vis Spectroscopy

The extinction spectra of the silver colloid were recorded after preparation using a Varian Cary 300 Bio spectrophotometer over a wavelength range of 200-800 nm. The baseline was recorded using doubly distilled water and the samples were diluted accordingly to remain in the linear response of the spectrometer. The concentration was calculated by Beer-Lamberts' law whereby the extinction coefficient used was 2.87×10^{10} M^{-1} cm^{-1} for a colloid with a maximum extinction wavelength of 407 nm.

3.2.2.2.2 Dynamic light scattering and zeta-potential measurements

The size and zeta-potential of the AgNP was measured using a Malvern Zetasizer (Nano-ZS) instrument. The standards for size were Nanosphere size standards 20 nm (± 1.5 nm, Lot. 339300) and 40nm (±1.8 nm, Lot. 33306), while the standard for the zeta-potential used was zeta-potential transfer standard (-68mV ± 6.8mV, Batch No. 051001).

3.2.3 Surface enhanced Raman spectroscopy

SERS analysis was carried out to see the difference in SERS signal obtained from ssDNA vs. dsDNA and the effect of phosphorothioate modification. Briefly the samples were prepared by adding 50 µL of dye-labelled oligonucleotide sequence (524 nM) to 50 µL of complementary oligonucleotide sequence (524 nM) and 400 µL of PBS (0.3 M, pH 7.3). The samples were pre-hybridised for 10 minutes at 90 ºC and 10 minutes at 20 ºC using a thermocycler (Agilent MX3005P). After which 7 µL of the sample was added to 10 µL of spermine tetrahydrochloride (0.1 M), 175 µL of

DEPC treated water and 175 μL of silver nanoparticles (0.2 nM) and analysed after 10 minutes in a poly (methyl methacrylate) (PMMA) micro-cuvette. An Avalon probe system Ramanstation R3 equipped with an optical fibre probe with a 532 nm diode laser excitation and a power of approximately 24 mW at the sample. The exposure time was 2 seconds and 5 accumulations. Data analysis was carried out by monitoring the 1650 cm^{-1} peak of the fluorescent dye TAMRA after being normalised to a hexane standard. A control was analysed using nonsense oligonucleotide instead of the complementary DNA. All samples were analysed in triplicates.

3.3 Results and discussion

Each dye-labelled oligonucleotide (O1, O2 & O3, see table 3-1) used in the previous chapter were hybridised with its phosphodiester complement (C1) and three different phosphorothioate complements (C2-C4) as listed in table 3-2. The modified complementary sequences were; one with all phosphorothioate linkages (C2), and two chimeric ones (C3 & C4). For C3 the first ten linkages from the 5' side are phosphorothioate modified, while for C4 the first 10 linkages from the 3' side are phosphorothioated. A nonsense sequence (NS) was used as a control. The melting curves and SERS intensity of each DNA duplex combination between the TAMRA-labelled oligonucleotide and their complementary was obtained.

It is to note that the modified DNA used is not stereospecific, as stereospecific synthesis although can be done[142] is not convenient and is not adapted to the use of automated synthesisers that produce large quantities of DNA. The number of

different stereoisomers produced is 2^{n-1}, where n is the number of bases in the oligonucleotide. Just as an example for all-phosphorothioate modified dye-labelled oligonucleotide (O2) has theoretically 524288 different stereoisomers. As was recognised by Eckstein *et al.*[143] since each phosphorothioate linkage can occur as either Rp or Sp diastereomer, it gives rise to nuclease stability as hydrolytic enzymes accept only the Rp or Sp forms of phosphorothioate mononucleotides. The chiral phosphorous atom also enables the oligonucleotide to form duplexes with RNA of variable stability[144] and promote triplex stabilisation[145].

Table 3-1 Dye-labelled oligonucleotide sequence

	5'-dye label	oligonucleotide sequence
O1	TAMRA	5'GGTTCATATAGTTATAATAA3'
O2	TAMRA	5'*G*G*T*T*C*A*T*A*T*A*G*T*T*A*T*A*A*T*A*A3'
O3	TAMRA	5'*G*G*T*T*C*A*T*A*T*AGTTATAATAA3'

* is a phosphorothioate linkage

Table 3-2 Unmodified and modified complementary oligonucleotide sequence (C1-C4) and a nonsense oligonucleotide sequence (NS).

	oligonucleotide sequence
C1	5' TTATTATAACTATATGAACC3 '
C2	5' T*T*A*T*T*A*T*A*A*C*T*A*T*A*T*G*A*A*C*C 3'
C3	5' T*T*A*T*T*A*T*A*A*C*TATATGAACC 3'
C4	5' TTATTATAAC*T*A*T*A*T*G*A*A*C*C 3'
NS	5' GAAGCCTACGGACGAGCAAT 3'

* is a phosphorothioate linkage

As can be seen from the temperature melt graphs (see figure 3-1) the changes in absorbance are all comparable to the unmodified duplex and only the melting temperatures (T_M) are significantly reduced when a phosphorothioate modification is introduced in the target and/or the complement DNA strand. If the slopes in the temperature melts have been significantly broader it would have indicated formation of many hybrids of relatively unstable duplexes due to the stereoisomerism. As observed in other similar studies[146] our melting data indicates a well-behaved two state transition. The general trend that can be seen from T_M data obtained is that the more phosphorothioate linkages present the lower is the melting temperature. This lowering of T_M ranges from 49 ºC for the normal duplex with no modifications to 28 ºC for the fully phosphorothioated duplex. It seems that part of the reason of the lowering of melting temperatures of the duplex is due to the lack of stereoregularity.

However Clark *et al.*[147] through circular dichroism (CD) spectroscopy have shown that the CD spectra of a DNA duplex in which both strands contained phosphorothioate modifications differed markedly from the spectra of either the unmodified DNA duplex or the DNA duplex containing modification in only one strand. They justify the difference due to an increase flexibility of the phosphorothioate oligonucleotide allowing the more rigid unmodified oligonucleotide to determine the structure. Therefore when both strands are modified this leads to a different structure to those where an unmodified strand is present.

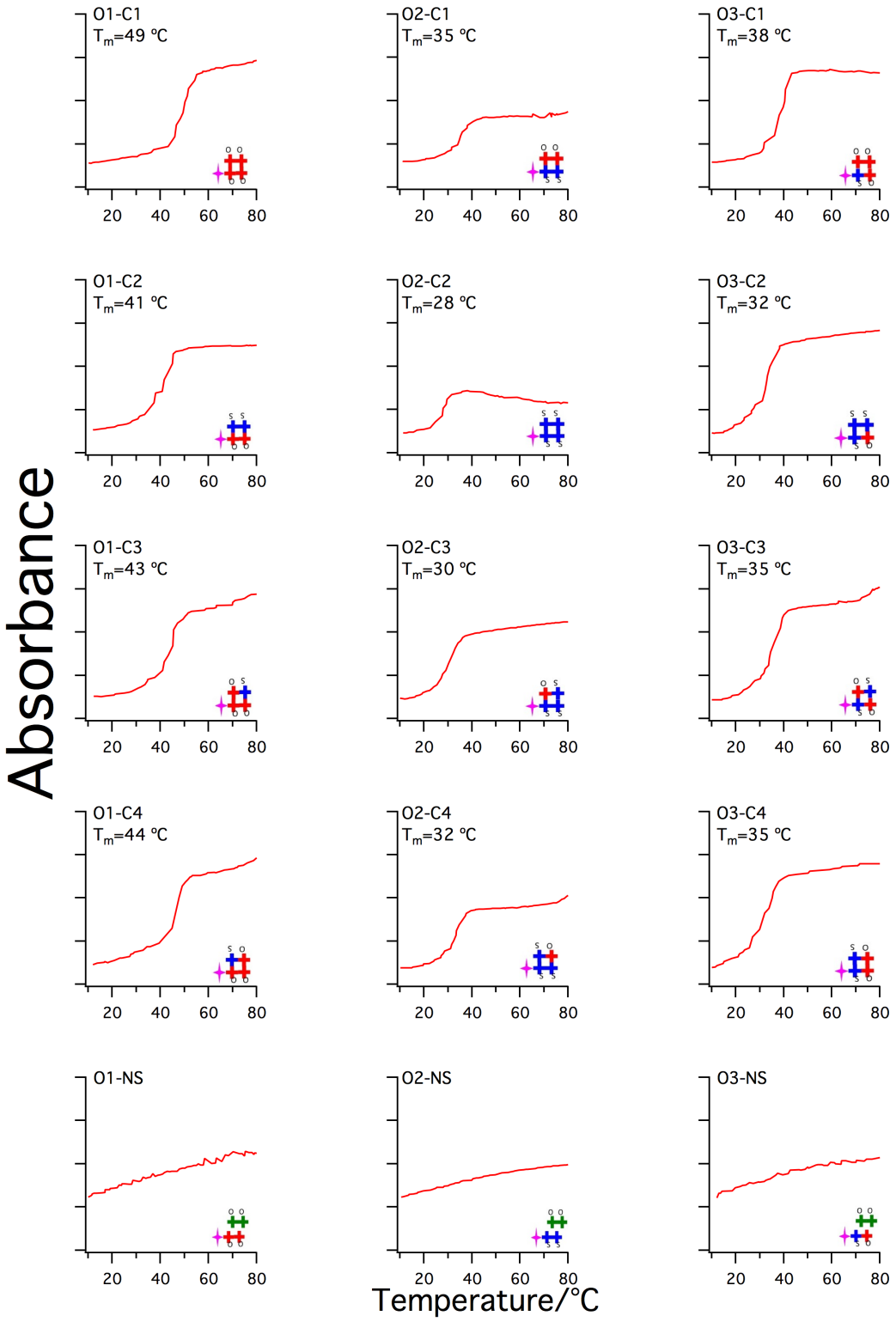

Figure 3-1Melting curves of O1, O2, O3 with C1, C2, C3, C4 and NS. Absorbance at 260 nm was measured every minute as the temperature cycled between 10 ºC and 90 ºC with 1 ºC per minute increment.

It is to note that a different study by Benimetskaya *et al.*[148] suggest an opposite view on the 'flexibility' of phosphorothioate-modified oligonucleotides. They suggest that phosphorothioate modified DNA is more rigid than unmodified ones as the bridging O-P-O angle is reduced with the introduction of sulfur, limiting the conformational entropy of the oligomer. However thermodynamic analysis[147] of modified and unmodified DNA duplexes show that the factor driving the reduction in T_M of the modified duplexes was a decrease in ΔS^o for formation of the complex, coinciding with the flexibility of phosphorothioates as supported by the CD spectra.

The focus of this chapter is to establish the differences in affinity of dye-labelled ssDNA, dsDNA with and without phosphorothioate modification. In the previous chapter it was shown that the chimeric and phosphorothioate-modified TAMRA-labelled oligonucleotide (ssDNA), disturbs the affinity to the AgNP surface and increases the LOD, when spermine is used as an aggregating agent. Therefore it is interesting to investigate the effect of phosphorothioate modification on the SERS detection of dsDNA. Assuming that the melting curves are indeed representing a two-state process, the experimental temperature used in the SERS analysis is below the lowest T_M of 28 ºC. Therefore more than half of the dsDNA has not dissociated. It also to note the addition of spermine which is part of the SERS analysis might increase the T_M as it is know that it further stabilises the DNA duplex[149].

Previous studies have shown that dsDNA give a lower SERS intensity signal compared to ssDNA and this difference was exploited to produce multiplexed SERS assay[150]. Furthermore Harper *et al.*[151] determined that surface attraction towards the AgNP surface of the oligonucleotide is driven through the constituent bases and

that TAMRA contributes minimally to surface adsorption. As seen from Figure 3-2 the unmodified TAMRA-labelled (O1) ssDNA as expected gave a higher intensity signal than the dsDNA. The more flexible ssDNA structure has its bases exposed which allows electrostatic attraction to the nanoparticle surface. On the other hand on the rigid and stable double helix the bases are not exposed and hence has lesser affinity to the surface. If the complement is all modified to phosphorothioate (C2) linkages the SERS intensity drops further more, however the presence of phosphodiester linkages in the chimeric complement sequences (C3-C4) have similar intensities to the unmodified complement (C1) (see Figure 3-2).

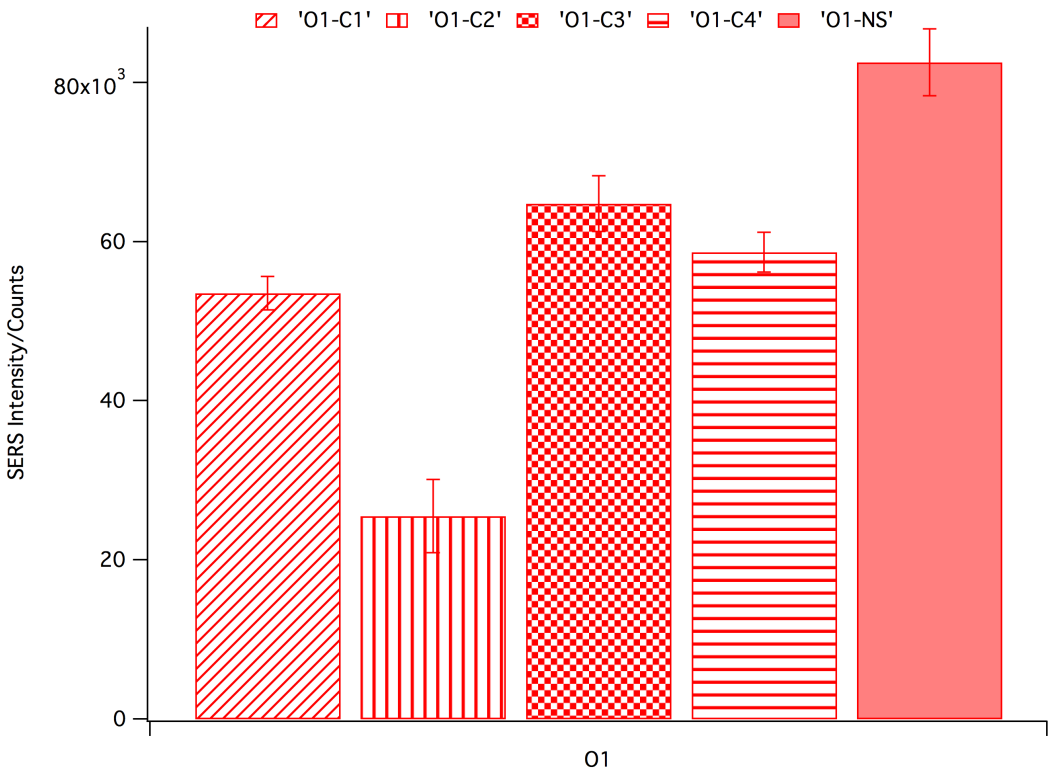

Figure 3-2 Comparison of SERS intensity for ssDNA (O1-NS) versus dsDNA (O1-C1, O1-C2, O1-C3 & O1-C4).

When the TAMRA-labelled oligonucleotide (O2) is fully modified the highest intensity signal is not given by the ssDNA but by dsDNA with an unmodified complement. If the complement is fully modified the intensity is comparable to that of the ssDNA. This shows that spermine is in fact ineffective in giving the DNA affinity to the silver nanoparticle surface if phosphodiester linkages are not present.

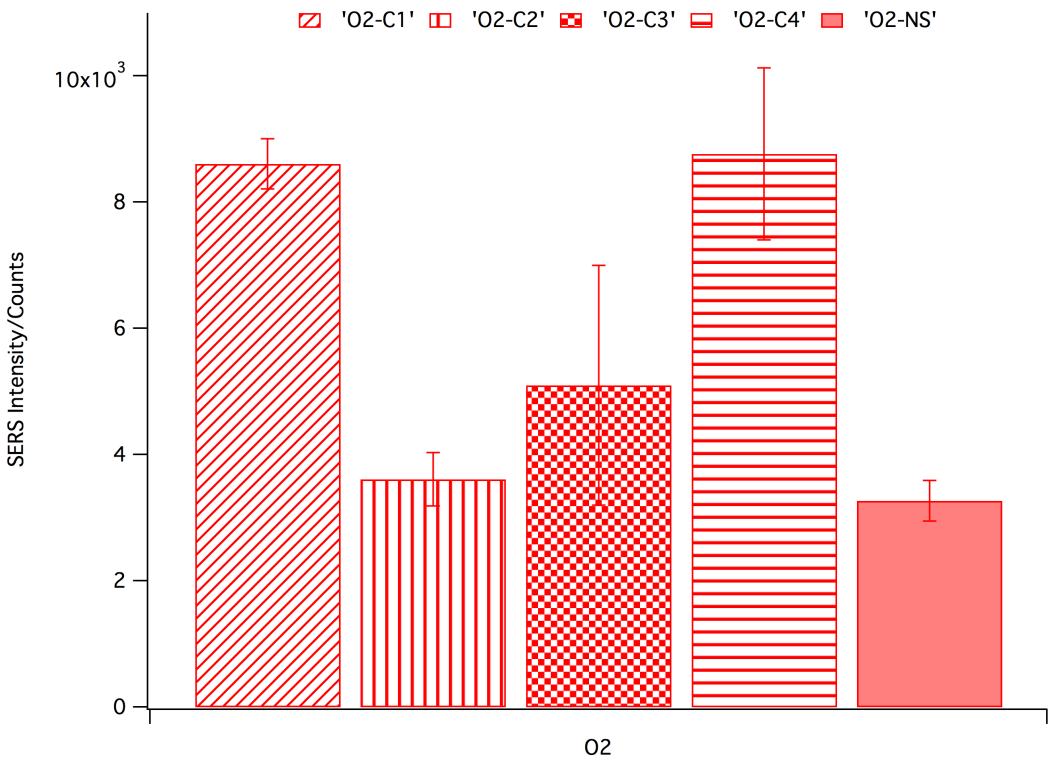

Figure 3-3 Comparison of SERS intensity for ssDNA (O2-NS) versus dsDNA (O2-C1, O2-C2, O2-C3 & O2-C4).

The chimeric dye-labelled oligonucleotide (O3) with a normal complement gives a higher SERS intensity than the ssDNA, however when more phosphorothioate linkages are present (C2, C3, C4) the intensity decreases and is less than the ssDNA. These results shows the importance of phosphodiester linkages if spermine is used as an aggregating agent.

These results show that there are differential effects of spermine with phosphodiester and phosphorothioate oligonucleotides. This could arise from the fact that Rp or Sp sulfur atom in a phosphorothioate linkage possesses a greater partial negative charge and increased polarisability relative to its oxygen (phosphodiester) counterpart[152]. This could affect the specificity of cations binding to these linkages.

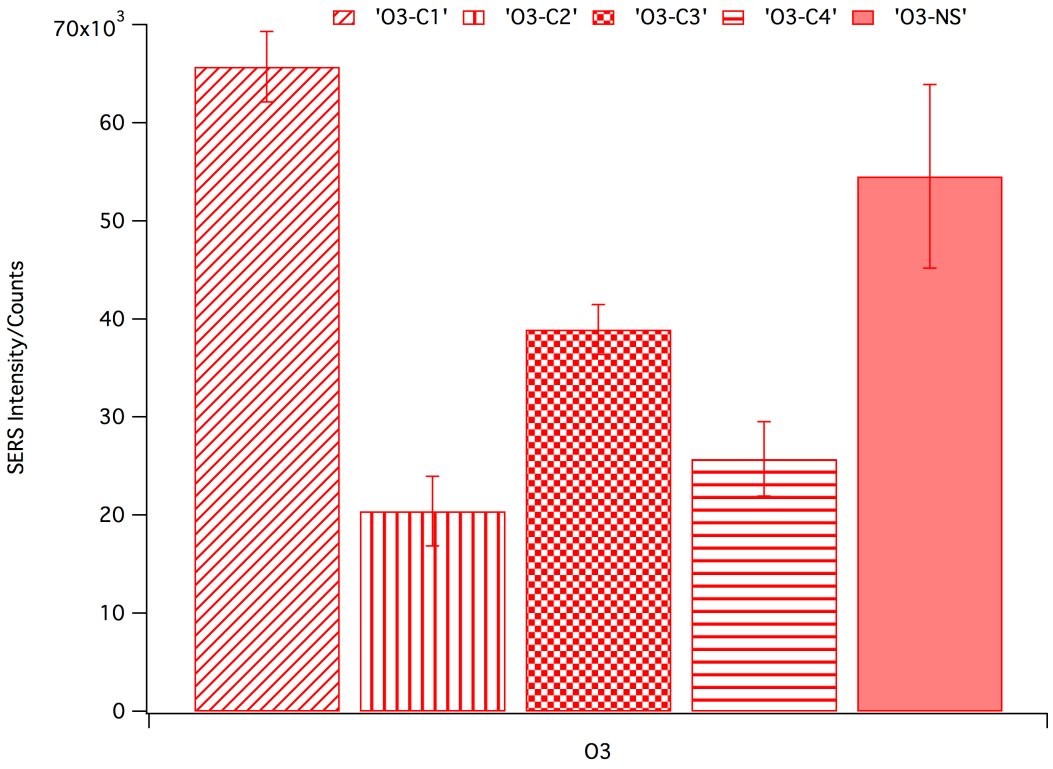

Figure 3-4 Comparison of SERS intensity for ssDNA (O3-NS) versus dsDNA (O3-C1, O3-C2, O3-C3 & O3-C4).

Differences in the interaction of polyamines with phosphorothioates compared to phosphodiesters has been observed in a study by Musso *et al.*[145] whereby an increased affinity was observed between polyamines and phosphorothioate-containing triplexes, however even with high-resolution NMR data it was insufficient to propose a mechanism for this difference.

3.4 Conclusion

In chapter 2 it was concluded that phosphorothioate modification increases the affinity of TAMRA –labelled ssDNA towards the AgNP surface. To profit from this increased affinity the aggregation agent used and its concentration has to be taken in consideration. In this chapter the study was extended to dsDNA, to better understand the effect of spermine on phosphorothioate modification dsDNA. Starting off with a melting curve study for the different combination of probe (O1, O2 & O3) and unlabelled compliments (C1, C2, C3 & C4) confirmed previous studies that phosphorothioate modification lowers the melting temperature which indicates a lack of stereoregularity and flexibility of the duplex. Previous studies have shown that unmodified dsDNA give a lower SERS intensity signal compared to unmodified ssDNA. The same trend was observed when using the unmodified O1 probe, that is the dsDNA gave a lower SERS intensity signal when compared to the ssDNA. It is to note however that the dsDNA with chimeric compliments (C3 & C4) gave a slightly higher signal than the unmodified compliment (C1) while the fully modified compliment C2, had a sharp decrease in SERS intensity compared to all the others. Going on to the O2 probe the importance of the presence phosphodiesters when spermine as an aggregating agent is used is shown. The O2 probe which is all phosphorothioate modified showed a different trend, whereby the dsDNA gave higher intensity than ssDNA. On gong to the O3 probe which is chimeric, the dsDNA with an unmodified compliment (O3-C1) gave a higher SERS intensity than the ssDNA (O3-NS) however when phosphorothioates compliments are present the dsDNA (O3-C2, O3-C3, and O3-C4) gave a lower SERS intensity than the ssDNA.

From this chapter one can conclude that spermine interacts with the phosphorothioate-modified oligonucleotides differently than it does with unmodified oligonucleotides. This interaction decreases the SERS intensity for phosphorothioate-modified DNA. More work needs to be done to understand the mechanism behind such a phenomenon. In the next chapters the effect of nanoparticle size will be investigated.

Chapter 4: A Preliminary Study on the Effect of Nanoparticle Size on SERS Enhancement.

4.1 Introduction

Inorganic nanoparticles are being used in an increasing amount of applications due to their properties such as photoluminescence (e.g. CdSe and CdTe), magnetic moment (e.g. iron oxide and cobalt), surface plasmon resonance absorption (e.g. silver and gold)[153,154]. The latter are finding huge potential in applications for sensitive optical diagnostic tools due to the high electron and strong optical absorption, which makes them ideal candidates as substrates for SERS. This spectroscopic method, the Raman signal of an analyte which is intrinsically weak can be enhanced when absorbed or in close proximity to a silver or gold nanoparticle surface. AgNP's were used in the first claims of single molecule detection both in colloid solutions[64] and on a planar substrate[65].

Since the surface plasmon resonance absorption is dependent on various factors such as the surface, the dielectric constant of the metal, the shape and the size of the particle, it is important to have a well-characterized substrate. This gives rise to the need of reproducible nanoparticle syntheses that produces, homogenous and monodispersed nanoparticles. There are various synthesis routes by which silver and gold nanoparticles[66] are obtained. While the preparation of spherical monodispersed gold nanoparticles are well characterized the preparation of AgNP's still seems to pose a challenge to produce spherical monodispersed nanoparticles which are suitable as SERS substrates. Most of these preparations result in polydispersed sols with different morphologies[2,67,77].

In this preliminary study 4 different sizes of nanoparticles were prepared. Citrate-reduced AgNP's were prepared and used as the smallest size and the 3 other larger sizes were prepared using a seeded growth method. Hydroxylamine hydrochloride was used as a reducing agent whereby silver is reduced onto AgNP seeds. The limit of detection using dye-labelled oligonucleotide probes was assessed for the four different sizes.

4.2 Experimental

4.2.1 Synthesis of Silver Colloid

4.2.1.1 General

All materials were purchased from Sigma-Aldrich and used without further purification unless otherwise stated. All water used was doubly distilled (18.2 *mΩ•cm*). All glassware was soaked in *aqua regia* for at leas two hours and rinsed with double distilled water.

4.2.1.2 Citrate reduced silver colloid (NP1)

The citrate reduced silver colloid preparation method used is a modification of the method reported by Lee and Meisel[67]. Water (500 mL) was heated up to 45 ºC in a three parallel-necked round bottom flask (1 L) and silver nitrate (90 mg in 10 mL H_2O) was added. The solution was heated up to 98 ºC and 1% w/v sodium citrate solution (10 mL) was added. The temperature was maintained at 98 ºC for 90 minutes with continuous stirring throughout the flask. The necks were covered with aluminium foil to prevent excessive water evaporation.

4.2.1.3 EDTA silver colloid preparation

The seed preparation method used is a modification of the method reported by Heard *et al.*[82]. Water (2 L) was heated up to 45 ºC in a beaker (3 L) and EDTA (94.7 mg) was added. The EDTA solution was then heat up to 98 ºC and sodium hydroxide solution (0.32 g in 20 mL H_2O) was added. The solution was brought to boil and 5 mL aliquots of silver nitrate (88 mg in 20 mL H_2O) were added consecutively. The solution was left boiling for 15 minutes with continuous stirring throughout the flask, after which it was left to cool to room temperature.

4.2.1.4 Silver colloid with controlled size ranges preparation

The different nanoparticle sizes were prepared using a modified version of the method reported by Lundahl *et al.*[81]. EDTA-reduced colloid (100 mL) as prepared in section 4.2.1.3 was diluted with water (100 mL) in a 3 parallel-necked round bottom flask (500 mL). Silver nitrate (0.5 mM) was added in varying amounts according to the desired nanoparticle diameter; 20 mL for NP2, 30 mL for NP3, and 200 mL for NP4. To each preparation 0.1% w/v hydroxylamine hydrochloride was then added drop wise until the nanoparticle solution started to scatter light strongly and took a red-brown colour. The solution was then heated to around 80 ºC and kept at that temperature for 10 minutes. This was followed by 1% w/v sodium citrate solution (10 mL) being added to the solution and allowed to cool to room temperature.

4.2.2 Silver colloid characterisation

4.2.2.1 UV/Vis spectroscopy

The extinction spectra of each silver colloid batch was recorded after preparation using a Varian Cary 300 Bio spectrophotometer. The samples were diluted accordingly if they were too concentrated. The concentration of each nanoparticle batch was calculated using the extinction coefficients for each different size presented by Yguerabide *et al.*[155].

4.2.2.2 Zeta-Potential

The ζ-potential of each batch prepared was measured using a Malvern Zetasier model 2000 (Worcestershire, U.K.). The standard used was zeta-potential transfer standard (-68 mV ± 6.8 mV) Batch No. 051001 (Malvern Instruments, U.K.)

4.2.2.3 Particle size measurements

4.2.2.3.1 DLS

The particle size distribution of each batch prepared was measured using a Malvern High Performance Particle Sizer (HPPS) model HPP5002 (Worcestershire, U.K.). The standards used were:

- Nanosphere size standards 40 nm nominal diameter (Polymer microspheres in H_2O, 40 nm ±1.8 nm) Lot. 33306 (Duke Scientific Corp. Palo Alto, CA, U.S.A.).

- Nanosphere size standards 20 nm nominal diameter (Polymer microspheres in H_2O, 21 nm ±1.5 nm) Lot. 33306 (Duke Scientific Corp. Palo Alto, CA, U.S.A.).

4.2.2.3.2 DCS

The particle size distribution of each batch prepared was measured using a CPS Disc Centrifuge model DC24000. The DCS was calibrated using a calibration standard (NIST traceable monodispersed polystyrene beads) of known size (0.377 μm) and density (1.385 g mL^{-1}). The samples were run at 24000 RPM. The particle density for silver nanoparticles was set as 10.5 g mL^{-1} and fluid density of 1.064 g mL^{-1}.

4.2.2.4 Microscopy

A sample from each batch of colloid prepared (NP1, NP2, NP3 & NP4) was dried on silicon wafer. Using a SEM (FEI Sirion 200 ultra-high-resolution Schottky Field emission gun), four 'snapshot' images were taken for each sample. From the images obtained the diameter was calculated using Image J[156], an image process and analysis software. An automated method was used to measure the particles with the following parameters in place:

- Particles must have a range between 10 nm – 100 nm
- Circularity of particles must be around 0.8 – 1, where circularity is defined as:

$$\boldsymbol{Circularity = 4\pi(Area/Perimeter^2)}$$

Equation 4-1

Before the particles were measured the images were converted to grey scale 8-bit images, enhanced by binary contrast enhancement (thresholding) and the scale was calibrated with the SEM image scale bar.

4.2.3 Quantitative Enhanced Raman Scattering of Labelled DNA

4.2.3.1 General

All materials were purchased from Sigma-Aldrich and used without further purification unless otherwise stated. All water used was double distilled (18.2 mΩ•cm).

4.2.3.2 Dye-labelled oligonucleotides

The dye-labelled oligonucleotide sequences used in this method are detailed in table 4-1. Dye-labelled oligonucleotides were purchased from MWG Biotech. The concentration of each dye was calculated before analysis using the Beer-Lambert law.

Table 4-1: Dye-labelled oligonucleotides used in this method

Dye label	λ_{max}	Oligonucleotide sequence
HEX	535 nm	5'TACGCAGTCGTA3'
Cy3.5	581 nm	5'CAGTGCTACTGA3'
Cy5	643 nm	5'GCTATCAGTCAG3'

4.2.3.3 Sample preparation and analysis

The sample preparation method used is a modification of the method reported by Stokes *et al.*[157], whereby each dye-labelled oligonucleotide was diluted with water to 8 stock solutions (50 μL) in the range of 52 to 525 nM, as to give a final dye concentration range of 1 to 10 nM. Samples were then prepared for SERRS analysis by adding the dye-labelled oligonucleotide (7 μL) and spermine solution (10 μL, 0.1 mol dm^{-3}) followed by sterile water (175 μL, 18.2 mΩ•cm) and silver colloid (175 μL, 0.2 nmol dm^{-3}). The samples were analysed within 60 s of the addition of the silver colloid and each concentration was analysed five times. A blank solution (i.e. without dye-labelled oligonucleotide) was recorded before each sample. The spectra were obtained with the spectrometer grating centred at 1500 cm^{-1} and integrating for 3 s. The spectra were baseline corrected using the GRAMS/32 software, and the average peak height of the strongest peak in the spectra was plotted (HEX, 1635 cm^{-1}; Cy3.5, 1279 cm^{-1}; Cy5 1468 cm^{-1}) against the concentration after being normalised to a silicon standard. This procedure was repeated for each silver nanoparticle size and dye-labelled oligonucleotide.

4.2.3.4 Instrumentation

The spectra were recorded at 514.5 nm laser excitation wavelength in a confocal arrangement. A Leica DM/LM microscope equipped with an Olympus 20x/0.4 long-working-distance objective was used to collect 180º backscattered light from a standard microtiter plate. The spectrometer system was a Renishaw inVia (Gloucestershire, U.K.) with an Ar^{+} Spectra Physics laser as the excitation source. The power output was measured to be approximately 6 mW at the sample. Dielectric

edge filters were used to reject Rayleigh scattered light. The detector used was a deep-depletion RenCAM charge-coupled device (CCD). Signal intensities were normalised to silicon standards throughout all experiments. The LOD was calculated by equation 4-2

$$LOD = \frac{\chi_{BL}+3\sigma_{BL}}{m} \qquad \textbf{Equation 4-2}$$

where χ_{BL} is the mean of the blank sample measurements, σ_{BL} is the standard deviation of the blank sample baseline and *m* is the gradient of the calibration line.

4.3 Results and Discussion

4.3.1 Nanoparticle characterisation

Various commercially available gold nanoparticles with different sizes are found and commonly used as SERS substrates since they are well characterised, as shown by the number of articles in literature that deal with controlled synthesis of gold nanoparticles of different size[158,159]. On the other hand silver nanoparticles are less well characterised, and the common methods used of citrate reduction[67] and borohydride reduction[2] give polydispersed colloid with a variety of shapes, with the latter giving an unstable suspension. In this chapter silver nanoparticles are used as to shed more light on the properties of such substrate, since silver nanoparticles are ideal candidate for SERS based applications as they have a stronger optical response and a narrower surface plasmon resonance (SPR) when compared with gold nanoparticles[155,160-162]. The wavelength used as the excitation source for SERS and SPR is in the range of 450 nm to 650 nm, for which the ideal size of the particle

would be around 60 nm. This size is ideal as it minimises collision with particle surface boundary (smaller sizes) and retardation effects (larger sizes)[160].

In this preliminary study four different sizes of silver nanoparticles were produced to test the effect of nanoparticle size would have on the SERS response when detecting dye-labelled oligonucleotides. The silver nanoparticles were prepared as described in section 4.2.1. The smallest nanoparticle size NP1 was prepared using a modified version of Lee and Meisel[67] as described by Munro *et al.*[75] which gives a monodispersed colloid of around 27 nm. The other larges sized nanoparticles (NP2, NP3 & NP4) were prepared by the method reported by Lundahl *et al.*[81] to give particles of 50, 60 and 80 nm respectively. The method involves seeded growth from smaller EDTA-reduced nanoparticles[82], using hydroxylamine hydrochloride as a reducing agent.

The samples were first characterised by UV/Vis spectroscopy which gives an indication if the colloid produced has the right characteristics of a monodispersed silver nanoparticle colloid. The extinction spectra obtained were normalised and the results plotted against each other as seen in figure 4-1. It can be clearly seen that as one goes from NP1 to NP4 that there is a broadening of the spectra.

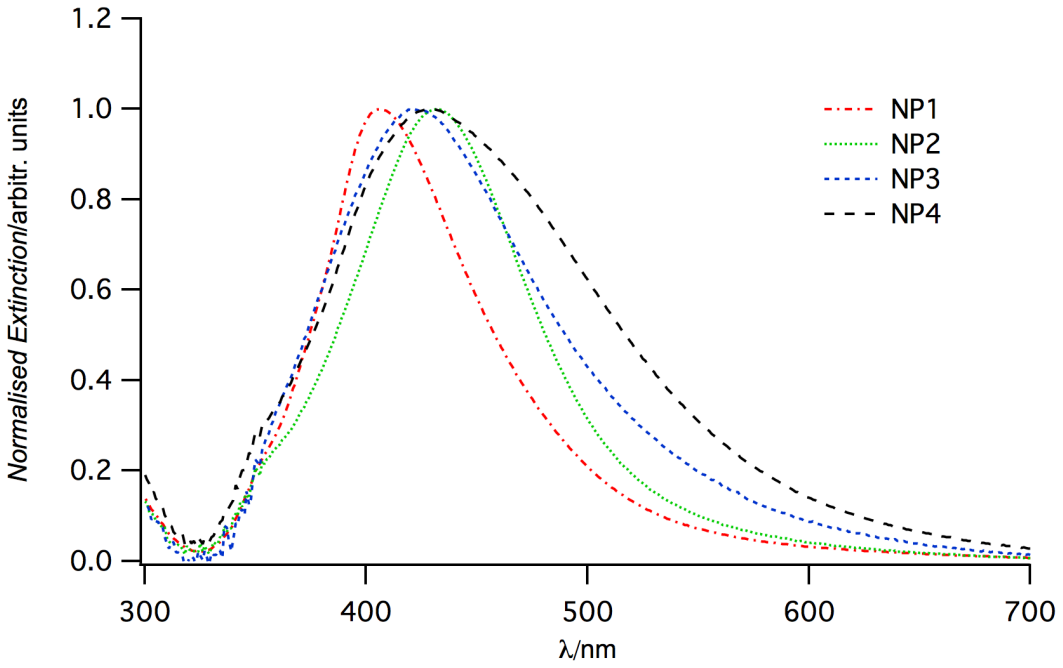

Figure 4-1 Extinction spectra of different silver nanoparticle diameters

This broadening effect can be attributed either to an increase in polydispersity as size is increased or else may be due to additional multipolar resonances superimposed onto the red-shifted single (dipolar) plasmon resonance. The red-shift as one moves from NP1 to NP4 clear shows that the diameter of the nanoparticles is increasing, however NP2 is more red-shifted than NP3 which was not expected. Also NP2 and NP4 have the same maximum absorbance wavelength at 431 nm. Further characterisation is needed to have a clearer picture of the nanoparticles produced. In table 4-2 the maximum absorbance wavelength and the absorbance are listed, including the data obtained from the 'seed' which batches NP2, NP3 & NP4 were grown from. Apart from the increase in the maximum absorbance wavelength when the batches are compared to the 'seed', the extinction spectra show as expected a lower particle concentration than the original EDTA-reduced nanoparticle solution, since the absorbance gets significantly lower (molar extinction coefficient increases

with particle size). The optical response of the batches is comparable to perfect spheres[160,163,164].

Table 4-2 Surface plasmon maximum and corresponding absorbance of the silver nanoparticles prepared

Preparation	Surface Plasmon Max./nm	Absorbance/arbit. units
NP1	407	1.990
Seed	423	0.666
NP2	431	0.646
NP3	428	0.468
NP4	431	0.315

The spherical shape of the nanoparticles can be confirmed by the SEM images taken (see figure 4-2). Four 'snapshots' of each batch were taken by SEM and the images in figure 4-2 are a representation of what is seen throughout. Important to note is that no rod shaped particles were found in the images, neither pronounced surface features or truncated shapes.

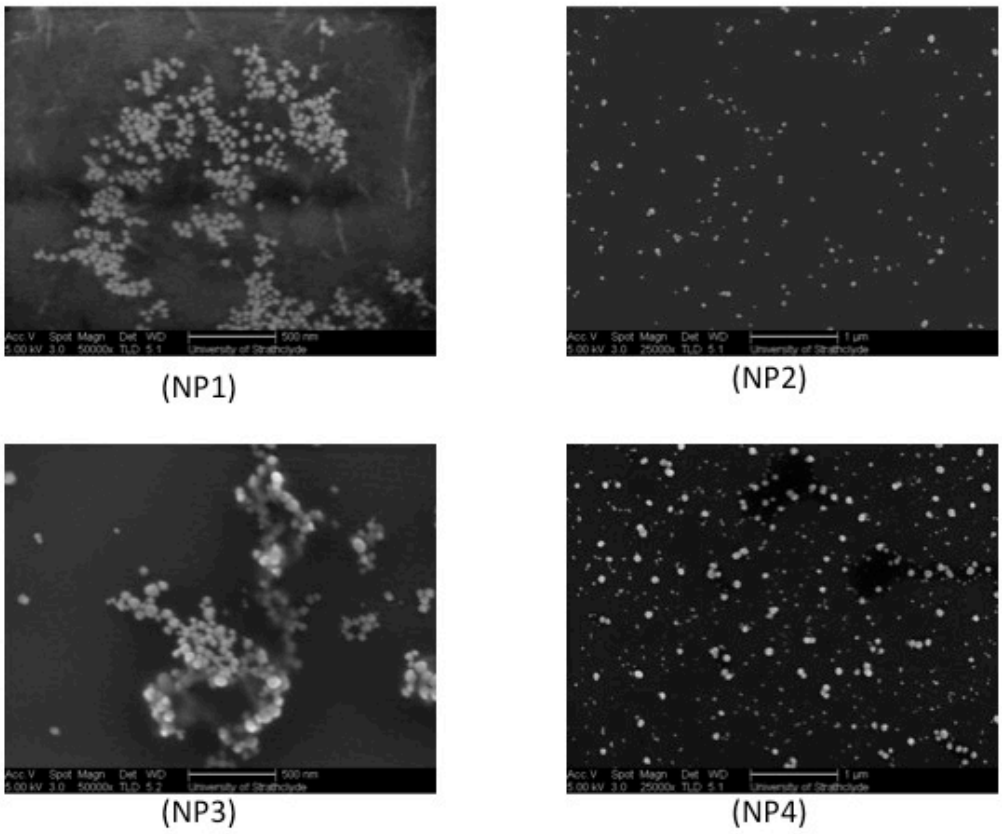

Figure 4-2 SEM images of the silver nanoparticles obtained from preparation 1 to 4. The particles were dried onto a silicon wafer. Note that images have different scale.

Table 4-3 shows the dimensions obtained when the particle images were measured through the Image J software. It shows that a gradual increase in size did occur for NP2, NP3, & NP4 and that the method through which NP1 was synthesised produced smaller particles than the unmodified version of the Lee and Meisel method[[67]. It must be remarked though that NP4 has a lot of small size nanoparticles. These can be attributed to the formation of new nucleation sites when the silver nitrate to seed ratio is increased hence the formation of new particles is inevitable. Further characterisation techniques were performed as to ascertain that analysis method used in Image J is effective and that the particles made are stable.

Table 4-3 Average silver nanoparticle diameters measured by Image J

Preparation	No. of particles measured	Average diameter/nm
NP1	244	33
NP2	530	45
NP3	69	55
NP4	231	70

Since the SEM images show that the particles are spherical (have a low aspect ratio) they could be measured with DLS and DCS with no additional manipulation of data to account for a non-spherical shape. The size results obtained by DLS are tabulated in table 4-4.

Table 4-4 Data from DLS for each preparation

Preparation	Z-Average/nm	Peak 1 Mean/nm	Peak 2 Mean/nm	PDI
NP1	59.8	86.6	18.5	0.266
Seed	42.7	49.6		0.111
NP2	45.3	55.2		0.135
NP3	54.4	69.6		0.168
NP4	59.3	79		0.189

The results show the Z-average size (also known as the cumulants mean), the peak modes by intensity and the polydispersity index (PDI). The seed produced by EDTA-reduction of silver nitrate gave a low PDI and small particles of around 40 nm as expected from such method. The batches grown from the EDTA-reduced seed (NP2, NP3 & NP4) are all larger then the seed and both Z-average and peak mode mean increase progressively as expected. The PDI is fairly low and thus indicates that the

colloids are monodispersed, however it seems that it increases with growth size. A thing to keep in mind with this technique is that larger particles may ‘hide’ smaller particles and thus are not represented in the result. A point in case is NP4 were from SEM images a large population of small particles were seen however are not represented in the DLS results. The results obtained for NP1 are ambiguous as the Z-average is higher that that for the supposedly larger NP4 particles and two peaks were found in the peak modes results that show two distinct populations, and a high PDI. These results do not reflect the SEM images obtained for the NP1. The DLS results of NP1 do not match with other characterisation techniques may be a result of the small particle size and thus factors such as Brownian motion effect the results output.

The DCS results shown in table 4-5 and figure 4-3 show that NP1, NP2 and NP3 are monodispersed, but as size is increased the peaks become broader. On the other hand, as also confirmed by the SEM images, NP4 is not monodispersed but has distinct population of large particles and a smaller population of smaller particles as seen in table 4-5 and figure 4-3. It should be noted that NP3 are not larger than NP2 as expected and this can be attributed to a larger distribution of particles. The overlay in figure 4-4 shows clearly that different sizes have been obtained (NP3 omitted). The DCS diameter values shall from now on be used in the discussion if not stated otherwise.

Table 4-5 DCS data for each preparation

Preparation	Peak 1/nm	Peak Half Width	Peak 2/nm	Peak 3/nm
NP1	44	0.0109		
NP2	53	0.0139		
NP3	45	0.0273		
NP4	70	0.0239	31	26

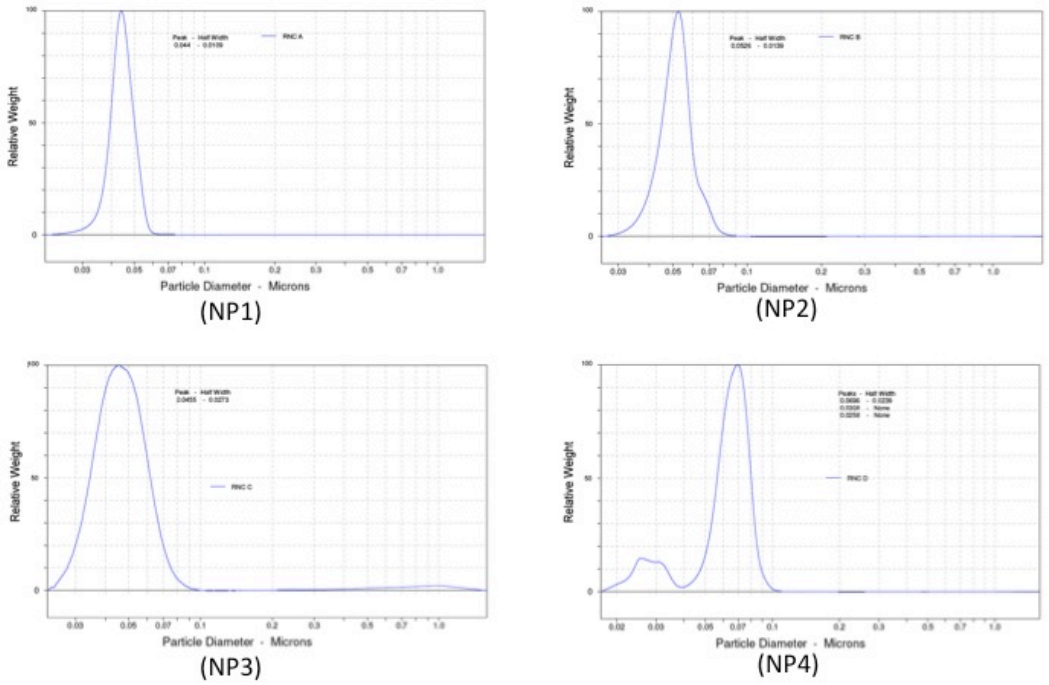

Figure 4-3 Particle sizing graphs from DCS for each preparation

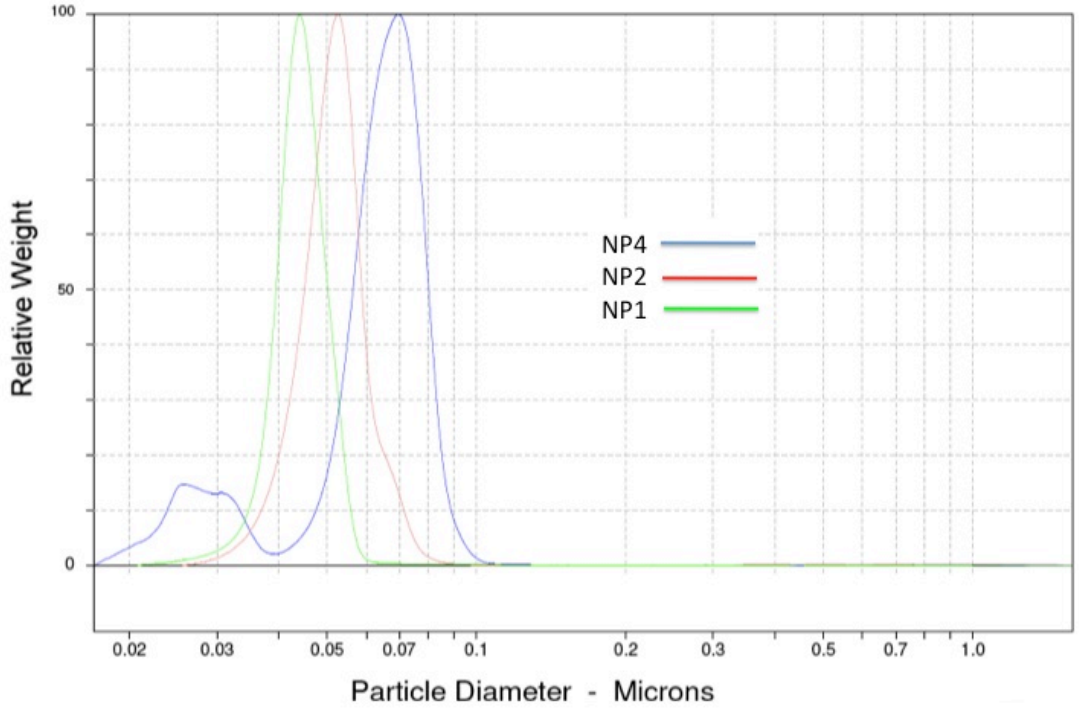

Figure 4-4 Overlay of particle sizing graphs of NP1, NP2, & NP4 from DCS

The ζ-potential of the seed (EDTA-reduced) and the four samples were recorded and tabulated in table 4-6. As expected all colloid solutions gave a high negative ζ-potential hence they are stable in solution. The citrate used to stabilise the nanoparticles (NP1, NP2, NP3 & NP4) gives adequate monolayer coverage at the surface, giving a negative charge to the silver nanoparticles (see table 4-6), as proposed by Munro *et al.*[75].

Table 4-6 ζ-potential for each preparation made.

Preparation	Average ζ-potential/mV	Standard deviation/mV
NP1	-49.8	±2.7
Seed	-44.7	±1.5
NP2	-50.1	±15.1
NP3	-46.7	±1.3
NP4	-58.2	±1.6

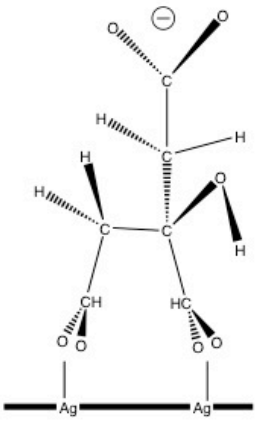

Figure 4-5 Proposed model of interaction and orientation of citrate at colloid surface. Figure adapted from Munro *et al.*[75].

4.3.2 Effect of nanoparticle size on the SERRS response

The method used to investigate the effect of nanoparticle size on the SERRS response combines the SERS from the silver nanoparticles prepared in section 4.2.1 and resonance Raman scattering from the dyes attached to the oligonucleotides. The dyes are fluorescent probes whose fluorescence signal is largely quenched by direct contact or close proximity to the silver metal. This composite technique is very

powerful and has reportedly achieved single-molecule detection[64,65,102,165]. Even if SERS spectra give narrow spectral lines ideal for multiplexed analysis[166], such a method can be further optimised for better multiplexing as SERRS spectra are simpler than SERS as only selected vibronic states are enhanced, giving the possibility to adopt this technique to real biological systems where only narrow SERRS peaks that conform to Raman resonance and surface selection rules would be observed.

The dye-labelled oligonucleotide sequences used in this study are listed in table 4-1 and the structures of the modified dyes are represented in figure 4-6. A terminal NH_2 was added to allow further modification with alternative groups or for conjugation purposes if the need arises in future work. Previous studies have already confirmed that SERRS yields a significant increase in sensitivity than fluorescence when dye-labelled oligonucleotides are analysed[115]. The dyes used (HEX, Cy3.5 and Cy5) are common fluorescent dyes and their use for quantitative oligonucleotide detection by SERRS have been already demonstrated by Faulds *et al.*[116,118].

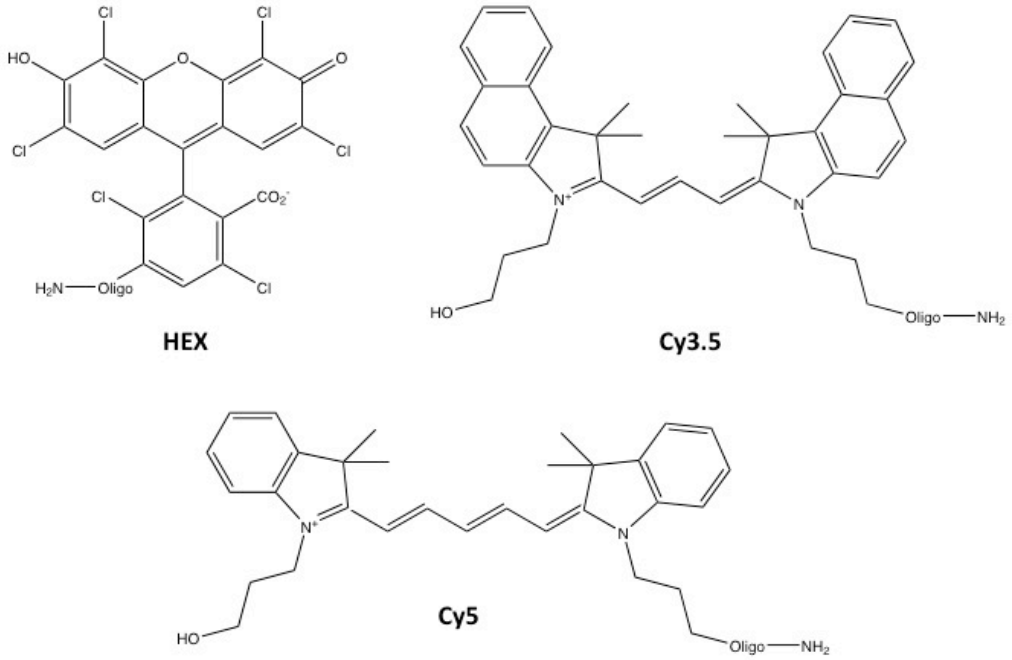

Figure 4-6 Structures of dyes used for the labelling of the oligonucleotides.

Faulds *et al.*[116,118] demonstrated that oligonucleotides labelled with dyes that have a negative charge perform better in SERRS if the oligonucleotide sequence is modified with 5-propargylamine-2'-deoxyuridine. This modification gives the oligonucleotide a positive charge once the spermine is added, facilitating its attraction to the negative surface of the silver nanoparticle[75]. If the dye has an overall neutral or positive charge then these modifications are not necessary although sensitivity could be increased if using them. Cy3.5 and Cy5 used in this experiment are positively charged while HEX is negatively charged. The oligonucleotide sequences attached to the dye were used as purchased without any internal modifications. SERRS spectra could still be obtained from them when added to the silver nanoparticles. This could

be due to the NH_2 terminal found at the 3' end of the sequence, which is positively charged and helps in the attraction towards the silver nanoparticle surface.

As in previous studies[115-118] the same conditions were used for SERRS analysis whereby a 514.5 nm source was used and the silver nanoparticles were aggregated. In these experiments a fibre-probe system was used and the laser beam was focused into a cuvette. In this method a setup as described by Stokes *et al.*[157] was used where the limit of detection for the different dyes with the four sizes of silver nanoparticles were obtained within a small volume of a microtitre plate using spermine as an aggregating agent. The laser beam was focused on the air/water interface and a more suitable 180º backscattered Raman light was used. This eliminates the need for the light to travel through the highly absorbing nanoparticle solution, thus increasing sensitivity.

Aggregation is important to have good SERRS results as it promotes a larger local electric field. For DNA analysis the tetramine spermine is used as it not only aggregates the nanoparticle by reducing the surface charge but it also neutralises the negatively charged phosphate backbone of the oligonucleotides when added before the nanoparticles. This improves the surface interaction and hence the SERRS sensitivity. For this set of analyses the spectra were taken at about 40 to 60 seconds after the addition of nanoparticles to the oligonucleotide/spermine sample. If left longer the aggregates might grow to larger clusters and the resonance is likely to become multipolar and thus the dipolar resonance required by SERRS is lost[157].

The three dye-labelled oligonucleotides were analysed in conjunction with the four different sizes of silver nanoparticles have a limit of detection lower than the base

concentration of each dye which is $1x10^{-8}$ mol dm^{-3} (see table 4-7). This confirms that the dyes used were in close proximity of the nanoparticles or adsorbed to their surface during the aggregation step since a good SERRS response was obtained as can be seen from the SERRS spectrum of Cy3.5, Cy5 and HEX oligonucleotide probes aggregated with silver nanoparticles (see figure 4-7). No internal modification of the oligonucleotide sequence is required. For the negatively charged dye HEX the NH_2 terminal group could have aided in giving a SERRS response apart form the DNA bases in the oligonucleotide that might play a role in absorption as well.

Table 4-7 SERRS limits of detection for the three different dye-labelled oligonucleotides with the different sized silver nanoparticles. No values indicates that the experiment was performed but the limit of detection is higher than the base concentration of the dye ($1x10^{-8}$ M).

	λ_{ex}:514.5 nm					
Dye label	λ_{max}/nm	NP1/mol dm^{-3}	NP2/mol dm^{-3}	NP3/mol dm^{-3}	NP4/mol dm^{-3}	Stokes[157]/mol dm^{-3}
HEX	535	$1.2x10^{-10}$	$4.4x10^{-11}$	$1.8x10^{-11}$	$2.6x10^{-11}$	$7.8x10^{-12}$
Cy3.5	581	$8.4x10^{-11}$	$1.9x10^{-11}$	$5.1x10^{-12}$	$9.9x10^{-12}$	$2.5x10^{-11}$
Cy5	643	$9.7x10^{-10}$	$6.6x10^{-10}$	$4.4x10^{-10}$	$4.2x10^{-10}$	_

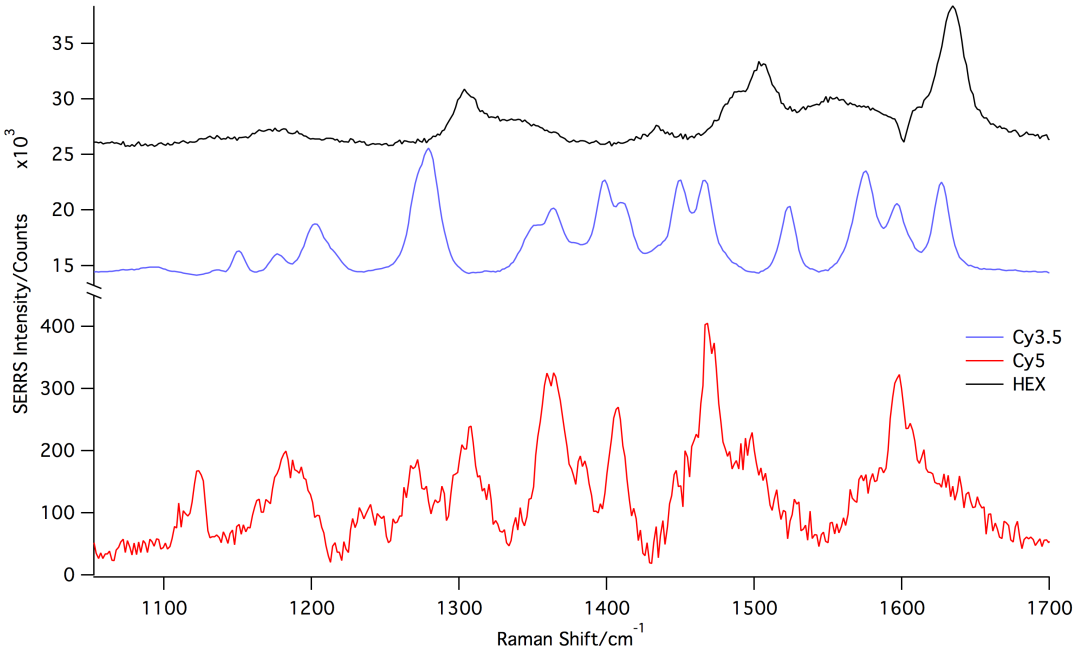

Figure 4-7 SERRS spectra of Cy3.5, Cy5, and HEX dye-labelled oligonucleotide probes (2.7 nM) and aggregated with silver colloid (NP4) with excitation at 514.5 nm, 3 seconds exposure time and 1 accumulations. For visualisation purposes the spectra have been baseline corrected and offset on the *Y*-axis.

The strongest peaks in the spectra were used to identify each label, these were: 1634.5 cm^{-1} for HEX; 1279.3 cm^{-1} for Cy3.5; 1468.3 cm^{-1} for Cy5. For all dyes and all different nanoparticle sizes the SERRS response was linear at low concentrations (1 nM to 4.8 nM) as can be seen from the calibration lines obtained (see figure 4-8). However at higher concentrations linearity is lost. This can be attributed to the fact that as more probe is available the coverage on the nanoparticle would not be monolayered anymore thus giving discrepancies.

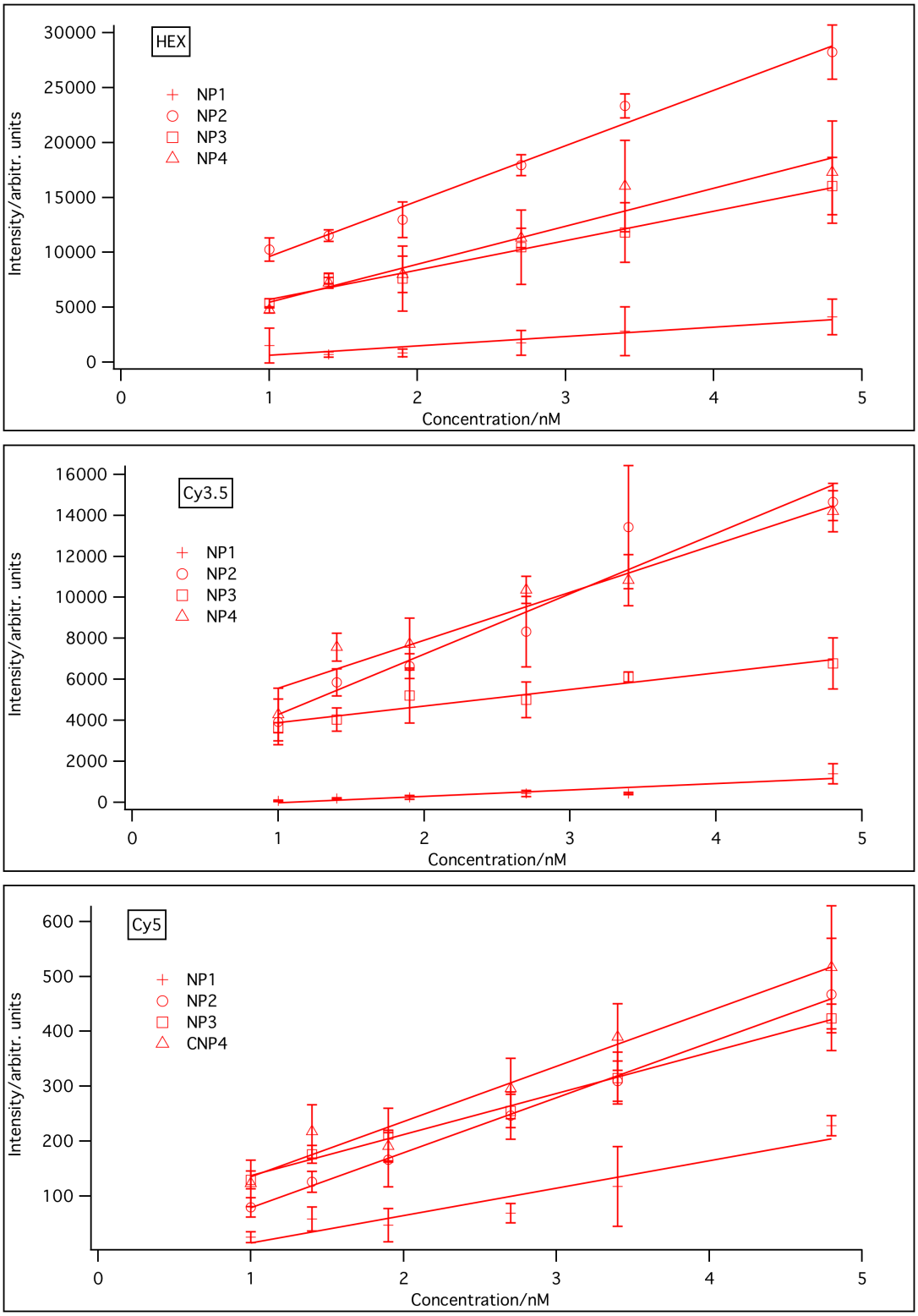

Figure 4-8 SERRS dilution series using silver nanoparticles and 514.5 nm laser excitation. The Raman intensity for each dye and particle size was plotted against concentration. The peaks used to identify each label were HEX, 1634.5 cm^{-1}; Cy3.5, 1279.3 cm^{-1}; Cy5, 1468.3 cm^{-1}.

From the LOD results (see table 4-7) obtained it is clearly shows that Cy3.5 probe holds the lowest LOD for all nanoparticle sizes. This stems from the fact that Cy3.5 is positively charged enabling it to adsorb to the negatively charged surface of the silver nanoparticles giving thus better sensitivity at very low concentrations. The Cy5 dye apart from being positively charged has a λ_{max} of 643 nm, more than 100 nm from the 514.5 nm laser source hence the significantly higher LOD than HEX and Cy3.5.

Clear and straightforward conclusions cannot be drawn for the effect of nanoparticle size on the SERRS response as other factors such as different dispersity and surface area. From table 4-7 NP1 and NP3 (44 nm and 45 nm respectively) have a similar average size, however do not have approximately similar LOD as would be expected, in fact NP3 gives a lower LOD. The different LOD can be attributed to the different preparation methods and more significantly the different size distribution of each batch. NP3 as stated before has a wider size distribution than NP1 as demonstrated by the half width of the peak in DCS (NP3: 27.3 nm, NP1: 10.9 nm).

For HEX and Cy3.5 probes NP2 with a mean size of 53 nm gave the lowest LOD while for Cy5 probe NP4 (70 nm) gave the lowest LOD, although it is worth noting that the LOD for NP2 was close and that Cy5 probe gave high LOD when compared to other dyes. The problem with the NP4 batch is that smaller sized nanoparticles are found in the population as was confirmed with the SEM images (see figure 4-2) and DCS results (see table 4-5). The results are promising and encourages further investigation as it can be seen from here that as size is increased the LOD is getting lower especially when comparing NP1 with the larger sizes NP2 and NP4.

An analogous study by Stokes *et al.*[157] show similar LODs although the study was not comparing different sizes of nanoparticles and used 5'-propargylamine-2'-deoxyuridine modified dye-labelled oligonucleotide sequences with silver nanoparticles (32 nm diameter) however comparisons can still be drawn. For the Cy5 dye, the LOD was better for unmodified oligonucleotides than the modified ones used by Stokes[157], where the LOD of detection is higher than the base concentration of the dye ($1x10^{-8}$ M) (see table 4-7). Such results can be attributed to the larger silver nanoparticles used, as a modified oligonucleotide that facilitates adsorption to the nanoparticle surface did not give better limit of detection than modified ones. A similar trend is found for Cy3.5 where the larger nanoparticles show a better LOD when compared to Stokes *et al.*[157]. However for the HEX dye the limit of detection is higher for the modified oligonucleotides.

4.4 Conclusion

In the previous chapters the focus was primarily on the SERS probe, while this chapter was a preliminary study on the effect of nanoparticle size on the SERS enhancement. The Lundahl method used for preparing the different sizes after a thorough characterisation of the colloids was found not as effective in preparing a range of different sized monodispersed nanoparticles. Problems were also encountered during the SEM characterisation as the images obtained showed sample aggregation. This issue was resolved in the next chapter. Using 3 different dye-labelled oligonucleotides that have different maximum absorbance wavelength, the LOD for the four different nanoparticle sizes were measured. The results obtained showed that a nanoparticle size of 55 nm gave a better LOD, than smaller and larger

nanoparticles. The results obtained during the characterisation of the colloid and the LOD of the different probes are encouraging and hence a better method to prepare different sized nanoparticles was investigated in the next chapter. This would lead to a more rigorous method to calculate the enhancement factor provided by a change in nanoparticle size, taking in consideration the change in surface area that inherently occurs.

Chapter 5: Synthesis of Size Tuneable Monodispersed Silver Nanoparticles and the Effect of Size on SERS Enhancement

5.1 Introduction

In the preliminary study conducted in chapter 4, it was shown that larger nanoparticles give a better limit of detection. In this chapter a different approach from the previous chapter will be used to calculate effectively the SERS analytical enhancement factor (AEF) for each of the different sizes of AgNP. In fact, in this chapter, the particles are not aggregated, thus eliminating the aggregation factor, 'small' probe molecules are used for an easier approximation of the surface coverage of the analyte on the nanoparticle surface and most importantly a more effective and simpler method for the preparation of spherical monodispersed nanoparticles. This was done by a seeded growth method, however contrary to the previous chapter the desired size of nanoparticle was obtained by changing the seed concentration and keeping all other reagents constant. This was done by using sodium borohydride reduced silver nanoparticles as seeds and hydroquinone (HQ) as the reducing agent for the $AgNO_3$ salt. HQ is a selective reducing agent as it allows silver ions to be reduced only on the seed particles present and thus reduces secondary nucleation sites giving better monodispersity. The different size ranges of nanoparticles produced were subsequently tested for their efficiency as SERS substrates to find the optimal size at which the maximum intensity is delivered. Such a study is important as it is known that enhancement increases with particle size increase[163,167], however it follows that an increase in size also means nanoparticles absorb less and scatter more through inelastic scattering[45]. An increase in size of AgNP whilst the Ag

concentration remains constant implies that the surface area available for the analyte to adsorb decreases. Hence the overall effect on the SERS response is a balance between the enhancement, scattering and surface area. To avoid overestimation of the SERS enhancement, the enhancement factor has to be real, that is an enhancement that would not be present under non-SERS conditions for the same molecule. SERS enhancement factors are usually separated into two main multiplicative contributions; the electromagnetic (EM) enhancement and the chemical enhancement (CE). The EM enhancement is due to the coupling of the incident and Raman electromagnetic field with the SERS substrate, while the CE origins are still controversial[168]. The most widely accepted mechanism for the latter is through a charge transfer mechanism[169]. The EM enhancement factor is thought to be the dominant contribution, however it is not necessary to know the exact origin to measure the overall enhancement factor.

In this chapter three analytes (rhodamine 6G (R6G), malachite green oxalate (MGO) and thiophenol (TP)) with different optical and chemical properties are used giving the possibility of understanding better the effect of nanoparticle size on different analytes by measuring the AEF. Since the AEF strongly depends on the adsorption properties and surface coverage of the probe identical experimental conditions were used with all the different sizes and analytes used. AEF measurements are easily obtained and reproducible therefore can be used to monitor the average effect of nanoparticle size on the SERS signal.

5.2 Experimental

5.2.1 Chemicals and materials

Silver nitrate ($AgNO_3$, ≥99%), hydroquinone ($C_6H_6O_2$, ≥99%), trisodium citrate dihydrate ($Na_3C_6H_5O_7 \cdot 2H_2O$, 99%), sodium borohydride ($NaBH_4$, 99%) rhodamine 6G (R6G) ($C_{28}H_{31}N_2O_3Cl$, 98%), malachite green oxalate ($C_{52}H_{54}N_4O_{12}$), thiophenol (C_6H_6S, ≥99%), ethanol (C_2H_6O, 99%). All chemicals were purchased from Sigma-Aldrich and used without further purification. All water used was doubly distilled (18.2 mΩ cm).

5.2.2 Synthesis of AgNP

The synthesis of the different sizes of AgNP were prepared by a two step process; the preparation of AgNP seeds by sodium borohydride reduction, followed by a controlled seeded growth of the AgNP seeds with the reduction of $AgNO_3$ with hydroquinone. All glassware was soaked in *aqua regia* for two hours and thoroughly rinsed with doubly distilled water.

5.2.2.1 Seed preparation

The sample preparation method used is a modification of the method reported by Creighton *et al.*[2]. The Ag colloid seed solution was prepared by preparing a 0.002 m sodium citrate solution (10 mL). Under vigorous stirring to the latter solution of 0.1 m $AgNO_3$ (50 μL) was added followed by a drop wise addition of 0.1 M $NaBH_4$ (1 mL).

5.2.2.2 AgNP with controlled size ranges preparation

The sample preparation method used is a modification of the method reported by Gentry *et al.*[80]. The different sizes of AgNP's were prepared by varying the amount of seed concentration whilst keeping all other reagents concentration constant. Hence a 0.1 M $AgNO_3$ (100 µL) solution was added to a varying volume of H_2O (7.2 mL – 9.7 mL) in a 15 mL scintillation flask. Under rapid stirring at room temperature a varying volume of sodium borohydride reduced silver nanoparticles (0.08 mL – 2.56 mL) were added followed by 0.1 M sodium citrate (22 µL) and of 0.03 M (100 µL) hydroquinone, thus giving a final solution volume of 10 mL.

5.2.3 Instrumentation and measurements

5.2.3.1 UV-Vis spectroscopy

The extinction spectra of the colloids were recorded using a Varian Cary 300 Bio spectrophotometer directly after preparation of each nanoparticle size over a wavelength range of 200-800 nm. The extinction spectra of the colloid were recorded again after addition of the analytes. The baselines were recorded using doubly distilled water and the samples were diluted accordingly to remain in the absorption response limit of the spectrometer. The seed concentration was calculated by Beer-Lamberts' law whereby the extinction coefficient used was 4.16×10^9 M^{-1} cm^{-1}.

5.2.3.2 Scanning electron microscopy

A sample from each nanoparticle preparation was prepared on a polycation functionalized silicon wafer. The wafer was first cleaned using water and ethanol,

then dried in a nitrogen flow. The wafer was then placed in an oxygen plasma cleaner for 60 seconds. PDDA (30 μL) was dissolved in 1 mM NaCl (1 mL), the solution was used to coat the clean wafer by spotting the wafer with the solution with a pipette and then leaving it for 30 minutes under a water-saturated atmosphere. After this step it was washed off and dried in a nitrogen flow. Each AgNP (100 μL) sample was put onto the PDDA-functionalized silicon wafer for 15 minutes under a water-saturated atmosphere. The sample was then washed off and dried in a nitrogen flow. Using a scanning electron microscope (FEI Sirion 200 ultra-high-resolution Schottky Field emission gun), eight 'snapshot' images were taken for each sample. From the images obtained the diameter was calculated using Image J[156], an image processing and analysis software. An automated method was used to measure the particles, whereby the particles must have a range between 10 nm – 100 nm and the circularity of the particles must be around 0.8 – 1 (where circularity is defined as Circularity = $4\pi(\text{Area}/\text{Perimeter}^2)$) as to avoid any aggregates that might be present. Before the particles were measured the images were converted to grey scale 8-bit images, enhanced by binary contrast enhancement (thresholding) and the scale was calibrated. More than 600 particles were measured for each size.

5.2.3.3 Dynamic light scattering and zeta-potential measurements

The size and zeta-potential of the different sized AgNP were measured before and after addition of MGO, R6G and TP using a Malvern Zetasizer (Nano-ZS) instrument. The standards for size were Nanosphere size standards 20 nm (± 1.5 nm, Lot. 339300) and 40nm (±1.8 nm, Lot. 33306), while the standard for the zeta-

potential used was zeta-potential transfer standard (-68mV ± 6.8mV, Batch No. 051001).

5.2.4 SERS Measurements

5.2.4.1 Preparation of samples for SERS analysis

To 300 µL of AgNP, 33 µL of $1.6x10^{-5}$ M R6G solution were added to give a final concentration of dye of $1.6x10^{-6}$ M. The same volumes and concentrations were used for the other analytes MGO and TP.

5.2.4.2 Surface enhanced Raman spectroscopy

The SERS spectra of three identical samples was recorded after one minute of mixing the analyte with the AgNP with an instrumental setup in a confocal arrangement at an extinction wavelength of 633 nm. The SERS spectra were obtained with an exposure time of 2 seconds and 5 accumulations and all data was normalised to a silicon standard. The setup consisted of a Leica DM/LM microscope equipped with an Olympus 20x/0.4 long-working distance objective that collects 180º backscattered light from a cuvette. The spectrometer system was Renishaw Ramascope System 2000 (Gloucestershire, UK) with a Renishaw diode laser with a power output of 1 mW at sample. Holographic edge filters were used to reject Rayleigh scattered light. The detector used was a deep-depletion RenCAM charge-coupled device (CCD). The same procedure using the same experimental setup was used using an excitation wavelength of 785 nm with an exposure of 20 seconds and 5 accumulations and all data was normalised to a silicon standard.

5.2.5 Raman measurements

5.2.5.1 Preparation of samples for Raman spectroscopy

A 0.01 M solutions of MGO andR6G, and a 9.3 M TP ethanolic solution TP. A $1x10^{-6}$ M MGO solution was prepared to obtain a Raman spectrum at 633 nm laser excitation wavelength.

5.2.5.2 Raman spectroscopy

The Raman spectra of three identical samples were recorded using the same experimental conditions and setup as described previously for obtaining the surface enhanced Raman spectra.

5.3 Results and discussion

In this study a range of sizes of silver nanoparticles were prepared using an improved method, which give monodispersed spherical particles. The optimal size for surface enhanced Raman scattering (SERS) was then assessed by comparing the signals from the different sizes prepared to Raman spectra. Silver was chosen for the study not only because it has a strong optical response and a narrower SPR than gold[155,160-162] but also due to the need of a well characterized method for preparation of homogenous monodispersed AgNP.

The AgNP's were synthesized using HQ as a selective reducing agent using a modified version of the seeded growth method used by Gentry *et al.*[80]. In this study it is shown that different sized nanoparticles can be prepared by varying the seed concentration. Other seeded growth methods have already been reported both for

gold and silver nanoparticles[170-173] but not with HQ as a reducing agent. HQ is widely used in photographic film development and selectively reduces silver ions in the presence of metallic silver nanoclusters[80,174,175]. The weak reducing potential of HQ (E^o = -0.699 v NHE) is unable to reduce isolated Ag^+ as it has a more negative reducing potential of -1.8V. However Ag^+ can be reduced in the presence of silver (Ag^0) as the reducing potential changes to +0.799 V.

For the synthesis of different sized silver nanoparticles, HQ was used as it is a weak reducing agent and as mentioned above it selectively reduces silver ions only in the presence of AgNP seeds as represented in figure 5-1. Reduction by HQ has its own practical aspects as the reduction reaction is complete in a short period of time (15 minutes maximum) and it occurs at room temperature. Also HQ gives poor steric hindrance but also binds weakly to the silver surface of nanoparticles therefore such nanoparticles can be easily modified with different modifiers which would be better suited for subsequent applications. The nanoparticles prepared by HQ in this paper were stabilized with sodium citrate.

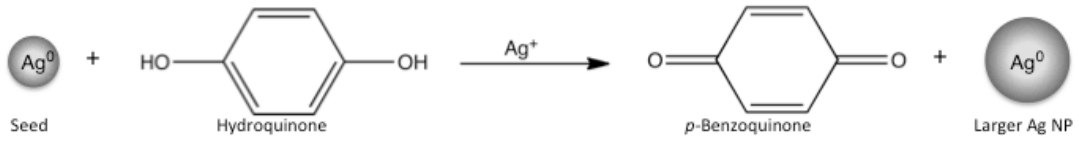

Figure 5-1 Schematic representation of growth of silver nanoparticle seeds (left) into larger silver nanoparticles by the reduction of silver ions by hydroquinone.

The seed used for the growth of the nanoparticles were prepared by sodium borohydride reduction of silver nitrate, which give small enough nanoparticles to

serve as seeds onto which further layers of silver can be added on. This nanoparticle preparation is reported to produce polydispersed sols and particles of different morphologies[2], as can be confirmed from the SEM images obtained (see figure 5-2 a). The nanoparticles grown from the seeds however are monodispersed and of a spherical shape as the images and particle size count obtained by the SEM confirm (see figure 5-2 b-e and figure 5-3).

The different sizes were produced by varying the concentration of the seed while keeping the amount of silver nitrate and HQ constant (see table 5-1). As the seed concentration is gradually decreased less nanoparticles will be available for the silver nitrate to be reduced on to therefore larger nanoparticles are gradually produced. It is to note that the silicon wafers were treated with PDDA a polycation which due to the positive charges on its backbone prevents aggregation of the negatively charged AgNP's during the drying process in the SEM preparation steps due to Coulombic attractions. The images obtained then give a better representation of what is in solution. As seen in figure 5-2 b-e very few aggregates are present, suggesting that no nanoparticle clusters are present in solution.

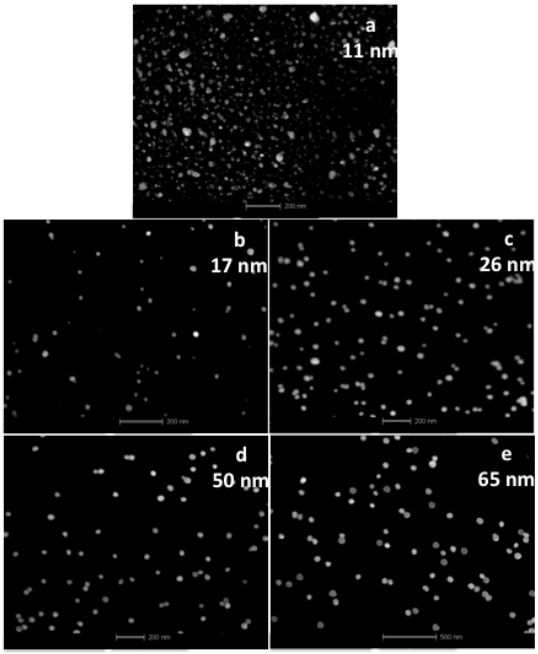

Figure 5-2 Sample SEM images of seed (a) and AgNP (b-e) produced by the seed growth method. Images a to e correspond to average sizes of 11, 17, 26, 50 and 65 nm respectively. Note that scale bars in images a to d are 200 nm while for image e the scale bar is 500 nm

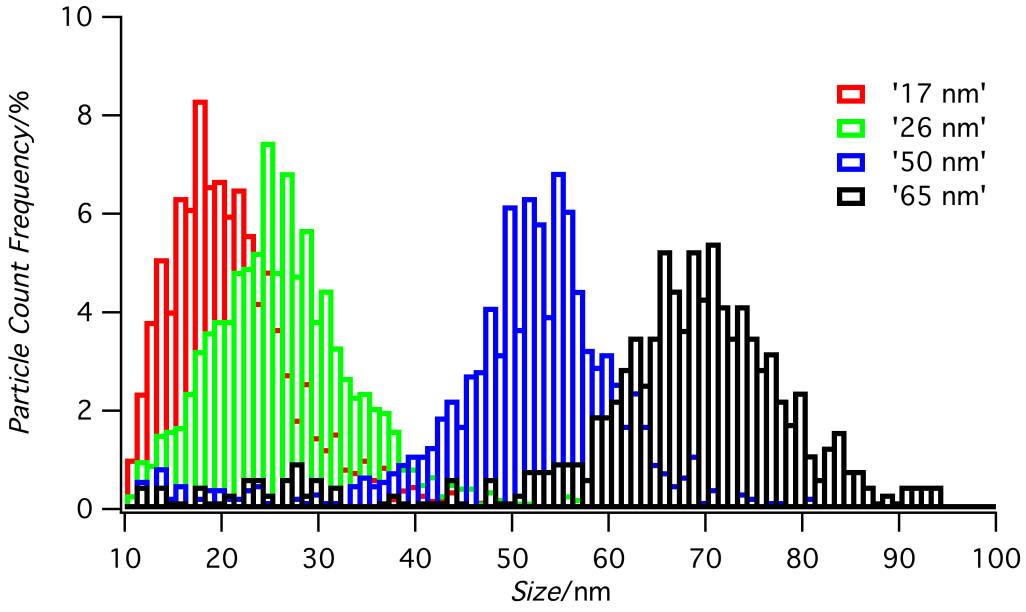

Figure 5-3 Histogram of measured particles by SEM corresponding to eight sample SEM images of AgNP's of each size prepared.

Table 5-1 Seed concentration and resulting nanoparticle size and extinction peak maximum.

Seed conc. (nm)	Final AgNP diameter (nm)	Absorption maximum (nm)	Standard deviation (nm)	FWHM (nm)	PDI
seed	11	390	± 13	71	0.56
0.542	17	407	± 5	103	0.25
0.145	26	421	± 8	169	0.3
0.018	50	467	± 11	199	0.21
0.009	65	513	± 15	227	0.22

The four samples produced were characterized by SEM, whereby eight SEM images from each sample were measured by an automated process on Image J[156] software from which it was calculated that as the seed concentration is decreased from 0.542 to 0.009 nM the size increased from 17 nm to 65 nm (see table 5-1) and that the samples produced are relatively monodispersed as the SEM images in figure 5-2(b-e) and histograms in figure 5-3 confirm. The full width at half maximum (FWHM), as well as the standard deviation increase as the size of the AgNP increases (see table 5-1). This is further confirmed by the PDI data gathered from DLS measurements (table 5 – 1). The seed has a high PDI of 0.56 which as shown by the SEM images, it signifies that is not only polydispersed but also non-spherical in shape. The PDI sharply decreases to an average of 0.25, when the seeds are used to produce the different NP sizes, this is due to the monodispersed and spherical nature of the NP produced. This broadening of the extinction spectra can be attributed to additional multipolar resonances which become more significant as the particles get larger[155] and as expected a red shift was observed as the size is increased starting from a

maximum of 390 nm for the seed up to 513 nm for the larger nanoparticles[81,163,176-179] (see figure 5-4).

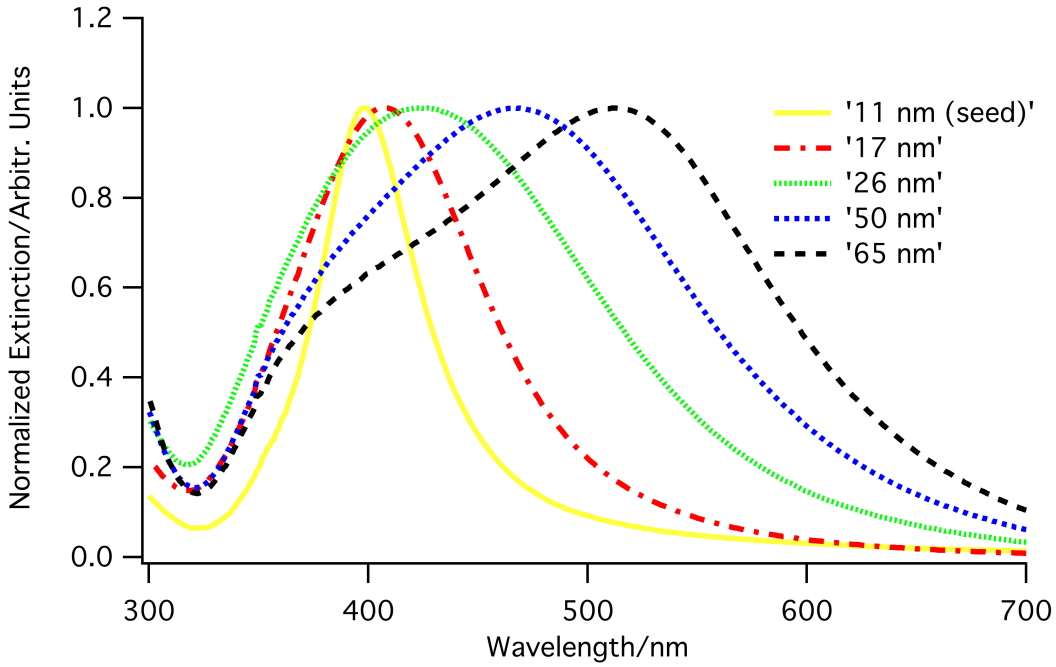

Figure 5-4 Normalised extinction spectra of seed and seed grown nanoparticles corresponding to SEM images in figure 5-2.

The extinction spectra of the nanoparticles produced have a low extinction above 600 nm therefore being off-resonance with the 633 and 785 nm laser excitation used. The analytes chosen to study the effect of spherical AgNP size on SERS intensity were the dyes rhodamine 6 G (R6G) and malachite green oxalate (MGO) and the sulfur containing molecule thiophenol (TP).

The three analytes adsorb to the surface (chemisorbed for TP and physisorbed for MGO & R6G) of the negatively charged AgNP as R6G and MGO are positively charged dyes, while TP has a thiol group which has a great affinity towards silver[75,180,181]. The two dyes have been extensively studied in SERS experiments as

they have reliable photostability[181-183]. R6G has a maximum adsorption of 530 nm and is off-resonance with both excitations used however MGO which has an excitation maximum at 621nm, therefore at 633 nm is in resonance with the laser. This gives the possibility to compare between off-resonance and resonance SERS intensity with different sizes. The non-dye analyte thiophenol was used which is off-resonance to both laser wavelengths used, and no fluorescence or photobleaching hinders the SERS measurement.

The Raman enhancement effect in the SERS experiment was determined by *G* which describes the enhancement of the Raman signal per molecule adsorbed on the surface of a SERS-active species (in this case AgNP)[52,184]. *G* is calculated as:

$$G = \frac{I_{SERS}}{I_{Raman}} \frac{M_{Bulk}}{M_{Monolayer}}$$

Equation 5-1

where I_{SERS} and I_{Raman} are the Raman intensities enhanced by AgNP and unenhanced intensity respectively. M_{Bulk} and $M_{Monolayer}$ are the molar concentrations of the analyte in an unenhanced experiment and enhanced experiment respectively. $M_{Monolayer}$ for the different sizes of AgNP's produced was calculated assuming total nanoparticle surface coverage of the analytes, whereby a single R6G molecule occupies an area of 0.4 nm^2 on the surface of the AgNP[185]. This value was used as an approximate value for MGO. While for TP a single molecule occupies and area of 0.3 nm^2 [180]. To ensure monolayer coverage around the nanoparticles a concentration of 1.6×10^{-6} M of analyte was used (see figure 5-5). Further information on these calculations are found in Appendix A.

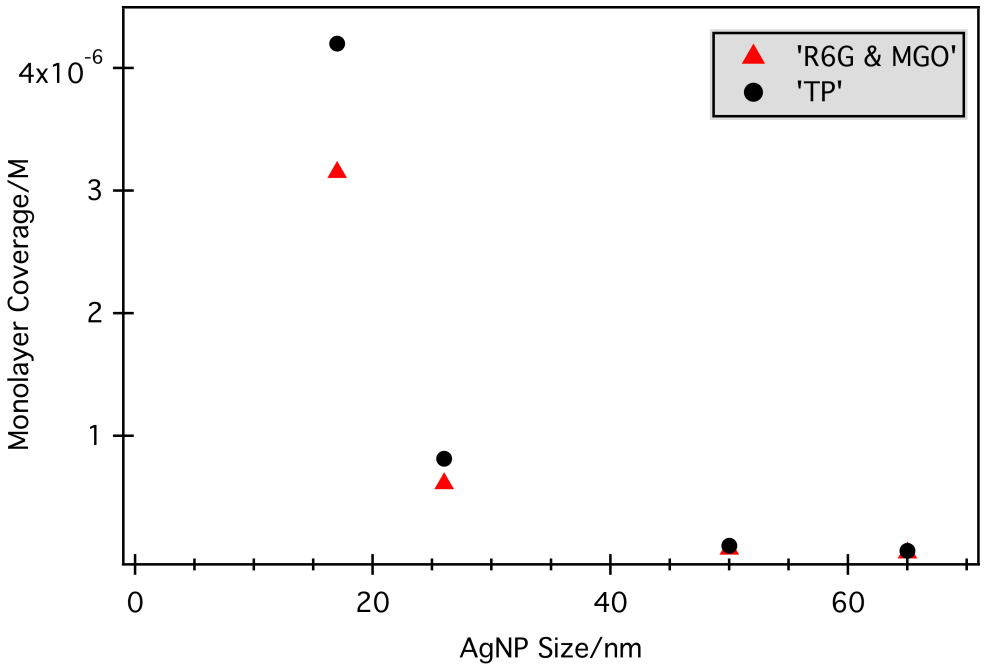

Figure 5-5 Monolayer coverage for the different sizes of nanoparticles where R6G and MGO have a 0.4 nm^2 coverage and TP covers on average 0.3 nm^2.

The Raman spectra for all three analytes from which I_{Raman} were obtained at a higher analyte concentration than in the SERS condition experiments, as peaks could not be resolved at those low concentrations. The Raman spectrum of MGO at 633 nm excitation wavelength however had to be taken at a concentration of 1µM due to the high fluorescence background as the laser excitation wavelength was close to the absorption peak of the dye.

The SERS intensity for the different AgNP sizes were monitored at two different Raman peaks for each analyte used (see figure 5-6). The Raman shift of 1361 cm^{-1} (in-plane bending and aromatic C-C stretching) and 1508 cm^{-1} (aromatic C-C stretching) for R6G were used, while for MGO 1365 cm^{-1} (N-C stretch) and 1395 cm^{-1} (C-C and C-H in-plane motion aromatic) and for TP 997 cm^{-1} (in-plane ring breathing mode) and 1022 cm^{-1} (in-plane C-H bend) were used[186,187].

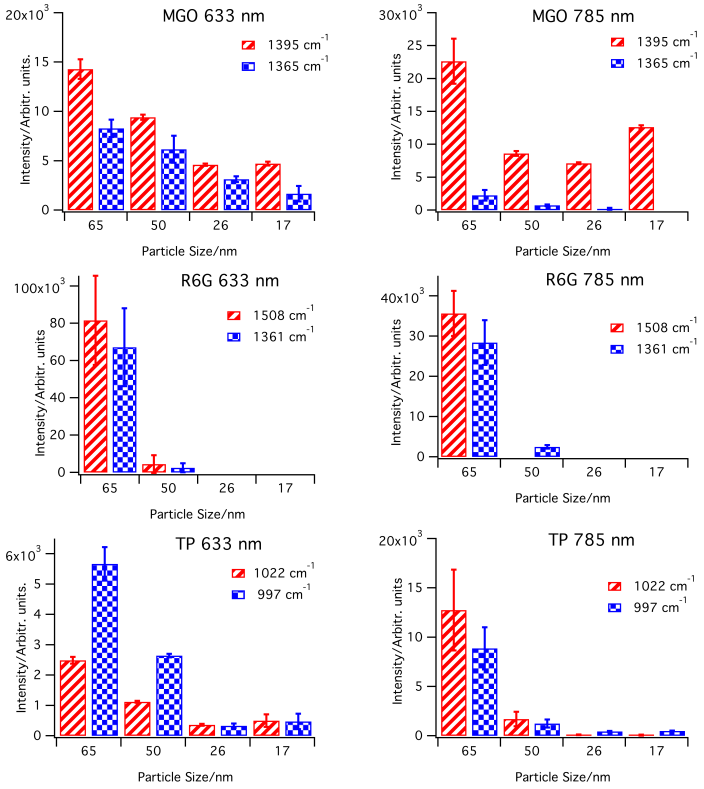

Figure 5-6 SERS intensities for the different AgNP sizes with the different analytes used at both 633 nm and 785 nm laser excitation wavelengths.

These bands were chosen as no shift in frequency is observed when going from the Raman spectrum of the neat analyte solution to the spectrum taken under SERS conditions, that is the frequency of the vibration chosen are not effected by the adsorption to the surface of the nanoparticle (see figure 5-7). It is to note however that the SERS spectrum of TP has a few changes when compared to neat TP. These changes are due to the adsorption of the molecule to the silver surface[186,188]. The band at 917cm^{-1} in the Raman spectrum which is attributed to the bending vibration of the S-H bond is no longer detected which indicates that the TP is chemisorbed on silver surface by the breaking of the S-H bond. Further evidence of TP is S-bonded

to the metal surface is the shift of the 1092cm^{-1} peak (ring-breathing mode coupled to the ν(C-S) mode) further down to 1068cm^{-1} [188](see figure 5-7).

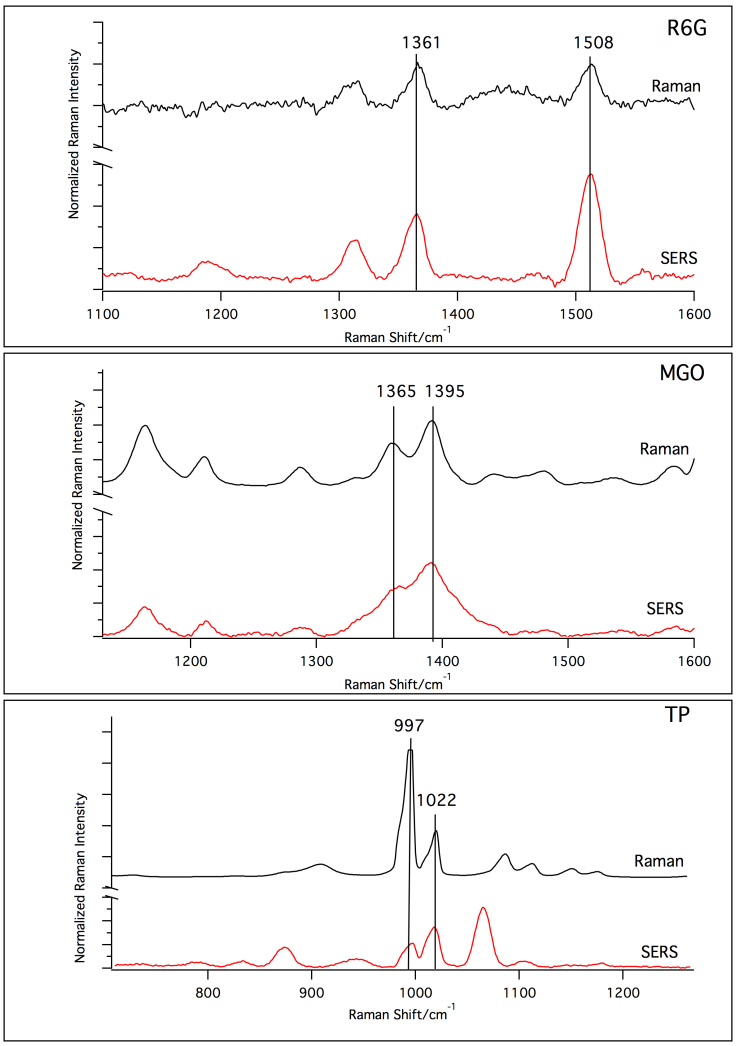

Figure 5-7 Raman and SERS spectra of R6G, MGO and TP. 65 nm AgNP's were used as the SERS substrate. A laser excitation wavelength of 785 nm was used with a 20 seconds exposure time and 5 accumulations. For visualisation purposes the spectra have been baseline corrected and offset on the *Y*-axis.

The extinction spectra (figure 5-8), size (figure 5-9) and zeta-potential (figure 5-10) of the AgNP's were measured before and after addition of the analytes. The DLS shows different particle size for the different samples of AgNP's produced, for which

after most analyte addition no significant shift in the nanoparticles' extinction spectra were observed and the DLS data show no significant increase in the hydrodynamic diameter. The zeta-potential for all different sized AgNP's produced show that stable particles are produced as the zeta-potential is around -30mV, due to the citrate layer that is adsorbed to the nanoparticle surface. A slight decrease in zeta-potential can be observed suggesting that the analytes has adsorbed to the surface without causing any aggregation of the colloid (see figure 5-10).

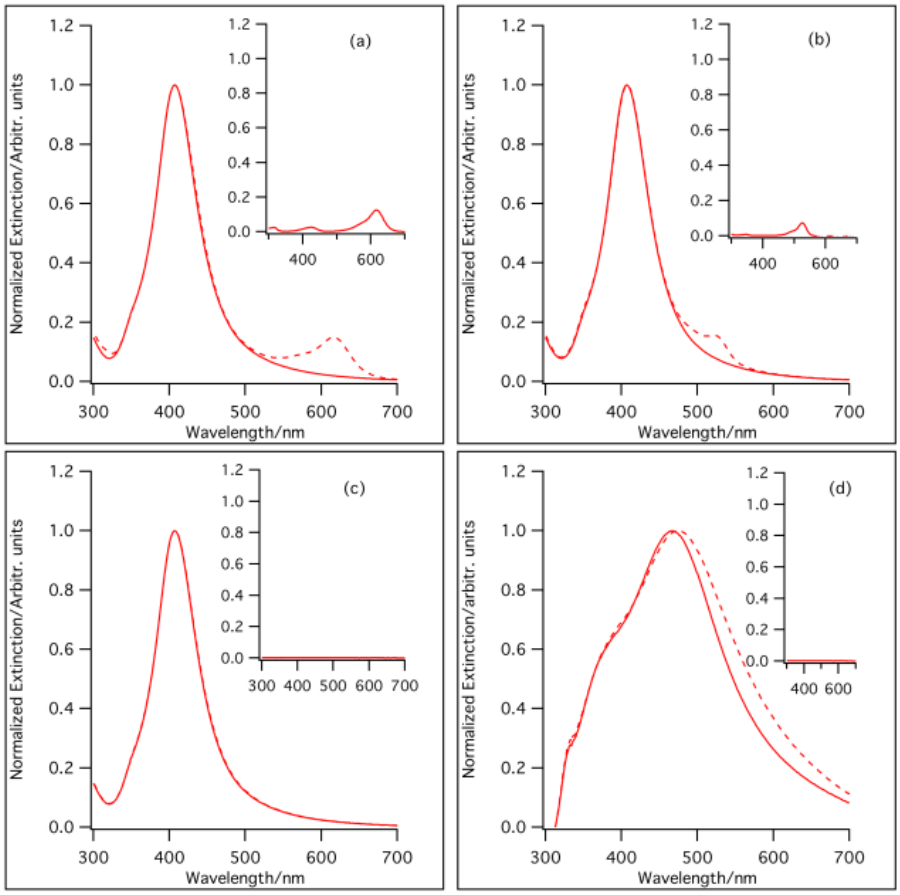

Figure 5-8 (a-c) Normalised extinction spectra of 17 nm AgNP before (—) and after (---) addition of MGO, R6G and TP respectively. (d) Normalised extinction spectrum of 50 nm AgNP before (—) and after (---) addition of TP. Analyte concentration used for all spectra was the same as in the SERS experiment, 1.6×10^{-6} M. (Inset) Respective analytes without AgNP.

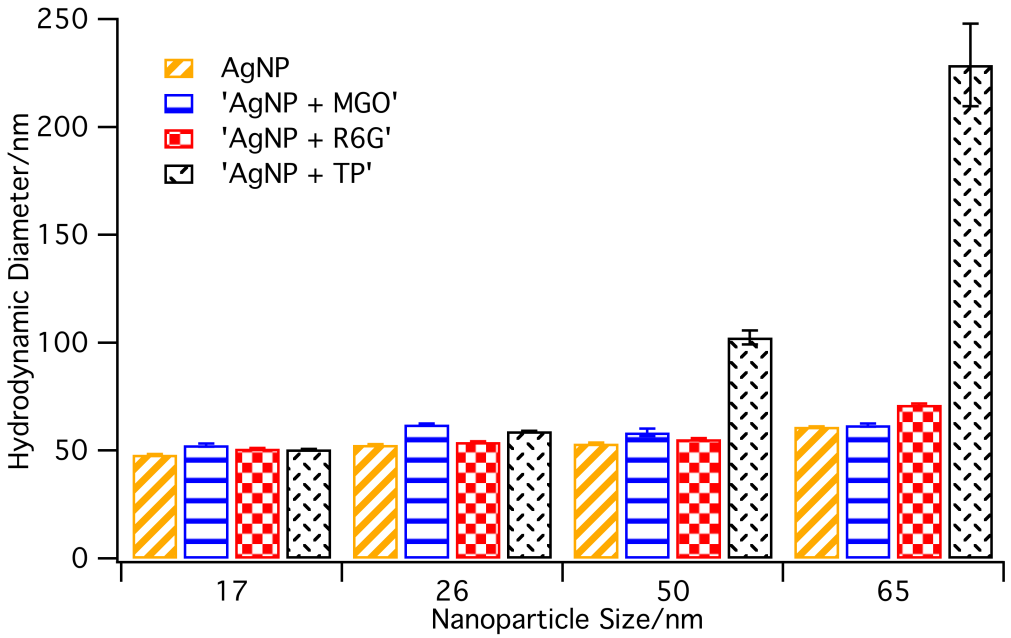

Figure 5-9 DLS size measurement of the different AgNP sizes before and after addition of MGO, R6G and TP.

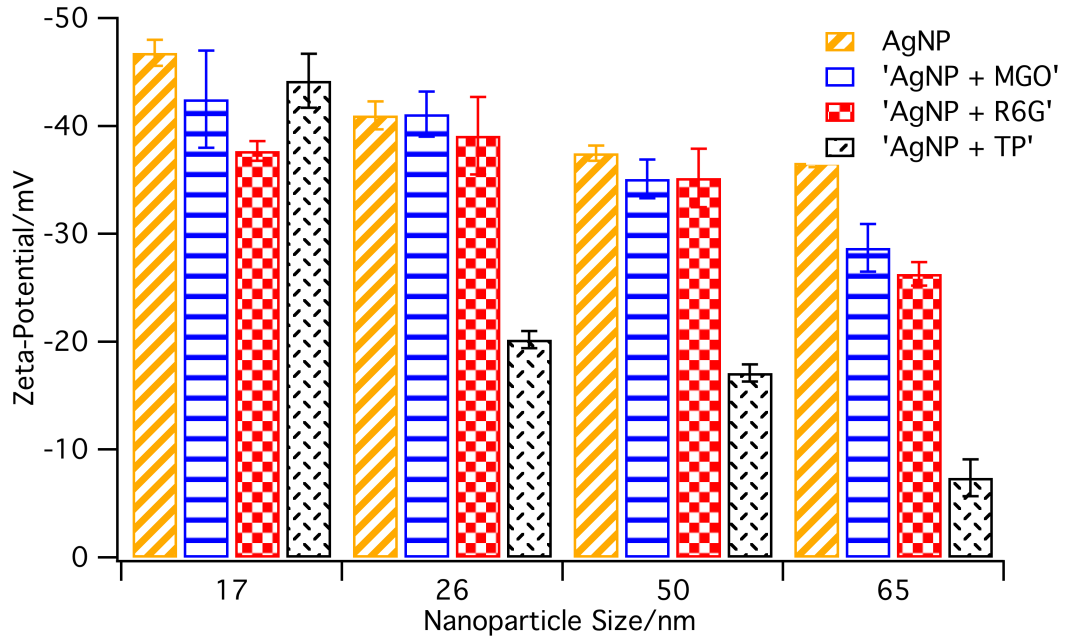

Figure 5-10 Zeta-potential measurements of the different AgNP sizes before and after addition of MGO, R6G and TP.

On the other hand when TP was added it is interesting to note that for the larger sized nanoparticles aggregation occurs as a red-shift is observed in the extinction spectra, aggregation was also confirmed by the DLS data and the zeta-potential measurements. (see figures 5-8 to 5-10).

For the samples where no aggregation occurred after addition of the analyte as expected[184], the SERS intensity and the *G* value increases with particle diameter as electromagnetic enhancement increases with size (see table 5-2). For TP addition an increase in intensity and *G* value was also observed however contribution by aggregation for the larger sized nanoparticles affected the SERS intensity. Nonetheless the fact that an increase in enhancement factor was observed for all three different analytes suggests that SERS intensity is not only probe dependent.

Table 5-2 The Analytical Enhancement Factor *G* of MGO, R6G and TP for the different nanoparticle sizes at 633 and 785 nm laser excitation wavelengths at the different Raman peaks monitored. Highlighted are the maximum enhancements obtained. Blank cells signify no SERS peak could be obtained.

Analyte (Absorption Max.)	NP Size	Raman Peaks	AEF Laser λ		Raman Peaks	AEF Laser λ	
	(nm)	(cm^{-1})	G 633 nm	G 785 nm	(cm^{-1})	G 633 nm	G 785 nm
MGO(621 nm)	17	1365	0.6	-	1395	4.5	$2.8x10^{2}$
	26		6.4	$3.3x10^{1}$		$3.3x10^{1}$	$8.0x10^{2}$
	50		$1.0x10^{2}$	$9.9x10^{2}$		$3.7x10^{2}$	$7.7x10^{3}$
	65		$2.2x10^{2}$	$5.0x10^{3}$		$5.8x10^{2}$	$3.4x10^{4}$
	(nm)	(cm^{-1})	G 633 nm	G 785 nm	(cm^{-1})	G 633 nm	G 785 nm
R6G(524 nm)	17	1361	-	-	1508	-	-
	26		-	-		-	-
	50		$8.1x10^{4}$	$4.3x10^{4}$		$1.3x10^{5}$	-
	65		$3.7x10^{6}$	$8.1x10^{5}$		$3.9x10^{6}$	$8.7x10^{4}$
	(nm)	(cm^{-1})	G 633 nm	G 785 nm	(cm^{-1})	G 633 nm	G 785 nm
TP	17	997	$4.9x10^{3}$	$1.9x10^{3}$	1022	$1.7x10^{4}$	$7.9x10^{2}$
	26		$1.8x10^{4}$	$8.8x10^{3}$		$6.4x10^{4}$	$2.5x10^{3}$
	50		$1.1x10^{6}$	$1.9x10^{5}$		$1.6x10^{6}$	$8.8x10^{5}$
	65		$4.4x10^{6}$	$2.3x10^{6}$		$5.8x10^{6}$	$1.1x10^{7}$

MGO, which absorbs at 621 nm is close to the 633 nm laser wavelength used and an enhancement can be seen for all nanoparticle sizes. On going to a longer laser wavelength (785 nm) spectra can be still be obtained for most nanoparticle sizes, with enhancement increasing with size. It is to note that the enhancement at 785 nm is greater than at 633 nm laser excitation, this can be due to the dye being resonant at 633 nm and some degree of photobleaching of the dye occurs which in turn reduces the SERS intensity. When using R6G however which is off-resonance with both laser wavelengths used enhancement of the Raman spectra at the concentration used in the experiment can only be seen for larger sized nanoparticles, this can be attributed to a reduced adsorption efficiency of the dye molecule due to the lack of colloid activation by NaCl as suggested by Kneipp *et al.*[165]. A higher enhancement factor is given at 633 nm laser excitation wavelength close to R6G absorption maximum though still being off-resonance rather than at a longer 785 nm wavelength.

For TP (a good Raman scatterer molecule) SERS spectra were obtained for all of the peaks monitored, even for the small sized nanoparticles where no aggregation occurred upon addition of TP. Enhancement factors are high even for smaller sizes of AgNP when TP is used. This can be due to the adsorption of the molecule through the formation of a thiol bond between the silver and sulfur. If it is assumed that the benzene ring of TP extends out of the AgNP surface, the Raman modes which are aligned with the local field are favoured hence a larger enhancement factor for the peaks observed, even at small silver nanoparticle size. For the larger nanoparticles aggregation played an important role in enhancement of the Raman peaks hence the enhancement cannot be solely related to the size of the nanoparticles.

This study shows us that for non-aggregated SERS experiments larger AgNP's are ideal for both on- and off-resonance setups, whereby the larger SERS intensities and enhancements are given.

5.4 Conclusion

A simple and fast method for the production of spherical, monodispersed nanoparticles of tuneable size by the selective reduction of $AgNO_3$ on silver seeds with HQ was reported. The different sizes produced (17 nm, 26 nm, 50 nm and 65 nm) were characterised. The results obtained show that this method produced monodispersed spherical nanoparticles. Using a PDDA-functionalised silicon wafer solved the nanoparticle aggregation and thus facilitating nanoparticle size measurements from the SEM images obtained. The well characterised nanoparticles were then used to calculate the AEF for three different analytes at 633 nm and 785 nm laser excitation wavelength. It was found that in SERS conditions and in on- and off-resonance condition the maximum enhancement factor was obtained with the 65 nm AgNPs. These particles have the potential for being used for other diagnostic purposes in off-resonance and in-resonance setups, as their optical response can be modified by the simple tuning of their size. In light of these results in the following chapter will investigate using dye-labelled oligonucleotides, nanoparticles larger than 65 nm to see if SERS intensity would continue to increase in size.

.

Chapter 6: Effect of Nanoparticle Size on SERS Response of Dye-labelled Phosphorothioate Oligonucleotides

6.1 Introduction

In chapters two and three it was concluded that SERS analysis of phosphorothioate-modified DNA are dependent on the position and number of modifications, the concentration and the type of aggregating agent used. In this chapter the effect of AgNP size on phosphorothioate-modified ssDNA is investigated. Already SERS analysis for dye-labelled oligonucleotides and small reporter molecules obtained in chapters four and five have shown that an increase in AgNP size leads to a decrease in LOD and an increase of the AEF. Building on the work done four different sizes of monodispersed AgNP's are produced using the method reported in section 5.2.2 to assess the effect of nanoparticle size on the SERS response of dye-labelled phosphorothioate-modified oligonucleotides. A larger AgNP was prepared in this study to see if it will translate into a larger SERS intensity or if other factors such as inelastic scattering[45] will hinder the output. In addition AgNP's were characterised using a nanoparticle tracking analysis (NTA) system and the results compared to other methods used in previous chapters.

6.2 Experimental

6.2.1 Chemicals and materials

Silver nitrate ($AgNO_3$, ≥99%), hydroquinone ($C_6H_6O_2$, ≥99%), trisodium citrate dihydrate ($Na_3C_6H_5O_7 \cdot 2H_2O$, 99%), sodium borohydride ($NaBH_4$, 99%). All

chemicals were purchased from Sigma-Aldrich and used without further purification. Oligonucleotides were purchased from Eurofins (Germany) and purified by HPLC. All water used was doubly distilled (18.2 mΩ cm).

6.2.2 Synthesis of AgNP

The synthesis of four different sized batches of nanoparticles were prepared using the seeded growth method used in section 5.2.2, where by varying the sodium borohydride reduced AgNP seed concentration, different sizes of AgNP can be produced by the hydroquinone reduction of $AgNO_3$. The only difference is that the seed concentration range used was between 0.0045 nM to 0.072 nM as to prepare larger nanoparticles than the ones used for the investigation in chapter 5, however the procedure used was the same.

6.2.3 Instrumentation and measurement

6.2.3.1 Nanoparticle tracking analysis

Using a Nanosight LM10 instrument with NTA software the concentration and particle size was measured. The following is the method used to perform the analysis of each nanoparticle sample. The Nanosight chamber was cleaned with a series of ethanol and water washes to remove any nanoparticle stuck to the glass. The chamber was then dried out using dry nitrogen. Each nanoparticle sample was diluted by a factor of a 1000. This was carried out using a serial dilution, as to have an ideal concentration of about $1x10^8$ to $25x10^8$ particles/mL which is roughly about 20 to 60 particles in the camera view. The samples were then injected using a syringe into the chamber making sure that there are no air bubbles trapped. Using the microscope the

interrogation area of the laser beam was chosen. In general this is close to the 'thumbprint' like area produced by the laser beam. The focus was then set so that the under low camera capture and gain settings only the focused particles can be seen in that position. The gain and shutter were then adjusted making sure not to lose any particles. The nanoparticle movement was then recorded for 60 seconds. Before the captured video recording was analysed the detection threshold was set to 192 and the blur to 5x5. The brightness and gain were adjusted to get a black background and then the detection threshold was set to auto and the gain adjusted to get a tracking cross on every particle after which the video was ready to be analysed.

6.2.3.2 UV-Vis spectroscopy

The extinction spectra of the colloids were recorded using a Varian Cary 300 Bio spectrophotometer, right after the preparation of each nanoparticle size over a wavelength range of 300-700 nm. The baselines were recorded using doubly distilled water and the samples were diluted accordingly to remain in the absorption response limit of the spectrometer.

6.2.3.3 Scanning electron microscopy

A sample from each nanoparticle preparation was prepared on a polycation functionalized silicon wafer. The wafer was first cleaned using water and ethanol, then dried in a nitrogen flow. The wafer was then placed in an oxygen plasma cleaner for 60 seconds. PDDA (30 μL) was dissolved in 1 mM NaCl (1 mL), the solution was used to coat the clean wafer by spotting the wafer with the solution with a pipette and then leaving it for 30 minutes under a water-saturated atmosphere. After this step it was washed off and dried in a nitrogen flow. Each AgNP (100 μL)

sample was put onto the PDDA-functionalized silicon wafer for 15 minutes under a water-saturated atmosphere. The sample was then washed off and dried in a nitrogen flow. Using a scanning electron microscope (FEI Sirion 200 ultra-high-resolution Schottky Field emission gun), eight 'snapshot' images were taken for each sample. From the images obtained the diameter was calculated using Image J[156], an image processing and analysis software. An automated method was used to measure the particles, whereby the particles must have a range between 10 nm – 100 nm and the circularity of the particles must be around 0.8 – 1 (where circularity is defined as Circularity = $4\pi(\text{Area}/\text{Perimeter}^2)$) as to avoid any aggregates that might be present. Before the particles were measured the images were converted to grey scale 8-bit images, enhanced by binary contrast enhancement (thresholding) and the scale was calibrated. More than 600 particles were measured for each size as to have statistically significant results.

6.2.3.4 Dynamic light scattering and zeta-potential measurements

The size and zeta-potential of the different sized AgNP's were measured using a Malvern Zetasizer (Nano-ZS) instrument. The standards for size were Nanosphere size standards 20 nm (± 1.5 nm, Lot. 339300) and 40nm (±1.8 nm, Lot. 33306), while the standard for the zeta-potential used was zeta-potential transfer standard (-68mV ± 6.8mV, Batch No. 051001).

6.2.4 SERS measurement

6.2.4.1 Instrumentation

Spectra were recorded at 532 nm excitation wavelength using an Avalon Instrument Ramanstation R3. The laser power was 100 mW and the spectra were recorded with an exposure time of 5 x 1s in a PMMA cuvette.

6.2.4.2 Limit of detection studies

Concentration studies were carried out on the unmodified (O1) and modified (O2, O3) oligonucleotides by diluting them with water to various concentrations. The samples were prepared for SERRS analysis as before by adding 7 μL of TAMRA-labelled oligonucleotide, 10 μL of 0.1 mol dm^{-3} spermine, 175 μL of water and 175 μL of 0.02 nM silver colloid. The samples were analysed 10 min after the addition of the silver colloid. Each concentration was analysed 5 times, with a 2 s exposure and 5 accumulations. The average peak height of the strongest peak (1650 cm^{-1}) in the spectrum was plotted against the concentration of the dye-labelled oligonucleotide after being normalised to a hexane standard. This was repeated for every silver colloid size. The LOD was calculated using equation 6-1

$$LOD = \frac{\chi_{BL} + 3\sigma_{BL}}{m}$$

Equation 6-1

where χ_{BL} is the mean of the blank sample measurements, σ_{BL} is the standard deviation of the blank sample baseline and *m* is the gradient of the calibration line.

6.3 Results and discussion

The method used for the preparation of the different sized nanoparticles is the same one used in chapter 5. As demonstrated before one can control the size of the nanoparticles produced and in this experiment larger nanoparticles were fabricated by reducing the initial seed concentration. The AgNP's were characterised with UV-Vis spectrometer, DLS, and SEM and their zeta-potential measured. As shown from the SEM images (see figure 6-1), extinction spectra (see figure 6-2) an increase in size was obtained. All particles produced had a negative zeta-potential (see table 6-1). The size obtained by DLS and SEM were compared to the results obtained by the nanoparticle tracking analysis nanosight (see table 6-2). It seems that DLS and nanosight give a larger size than those obtained by the analysis of the SEM images. It is to note that nanosight operates for particles between 10 to 1000 nm, and in our measurements of the seed the analysis was not possible.

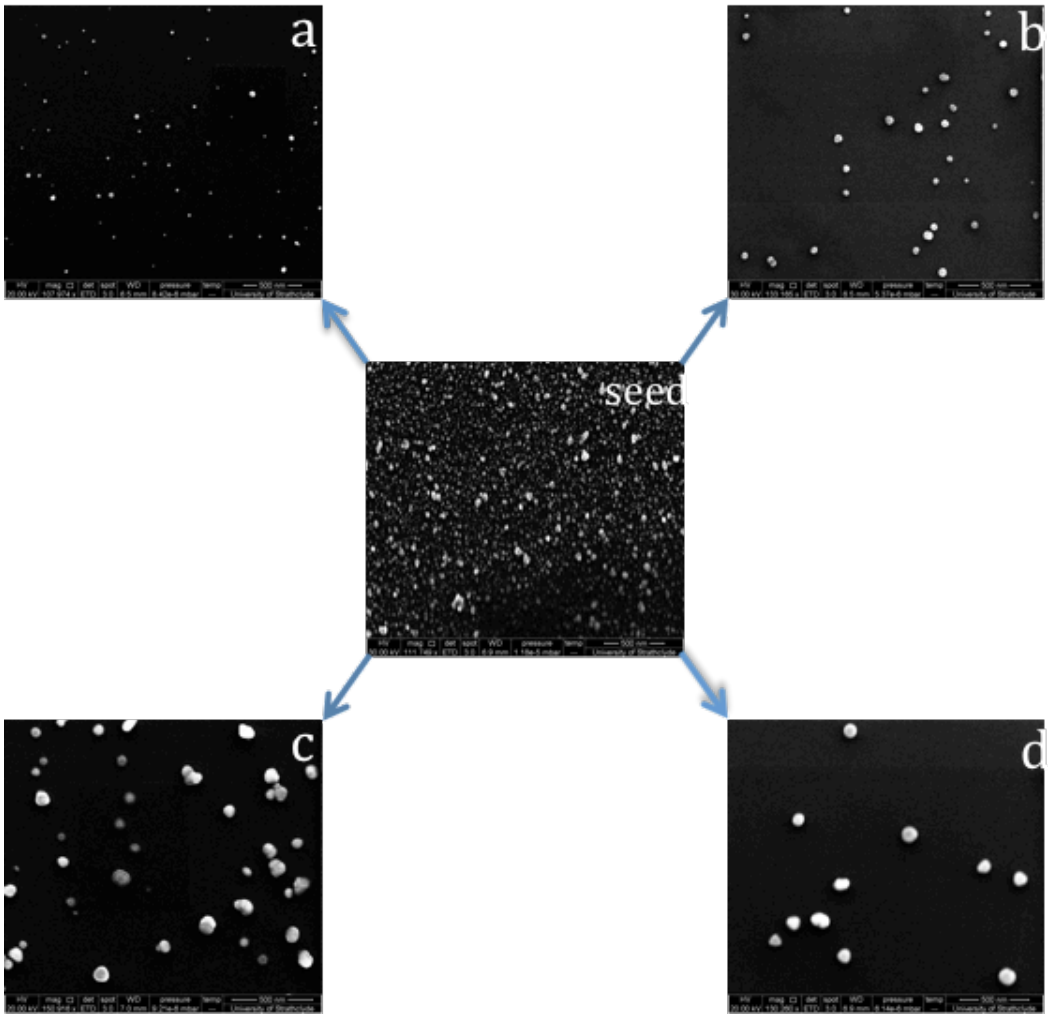

Figure 6-1 Sample SEM images of seed and AgNP's (a-d) produced by the seed growth method. Images a to d correspond to average sizes of 33, 46, 65, and 94 nm respectively. Note that scale bars in images a to d are 500 nm.

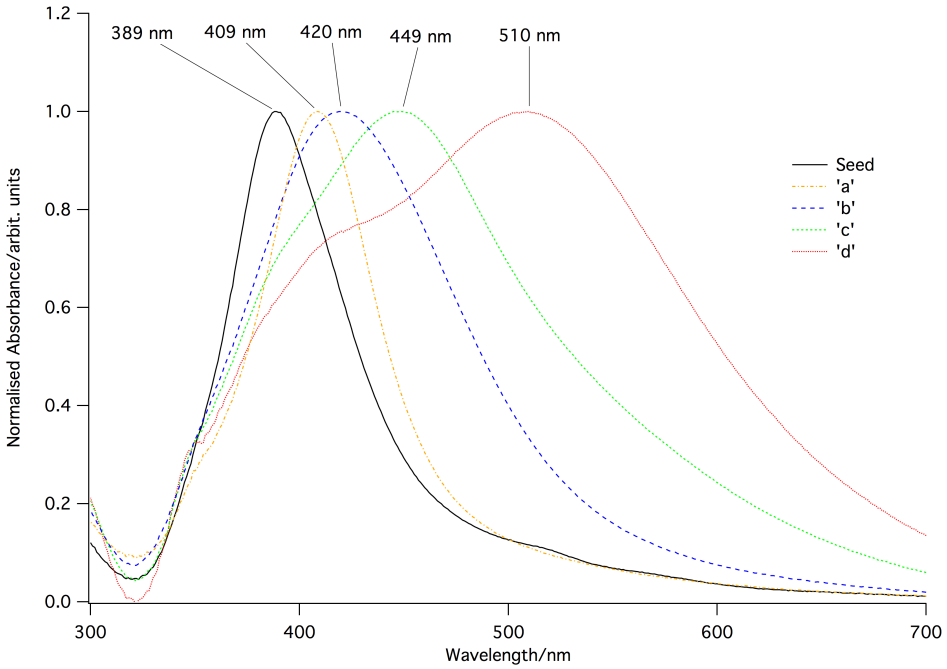

Figure 6-2 Normalised extinction spectra of seed and seed grown nanoparticles corresponding to SEM images in figure 6-1.

Table 6-1 Zeta-potentials for AgNP's

	Zeta potential	
Seed	-36.1 mV	±2.5
NP A	-40.0 mV	±2
NP B	-39.8 mV	±1.8
NP C	-25.2 mV	±0.3
NP D	-30.9 mV	±0.6

Table 6-2 Comparison of nanoparticle sizes obtained by different characterisation methods.

	SEM		DLS		Nanosight	
Seed	21 nm	±14	14 nm	±0.1	-	-
NP A	33 nm	±11	28 nm	±0.7	52	±10
NP B	46 nm	±13	61 nm	±4.3	67	±29
NP C	65 nm	±23	85 nm	±1.8	92	±38
NP D	94 nm	±32	103 nm	±5.1	114	±40

Using the absorbance from the extinction spectra and extension coefficients[155] of the different sizes (SEM sizes) of AgNP's, the concentration of each batch was obtained using the Beer-Lambert law. The concentrations obtained by nanosight were close to the ones obtained from the extinction spectra, hence one could use nanosight directly for estimating the extinction coefficients of Ag and Au nanoparticles.

Table 6-3 Comparison table of concentration obtained through the nanoparticle's extinction spectra and Nanosight.

	Ext. Coeff	Conc. (Uv/Vis)	Conc. (Nanosight)
NP A	2.23e+10	0.7 nM	0.6 nM
NP B	3.98e+10	0.14 nM	0.11 nM
NP C	6.66e+10	0.05 nM	0.04 nM
NP D	1.17e+11	0.02 nM	0.03 nM

The four different sized nanoparticles were then used to see the effect of size on the SERS response on a dye-labelled oligonucleotide. All four batches were diluted to the same concentration and after mixing with the oligonucleotide and the aggregating agent, they were analysed. As can be seen from figures 6-3, 6-4 and 6-5, where SERS intensity was plotted against particle size, the intensity increases with size. However on further size increment the intensity decreases. The highest intensity was recorded at 65 nm (NP C) for all concentrations. This trend can be attributed to the fact that as the spherical nanoparticles increase in size, scattering and radiation dampening is increasing as well which results in lower Raman signals.

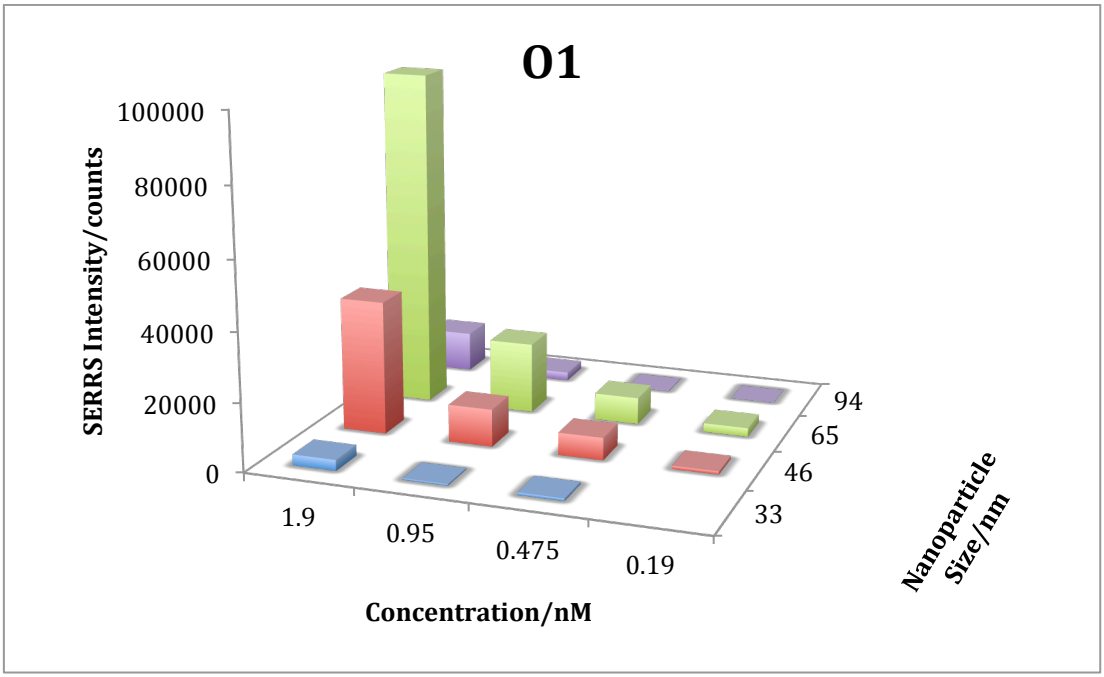

Figure 6-3 SERS intensities of O1 oligonucleotide (20 PO) at various concentrations with the different AgNP sizes at 532 nm laser excitation wavelength.

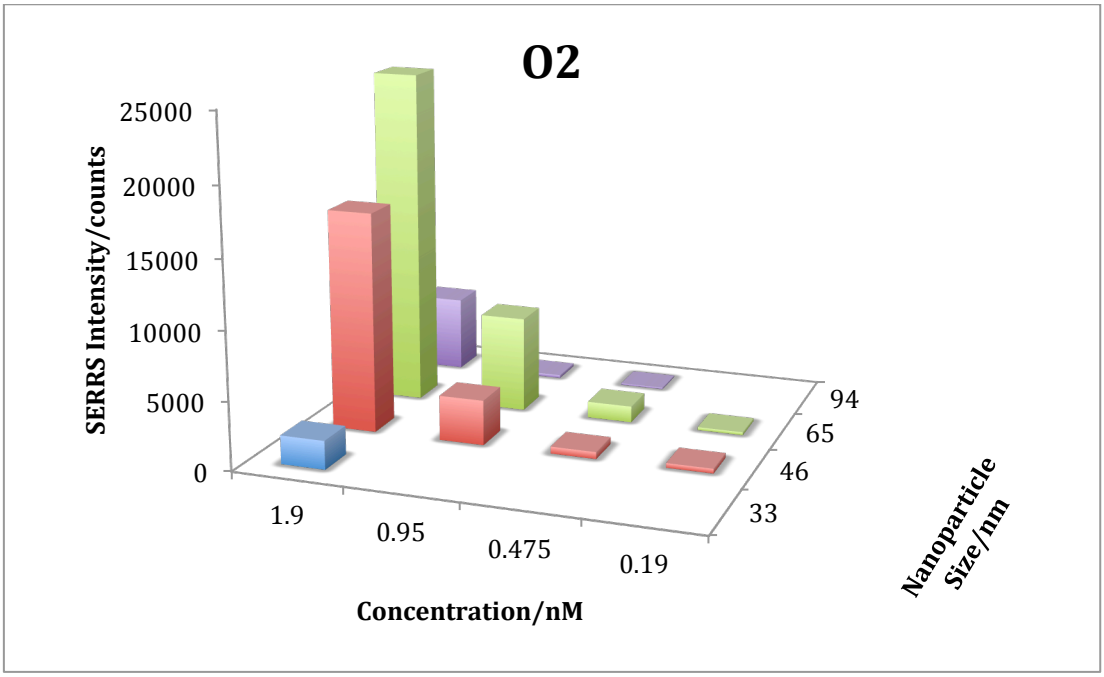

Figure 6-4 SERS intensities of O2 oligonucleotide (20 PS) at various concentrations with the different AgNP sizes at 532 nm laser excitation wavelength.

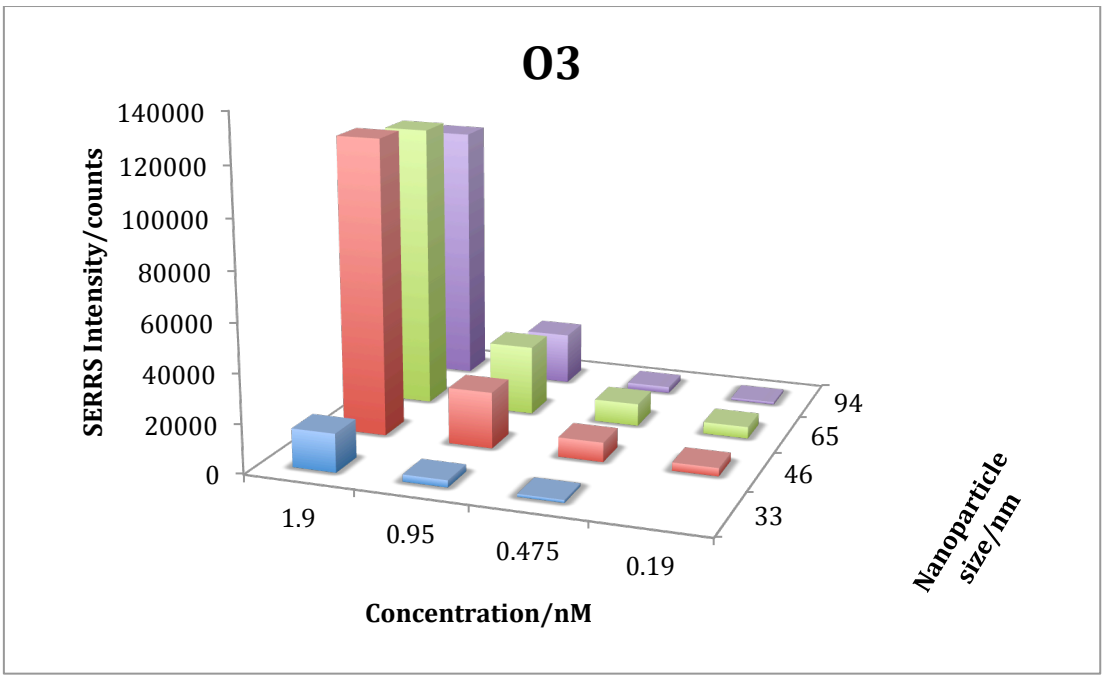

Figure 6-5 SERS intensities of O3 oligonucleotide (10 PO/10PS) at various concentrations with the different AgNP sizes at 532 nm laser excitation wavelength.

In chapter 2 when using a final spermine concentration of 2.72 mM and 0.3 nM of citrate reduced AgNP the unmodified DNA (O1) gave a lower LOD (1.1×10^{-12} mol dm^{-3}) than the chimeric DNA (O3) (3×10^{-11} mol dm^{-3}). However when using AgNP (0.02 nM) produced by the HQ seed-growth method, the chimeric DNA (O3) gives a better LOD than the unmodified DNA (O1) as seen in table 6-4 for all the nanoparticle sizes used. Apart from the lower nanoparticle concentration used in this chapter, the other difference is the method of nanoparticle preparation which could effect the surface chemistry. Further studies are needed to determine the effect of different nanoparticle preparation might have on the SERS response of phosphorothioate-modified DNA. For O2 all phosphorothioate-modified oligonucleotides as in chapter two shows an increase in the LOD when compared to O1 and O3 for NP B and NP C. This continues to affirm that an increase in phosphorothioate linkages does not result in a better LOD when using spermine as an aggregation agent. As for the relation of LOD with size as expected the lowest LOD was obtained by NP C (65 nm). The LOD for NP 1 (33 nm) could not be calculated as few data points (<4) were obtained.

Table 6-4 Limit of detection of the 3 labelled oligonucleotides with different nanoparticle sizes.

Oligo	NP A	NP B	NP C	NP D
	LOD/mol dm^{-3}	LOD/mol dm^{-3}	LOD/mol dm^{-3}	LOD/mol dm^{-3}
O1	-	2.0×10^{-12}	1.8×10^{-12}	6.0×10^{-12}
O2	-	4.6×10^{-12}	3.0×10^{-12}	-
O3	-	1.7×10^{-12}	1.5×10^{-12}	1.6×10^{-12}

6.4 Conclusion

In chapter five it was found that from the four different nanoparticle sizes produced (17 nm, 26 nm, 50 nm & 65 nm) the largest AEF was obtained from the 65 nm silver nanoparticles. In this chapter a larger silver nanoparticle size (94 nm) was produced and the effect on SERS intensity when using TAMRA-labelled oligonucleotides was investigated. The different AgNP sizes prepared re-confirmed that an optimal size for DNA SERS detection is achieved at around 65 nm, as a further increase in size leads to lower SERS intensity and higher LOD. This trend was seen for both unmodified and phosphorothioate-modified DNA. Furthermore it was found that the chimeric phosphorothioate-modified oligonucleotide (O3) gives a lower LOD than the unmodified oligonucleotide when using HQ seeded growth AgNP. This encourages further investigation on the use of phosphorothioate-modified DNA as SERS probes.

Furthermore in this chapter a NTA system has proved itself to be a versatile system, comparable to other nanoparticle characterisation techniques used giving both nanoparticle size and particle concentration.

Chapter 7: Conclusion and Further Work

This thesis was set about to investigate the effect of phosphorothioate-modified DNA and silver nanoparticle size on the quantitative enhanced Raman scattering. Further knowledge on both the SERS probes and SERS substrates helps in improving the limit of detection of DNA which is an important aspect of diagnostic tools to be used in commercial applications. In light of the fact that SERS has been effectively used as a quantitative technique for the direct analysis of dye-labelled oligonucleotides [117,122], in chapter 2 phosphorothioate modified oligonucleotides were investigated on the assumption that the LOD will be improved due to the known affinity of sulfur towards silver surfaces. Using different aggregating agents it was concluded that LOD is improved with modified DNA compared to unmodified DNA when using inorganic salts as aggregating agents. However when using spermine the LOD is not improved when using phosphorothioate modified oligonucleotides. Further investigations showed that by decreasing the spermine concentration and using a chimeric DNA (having both phosphodiester and phosphothioate linkages) the LOD is decreased compared to a normal dye-labelled oligonucleotide. These results show that when spermine is used as aggregating agent the LOD depends on the number of modifications done, their position in the oligonucleotide and the spermine concentration. Furthermore using phosphorothioate modified polyadenine oligonucleotides that the DNA actually adsorbs through the P-S bond. These results prompted further investigations on the effect of SERS signal when phosphorothioates modifications are used in dsDNA. It is known from previous studies that ssDNA and dsDNA have different adsorption to silver nanoparticle surfaces, hence dsDNA gives

a lower SERS intensity signal compared to ssDNA[150]. In chapter 3 results have shown that a chimeric dsDNA gives a higher intensity than a ssDNA with all linkages modified, in stark contrast to when unmodified DNA are used. The lower melting temperatures of phosphorothioate modified DNA indicates a lack of stereoregurality and flexibility of the duplex which causes a different interaction of spermine with DNA, leading to a decrease in SERS intensity.

After the effects of phosphorothioate modification on SERS were investigated the focus was turned onto the SER substrate. In chapter four, different sizes of nanoparticles were produced using the Lee and Meisel method[67] and the Lundahl method[81]. The LOD of three different dye-labelled oligonucleotides was obtained for the different sizes of silver nanoparticles. From this preliminary study it is noted the importance of the dye-species. Apart from the dye being in- or off-resonance with the laser excitation wavelength, the charge of the dye is also important. Since a negatively charged AgNPs were used positive dye Cy3.5 gave better LOD. The methods used to prepare the different sizes of AgNPs were not ideal, as they were polydispersed. Chapter five addresses this issue and a simple and fast method for the synthesis of spherical monodispersed nanoparticles of tuneable size by the selective reduction of $AgNO_3$ on silver seeds with HQ was introduced. Using this nanoparticle synthesis method the AEF was calculated for three different analytes MGO, R6G and TP. It was concluded that AgNPs with a diameter of 65 nm gave the highest enhancement factor. The study on nanoparticle size was continued in chapter six, using both unmodified and phosphorothioate modified dye-labelled DNA, whereby it was found that an increase in particle size above 65 nm leads to a lowering in SERS

intensity and an increase in the LOD. It was also shown that chimeric phosphorothioate modified oligonucleotides (O3) gives a lower LOD when compared to the unmodified oligonucleotide.

The work done on the use of phosphorothioates as SERS probes and the different size of AgNPs to find the correlation between SERS enhancement and size, gave us a clear picture that to develop any biodiagnostic tools the factors effecting the analysis such as chemical modifications, aggregation agent, nanoparticle size etc., have to be understood. Any future work on the use of phosphorothioate oligonucleotides in SERS based DNA detection should thus be focused on understanding better the interaction between the polyamines and the modified DNA. Apart from studying other configurations of phosphorothioate modification in oligonucleotide (such as staggered PS-PO linkages) and their interaction with polyamines in a SERS experimental configuration, molecular modelling studies backed up by NMR and crystallographic studies of phosphorothioate-modified DNA would be essential to propose adequate mechanisms for the phenomena observed in our studies. The possibility of using the phosphorothioate modification as a means of functionalising silver and gold nanoparticles should be looked into and compared to other functionalization methods such as the use of thiol and thioctic acid modifications of oligonucleotides.

This corpus of study lays the ground for further work in SERS in the quest to optimise SERS based biodiagnostic assays, as it shows the consequences and also the pit-falls when changes are made to the SERS substrate and probe/analyte.

References:

[1] S. Y. Shim, D. K. Lim, J. M. Nam *Nanomedicine* **2008**, *3*, 215.
[2] J. A. Creighton, C. G. Blatchford, M. G. Albrecht *J. Chem. Soc., Faraday Trans. 2* **1979**, *75*, 790.
[3] *Nucleic acids in chemistry and biology*; 3rd. ed. ed.; G. M. Blackburn, M. J. Gait, D. Loakes, D. M. Williams, Eds.; RSC Publishing: Cambridge 2006.
[4] J. D. Watson, F. H. C. Crick *Nature* **1953**, *171*, 737.
[5] M. Strock 2006; Vol. 2013.
[6] A. M. Michelson, A. R. Todd *Journal of the Chemical Society (Resumed)* **1955**, *0*, 2632.
[7] A. Rich, S. Zhang *Nat Rev Genet* **2003**, *4*, 566.
[8] M. U. Ahmed, I. Saaem, P. C. Wu, A. S. Brown *Crit. Rev. Biotechnol.*, *0*, 1.
[9] S. A. Deepak, K. R. Kottapalli, R. Rakwal, G. Oros, K. S. Rangappa, H. Iwahashi, Y. Masuo, G. K. Agrawal *Curr. Genomics* **2007**, *8*, 234.
[10] W. Gilbert, A. Maxam *Proc. Natl. Acad. Sci. U. S. A.* **1973**, *70*, 3581.
[11] F. Sanger, S. Nicklen, A. R. Coulson *Proc. Natl. Acad. Sci. U. S. A.* **1977**, *74*, 5463.
[12] E. D. Hyman *Anal. Biochem.* **1988**, *174*, 423.
[13] S. L. Beaucage, M. H. Caruthers *Tetrahedron Lett.* **1981**, *22*, 1859.
[14] L. J. McBride, M. H. Caruthers *Tetrahedron Lett.* **1983**, *24*, 245.
[15] M. D. Matteucci, M. H. Caruthers *J. Am. Chem. Soc.* **1981**, *103*, 3185.
[16] G. R. Gough, M. J. Brunden, P. T. Gilham *Tetrahedron Lett.* **1981**, *22*, 4177.
[17] R. K. Saiki, T. L. Bugawan, G. T. Horn, K. B. Mullis, H. A. Erlich *Nature* **1986**, *324*, 163.
[18] T. M. Devlin *Textbook of biochemistry: with clinical correlations*; Wiley-Liss, 2002.
[19] C. B. Reese *Org. Biomol. Chem.* **2005**, *3*, 3851.
[20] G. Weimann, H. G. Khorana *J. Am. Chem. Soc.* **1962**, *84*, 419.
[21] J. C. Schulhof, D. Molko, R. Teoule *Nucleic Acids Res.* **1987**, *15*, 397.
[22] H. Vu, C. McCollum, K. Jacobson, P. Theisen, R. Vinayak, E. Spiess, A. Andrus *Tetrahedron Lett.* **1990**, *31*, 7269.
[23] G. M. Tener *J. Am. Chem. Soc.* **1961**, *83*, 159.
[24] R. L. Letsinger, K. K. Ogilvie *J. Am. Chem. Soc.* **1969**, *91*, 3350.
[25] J. Nielsen, M. Taagaard, J. E. Marugg, J. H. van Boom, O. Dahl *Nucleic Acids Res.* **1986**, *14*, 7391.
[26] J. S. Eadie, D. S. Davidson *Nucleic Acids Res.* **1987**, *15*, 8333.
[27] R. L. Letsinger, J. L. Finnan, G. A. Heavner, W. B. Lunsford *J. Am. Chem. Soc.* **1975**, *97*, 3278.
[28] R. L. Letsinger, W. B. Lunsford *J. Am. Chem. Soc.* **1976**, *98*, 3655.
[29] A. Sassolas, B. D. Leca-Bouvier, L. J. Blum *Chem. Rev.* **2007**, *108*, 109.
[30] S. Tyagi, F. R. Kramer *Nat Biotech* **1996**, *14*, 303.

[31] K. Sonogashira, Y. Tohda, N. Hagihara *Tetrahedron Lett.* **1975**, *16*, 4467.
[32] H. Kaur, B. R. Babu, S. Maiti *Chem. Rev.* **2007**, *107*, 4672.
[33] A. De Mesmaeker, R. Haener, P. Martin, H. E. Moser *Accounts Chem. Res.* **1995**, *28*, 366.
[34] J.-P. Bongartz, A.-M. Aubertain, P. G. Milhaud, B. Lebleu *Nucleic Acids Res.* **1994**, *22*, 4681.
[35] P. J. Garegg, I. Lindh, T. Regberg, J. Stawinski, R. Str√∂mberg, C. Henrichson *Tetrahedron Lett.* **1986**, *27*, 4051.
[36] R. P. Iyer, W. Egan, J. B. Regan, S. L. Beaucage *J. Am. Chem. Soc.* **1990**, *112*, 1253.
[37] R. P. Iyer, L. R. Phillips, W. Egan, J. B. Regan, S. L. Beaucage *The Journal of Organic Chemistry* **1990**, *55*, 4693.
[38] P. C. J. Kamer, H. C. P. F. Roelen, H. van den Elst, G. A. van der Marel, J. H. van Boom *Tetrahedron Lett.* **1989**, *30*, 6757.
[39] H. C. P. F. Roelen, P. C. J. Kamer, H. van den Elst, G. A. van der Marel, J. H. van Boom *Recl. Trav. Chim. Pays-Bas* **1991**, *110*, 325.
[40] H. Vu, B. L. Hirschbein *Tetrahedron Lett.* **1991**, *32*, 3005.
[41] L. Chen, T. R. Thompson, R. P. Hammer, G. Barany *The Journal of Organic Chemistry* **1996**, *61*, 6639.
[42] Q. Xu, G. Barany, R. P. Hammer, K. Musier-Forsyth *Nucleic Acids Res.* **1996**, *24*, 3643.
[43] Q. Xu, K. Musier-Forsyth, R. P. Hammer, G. Barany *Nucleic Acids Res.* **1996**, *24*, 1602.
[44] M. Y.-X. Ma, J. C. Dignam, G. W. Fong, L. Li, S. H. Gray, B. Jacob Samuel, S. T. George *Nucleic Acids Res.* **1997**, *25*, 3590.
[45] E. C. Le Ru, P. G. Etchegoin *Principles of Surface-Enhanced Raman Spectroscopy*; Elsevier: Amsterdam, 2009.
[46] C. V. Raman, K. S. Krishnan, *Nature* **1928**, *121*, 501.
[47] .
[48] W. Demtröder *Laser spectroscopy*; Springer: Berlin, 2008.
[49] B. Valeur *Molecular Fluorescence: Principles and applications.*; Wiley-VCH: Weinheim, 2002.
[50] H. Haken, H. C. Wolf, W. D. Brewer *Molecular physics and elements of quantum chemistry: introduction to experiments and theory*; Springer-Verlag: Berlin, 2004.
[51] P. M. Platzman, P. A. Wolf *Waves and interactions in solid state plasmas (Solid State Physics, Suppl. No 13)*; Academic Press: New York, London, 1973.
[52] E. C. Le Ru, E. Blackie, M. Meyer, P. G. Etchegoin *J. Phys. Chem. C* **2007**, *111*, 13794.
[53] G. Sabatte, R. Keir, M. Lawlor, M. Black, D. Graham, W. E. Smith *Anal. Chem.* **2008**, *80*, 2351.
[54] K. Chen, M. Leona, K.-C. Vo-Dinh, F. Yan, M. B. Wabuyele, T. Vo Dinh *J. Raman Spectrosc.* **2006**, *37*, 520.
[55] K. Chen, K.-C. Vo-Dinh, F. Yan, M. B. Wabuyele, T. Vo-Dinh *Anal. Chim. Acta* **2006**, *569*, 234.

[56] R. J. H. Clark *J. Mol. Struct.* **1995**, *347*, 417.
[57] S. Cinta-Pinzaru, N. Peica, B. K¸stner, S. Schl¸cker, M. Schmitt, T. Frosch, J. H. Faber, G. Bringmann, J. Popp *J. Raman Spectrosc.* **2006**, *37*, 326.
[58] J. Binoy, I. H. Joe, V. S. Jayakumar, O. F. Nielsen, J. Aubard *Laser Phys. Lett.* **2005**, *2*, 544.
[59] A. V. Szeghalmi, L. Leopold, S. Pînzaru, V. Chis, I. Silaghi Dumitrescu, M. Schmitt, J. Popp, W. Kiefer *Biopolymers* **2005**, *78*, 298.
[60] J. M. Sylvia, J. A. Janni, J. D. Klein, K. M. Spencer *Anal. Chem.* **2000**, *72*, 5834.
[61] O. Lyandres, N. C. Shah, C. R. Yonzon, J. T. Walsh, M. R. Glucksberg, R. P. Van Duyne *Anal. Chem.* **2005**, *77*, 6134.
[62] A. Rasmussen, V. Deckert *J. Raman Spectrosc.* **2006**, *37*, 311.
[63] M. Larsson, J. Lindgren *J. Raman Spectrosc.* **2005**, *36*, 394.
[64] K. Kneipp, Y. Wang, H. Kneipp, L. T. Perelman, I. Itzkan, R. R. Dasari, M. S. Feld *Phys. Rev. Lett.* **1997**, *78*, 1667.
[65] S. Nie, S. R. Emory *Science* **1997**, *275*, 1102.
[66] O. Masala, R. Seshadri *Ann. Rev. Mater. Res.* **2004**, *34*, 41.
[67] P. C. Lee, D. Meisel *J. Phys. Chem.* **1982**, *86*, 3391.
[68] R. Jin, G. Wu, Z. Li, C. A. Mirkin, G. C. Schatz *J. Am. Chem. Soc.* **2003**, *125*, 1643.
[69] C. A. Mirkin, R. L. Letsinger, R. C. Mucic, J. J. Storhoff *Nature* **1996**, *382*, 607.
[70] L. M. Demers, C. A. Mirkin, R. C. Mucic, R. A. Reynolds, R. L. Letsinger, R. Elghanian, G. Viswanadham *Anal. Chem.* **2000**, *72*, 5535.
[71] L. He, M. D. Musick, S. R. Nicewarner, F. G. Salinas, S. J. Benkovic, M. J. Natan, C. D. Keating *J. Am. Chem. Soc.* **2000**, *122*, 9071.
[72] J. Liu, J. H. Lee, Y. Lu *Anal. Chem.* **2007**, *79*, 4120.
[73] M. C. Daniel, D. Astruc *Chem. Rev.* **2004**, *104*, 293.
[74] G. Schmid *Chem. Soc. Rev.* **2008**, *37*, 1909.
[75] C. H. Munro, W. E. Smith, M. Garner, J. Clarkson, P. C. White *Langmuir* **1995**, *11*, 3712.
[76] Z. S. Pillai, P. V. Kamat *J. Phys. Chem. B* **2004**, *108*, 945.
[77] D. L. Van Hyning, C. F. Zukoski *Langmuir* **1998**, *14*, 7034.
[78] S. Schneider, P. Halbig, H. Grau, U. Nickel *Photochem. Photobiol.* **1994**, *60*, 605.
[79] U. Nickel, K. Mansyreff, S. Schneider *J. Raman Spectrosc.* **2004**, *35*, 101.
[80] S. T. Gentry, S. J. Fredericks, R. Krchnavek *Langmuir* **2009**, *25*, 2613.
[81] P. Lundahl, R. Stokes, E. Smith, R. Martin, D. Graham *Micro & Nano Letters, IET* **2008**, *3*, 62.
[82] S. M. Heard, F. Grieser, C. G. Barraclough, J. V. Sanders *J. Colloid Interface Sci.* **1983**, *93*, 545.

[83] H. S. Kim, J. H. Ryu, B. Jose, B. G. Lee, B. S. Ahn, Y. S. Kang *Langmuir* **2001**, *17*, 5817.
[84] E. C. Le Ru, C. Galloway, P. G. Etchegoin *Phys. Chem. Chem. Phys.* **2006**, *8*, 3083.
[85] J. J. Mock, M. Barbic, D. R. Smith, D. A. Schultz, S. Schultz *J. Chem. Phys.* **2002**, *116*, 6755.
[86] B. J. Berne *Dynamic light scattering, with applications to chemistry, biology and physics*; Wiley: New York, 1976.
[87] G. G. Stokes *Mathematical and physical papers* Cambridge University Press: Cambridge 1880.
[88] I. Laidlaw, M. Steinmetz In *Modern Analytical Ultracentrifugation: Techniques and Methods*; Scott DJ, Harding SE, Eds.; Royal Society of Chemistry: 2005.
[89] D. G. Thompson, A. Enright, K. Faulds, W. E. Smith, D. Graham *Anal. Chem.* **2008**, *80*, 2805.
[90] A. B. Steel, R. L. Levicky, T. M. Herne, M. J. Tarlov *Biophys. J.* **2000**, *79*, 975.
[91] S. R. Nicewarner Pena, S. Raina, G. P. Goodrich, N. V. Fedoroff, C. D. Keating *J. Am. Chem. Soc.* **2002**, *124*, 7314.
[92] W. J. Parak, T. Pellegrino, C. M. Micheel, D. Gerion, S. C. Williams, A. P. Alivisatos *Nano Lett.* **2002**, *3*, 33.
[93] T. Pellegrino, R. A. Sperling, A. P. Alivisatos, W. J. Parak *J. Biomed. Biotechnol.* **2007**.
[94] W. Zhao, W. Chiuman, J. C. F. Lam, S. A. McManus, W. Chen, Y. Cui, R. Pelton, M. A. Brook, Y. Li *J. Am. Chem. Soc.* **2008**, *130*, 3610.
[95] V. Bagalkot, L. Zhang, E. Levy-Nissenbaum, S. Jon, P. W. Kantoff, R. Langer, O. C. Farokhzad *Nano Lett.* **2007**, *7*, 3065.
[96] N. R. Jana, J. Y. Ying *Adv. Mater.* **2008**, *20*, 430.
[97] J. K. Herr, J. E. Smith, C. D. Medley, D. Shangguan, W. Tan *Anal. Chem.* **2006**, *78*, 2918.
[98] M. Levy, S. F. Cater, A. D. Ellington *ChemBioChem* **2005**, *6*, 2163.
[99] H. Cho, B. R. Baker, S. Wachsmann-Hogiu, C. V. Pagba, T. A. Laurence, S. M. Lane, L. P. Lee, J. B. H. Tok *Nano Lett.* **2008**, *8*, 4386.
[100] H. Pandana, K. H. Aschenbach, R. D. Gomez *IEEE Sens. J.* **2008**, *8*, 661.
[101] T. Vo-Dinh, M. Y. K. Hiromoto, G. M. Begun, R. L. Moody *Anal. Chem.* **1984**, *56*, 1667.
[102] K. Kneipp, H. Kneipp, G. Deinum, I. Itzkan, R. R. Dasari, M. S. Feld *Appl. Spectrosc.* **1998**, *52*, 175.
[103] D. Graham, K. Faulds *Chem. Soc. Rev.* **2008**, *37*, 1042.
[104] L. R. Allain, T. Vo-Dinh *Anal. Chim. Acta* **2002**, *469*, 149.
[105] Y. C. Cao, R. Jin, C. A. Mirkin *Science* **2002**, *297*, 1536.
[106] P. M. Holland, R. D. Abramson, R. Watson, D. H. Gelfand *Proc. Natl. Acad. Sci. U. S. A.* **1991**, *88*, 7276.

[107] E. J. Cho, J.-W. Lee, A. D. Ellington *Annual Review of Analytical Chemistry* **2009**, *2*, 241.
[108] M. S. Han, A. K. R. Lytton-Jean, B.-K. Oh, J. Heo, C. A. Mirkin *Angew. Chem. Int. Ed.* **2006**, *45*, 1807.
[109] J. J. Storhoff, A. D. Lucas, V. Garimella, Y. P. Bao, U. R. Muller *Nat Biotech* **2004**, *22*, 883.
[110] S.-J. Park, T. A. Taton, C. A. Mirkin *Science* **2002**, *295*, 1503.
[111] A. P. Alivisatos *Science* **1996**, *271*, 933.
[112] M. Nirmal, L. Brus *Accounts Chem. Res.* **1998**, *32*, 407.
[113] D. Cunningham, R. E. Littleford, W. E. Smith, P. J. Lundahl, I. Khan, D. W. McComb, D. Graham, N. Laforest *Faraday Discuss.* **2006**, *132*, 135.
[114] R. Brown, W. E. Smith, D. Graham *Tetrahedron Lett.* **2001**, *42*, 2197.
[115] K. Faulds, R. P. Barbagallo, J. T. Keer, W. E. Smith, D. Graham *Analyst* **2004**, *129*, 567.
[116] K. Faulds, W. E. Smith, D. Graham *Anal. Chem.* **2004**, *76*, 412.
[117] K. Faulds, W. E. Smith, D. Graham *Analyst* **2005**, *130*, 1125.
[118] K. Faulds, L. Stewart, W. E. Smith, D. Graham *Talanta* **2005**, *67*, 667.
[119] L. Fruk, A. Grondin, W. E. Smith, D. Graham *Chemical Communications* **2002**, 2100.
[120] D. Graham, L. Fruk, W. Ewen Smith *Analyst* **2003**, *128*, 692.
[121] D. Graham, B. J. Mallinder, W. E. Smith *Angew. Chem.-Int. Edit.* **2000**, *39*, 1061.
[122] D. Graham, W. E. Smith, A. M. T. Linacre, C. H. Munro, N. D. Watson, P. C. White *Anal. Chem.* **1997**, *69*, 4703.
[123] C. Rodger, W. E. Smith, G. Dent, M. Edmondson *J. Chem. Soc., Dalton Trans.* **1996**, 791.
[124] K. Faulds, F. McKenzie, D. Graham *Analyst* **2007**, *132*, 1100.
[125] F. Eckstein *Accounts Chem. Res.* **1979**, *12*, 204.
[126] J. Kurreck *Eur. J. Biochem.* **2003**, *270*, 1628.
[127] M. Brust, J. Fink, D. Bethell, D. J. Schiffrin, C. Kiely *J. Chem. Soc., Chem. Commun.* **1995**, 1655.
[128] M. Brust, C. J. Kiely *Colloids Surf. Physicochem. Eng. Aspects* **2002**, *202*, 175.
[129] M. Brust, M. Walker, D. Bethell, D. J. Schiffrin, R. Whyman *J. Chem. Soc., Chem. Commun.* **1994**, 801.
[130] J. A. Dougan, C. Karlsson, W. E. Smith, D. Graham *Nucleic Acids Res.* **2007**, *35*, 3668.
[131] N. Ma, E. H. Sargent, S. O. Kelley *Nat. Nanotechnol.* **2009**, *4*, 121.
[132] J. H. Lee, D. P. Wernette, M. V. Yigit, J. Liu, Z. Wang, Y. Lu *Angew. Chem. Int. Ed.* **2007**, *46*, 9006.
[133] A. Kumar, S. Phadtare, R. Pasricha, P. Guga, K. N. Ganesh, M. Sastry *Curr. Sci.* **2003**, *84*, 71.
[134] S. Pal, J. Sharma, H. Yan, Y. Liu *Chem Commun (Camb)* **2009**, 6059.
[135] E. Papadopoulou, S. E. J. Bell *J. Phys. Chem. C* **2010**, *114*, 22644.

[136] L. Jiang, H. Zhang, J. Zhuang, B. Yang, W. Yang, T. Li, C. Sun *Adv. Mater.* **2005**, *17*, 2066.
[137] E. Papadopoulou, S. E. J. Bell *Chemical Communications* **2011**, *47*, 10966.
[138] D. Graham, B. J. Mallinder, W. E. Smith *Biopolymers* **2000**, *57*, 85.
[139] E. Papadopoulou, S. E. J. Bell *Angew. Chem. Int. Ed.* **2011**, *50*, 9058.
[140] D. Whitcombe, J. Theaker, S. P. Guy, T. Brown, S. Little *Nat Biotech* **1999**, *17*, 804.
[141] H. Li, L. Rothberg *Proc. Natl. Acad. Sci. U. S. A.* **2004**, *101*, 14036.
[142] L. A. LaPlanche, T. L. James, C. Powell, W. D. Wilson, B. Uznanski, W. J. Stec, M. F. Summers, G. Zon *Nucleic Acids Res.* **1986**, *14*, 9081.
[143] F. Eckstein *Annu. Rev. Biochem.* **1985**, *54*, 367.
[144] M. K. Ghosh, K. Ghosh, O. Dahl, J. S. Cohen *Nucleic Acids Res.* **1993**, *21*, 5761.
[145] M. Musso, M. W. Van Dyke *Nucleic Acids Res.* **1995**, *23*, 2320.
[146] C. A. Stein, C. Subasinghe, K. Shinozuka, J. S. Cohen *Nucleic Acids Res.* **1988**, *16*, 3209.
[147] C. L. Clark, P. K. Cecil, D. Singh, D. M. Gray *Nucleic Acids Res.* **1997**, *25*, 4098.
[148] L. Benimetskaya, J. L. Tonkinson, M. Koziolkiewicz, B. Karwowski, P. Guga, R. Zeltser, W. Stec, C. A. Stein *Nucleic Acids Res.* **1995**, *23*, 4239.
[149] T. Antony, T. Thomas, A. Shirahata, T. J. Thomas *Biochemistry* **1999**, *38*, 10775.
[150] A. MacAskill, D. Crawford, D. Graham, K. Faulds *Anal. Chem.* **2009**, *81*, 8134.
[151] M. M. Harper, J. A. Dougan, N. C. Shand, D. Graham, K. Faulds *Analyst* **2012**, *137*, 2063.
[152] P. Frey, R. Sammons *Science* **1985**, *228*, 541.
[153] V. Biju, T. Itoh, A. Anas, A. Sujith, M. Ishikawa *Analytical and Bioanalytical Chemistry* **2008**, *391*, 2469.
[154] R. A. Sperling, W. J. Parak *Philosophical Transactions of the Royal Society A: Mathematical, Physical and Engineering Sciences* **2010**, *368*, 1333.
[155] J. Yguerabide, E. E. Yguerabide *Anal. Biochem.* **1998**, *262*, 137.
[156] M. D. Abramoff, P. J. Magelhaes, S. J. Ram *Biophotonics International* **2004**, *11*, 36.
[157] R. J. Stokes, A. Macaskill, P. J. Lundahl, W. E. Smith, K. Faulds, D. Graham *Small* **2007**, *3*, 1593.
[158] D. G. Duff, A. Baiker, P. P. Edwards *Langmuir* **1993**, *9*, 2301.
[159] K. C. Grabar, R. G. Freeman, M. B. Hommer, M. J. Natan *Anal. Chem.* **1995**, *67*, 735.
[160] C. F. Bohren, D. R. Huffman *Absorption and scattering of light by small particles*; Wiley: New York 1998.
[161] H. Xu, J. Aizpurua, M. Kall, P. Apell *Phys. Rev. E* **2000**, *62*, 4318.
[162] J. Yguerabide, E. E. Yguerabide *Anal. Biochem.* **1998**, *262*, 157.

[163] K. L. Kelly, E. Coronado, L. L. Zhao, G. C. Schatz *J. Phys. Chem. B* **2003**, *107*, 668.
[164] I. O. Sosa, C. Noguez, R. G. Barrera *J. Phys. Chem. B* **2003**, *107*, 6269.
[165] K. Kneipp, Y. Wang, R. R. Dasari, M. S. Feld *Appl. Spectrosc.* **1995**, *49*, 780.
[166] T. Vo-Dinh, K. Houck, D. L. Stokes *Anal. Chem.* **1994**, *66*, 3379.
[167] V. N. Pustovit, T. V. Shahbazyan *Microelectron. J.* **2005**, *36*, 559.
[168] R. Aroca In *Surface-Enhanced Vibrational Spectroscopy*; John Wiley & Sons, Ltd: 2007, p 185.
[169] J. R. Lombardi, R. L. Birke, T. Lu, J. Xu *The Journal of Chemical Physics* **1986**, *84*, 4174.
[170] L. Cao, T. Zhu, Z. Liu *J. Colloid Interface Sci.* **2006**, *293*, 69.
[171] N. R. Jana, L. Gearheart, C. J. Murphy *Adv. Mater.* **2001**, *13*, 1389.
[172] N. R. Jana, L. Gearheart, C. J. Murphy *The Journal of Physical Chemistry B* **2001**, *105*, 4065.
[173] H. Yu, P. C. Gibbons, K. F. Kelton, W. E. Buhro *J. Am. Chem. Soc.* **2001**, *123*, 9198.
[174] T. Linnert, P. Mulvaney, A. Henglein, H. Weller *J. Am. Chem. Soc.* **1990**, *112*, 4657.
[175] M. Mostafavi, J. L. Marignier, J. Amblard, J. Belloni *International Journal of Radiation Applications and Instrumentation. Part C. Radiation Physics and Chemistry* **1989**, *34*, 605.
[176] I. Pastoriza-Santos, L. M. Liz-Marzan *J. Mater. Chem.* **2008**, *18*, 1724.
[177] C. S. Seney, B. M. Gutzman, R. H. Goddard *The Journal of Physical Chemistry C* **2008**, *113*, 74.
[178] O. Siiman, L. A. Bumm, R. Callaghan, C. G. Blatchford, M. Kerker *The Journal of Physical Chemistry* **1983**, *87*, 1014.
[179] K. G. Stamplecoskie, J. C. Scaiano *J. Am. Chem. Soc.* **2010**, *132*, 1825.
[180] J. Y. Gui, D. A. Stern, D. G. Frank, F. Lu, D. C. Zapien, A. T. Hubbard *Langmuir* **1991**, *7*, 955.
[181] X. Qian, S. R. Emory, S. Nie *J. Am. Chem. Soc.* **2012**, *134*, 2000.
[182] V. S. Tiwari, T. Oleg, G. K. Darbha, W. Hardy, J. P. Singh, P. C. Ray *Chem. Phys. Lett.* **2007**, *446*, 77.
[183] J. Wrzesien, D. Graham *Tetrahedron* **2012**, *68*, 1230.
[184] K. G. Stamplecoskie, J. C. Scaiano, V. S. Tiwari, H. Anis *The Journal of Physical Chemistry C* **2011**, *115*, 1403.
[185] R. Sasai, T. Fujita, N. Iyi, H. Itoh, K. Takagi *Langmuir* **2002**, *18*, 6578.
[186] M. A. Bryant, S. L. Joa, J. E. Pemberton *Langmuir* **1992**, *8*, 753.
[187] A. C. Power, A. J. Betts, J. F. Cassidy *Analyst* **2011**, *136*, 2794.
[188] T. H. Joo, M. S. Kim, K. Kim *J. Raman Spectrosc.* **1987**, *18*, 57.

Appendix A

Table 0-1 Reagent amounts used to prepare the different nanoparticle sizes in chapter 5 & 6

Sample	0.1M $AgNO_3$	H_2O	AgNP Seed (µl)	0.1M Citrate	0.03M Hydroquinone
NP1	100	5200	4800	22	100
NP2	100	8498	1280	22	100
NPA	100	9138	640	22	100
NP3/NPB	100	9618	160	22	100
NP4/NPC	100	9698	80	22	100
NPD	100	9738	40	22	100

The molar concentration of the analyte bound to the surface of the different sizes of AgNPs in the SERS experiment was calculated as follows;

First the mass of one AgNP was calculated:

$$\boldsymbol{Mass\ of\ NP = \rho \frac{4}{3} \pi r^3} \qquad \text{Equation A1}$$

where ρ is the density of silver (10.49 $g \cdot cm^{-3}$) and r is the nanoparticle radius.

From the mass of each nanoparticle, the moles of silver per particle can be obtained:

$$\boldsymbol{Moles\ of\ Ag\ per\ particle = Mass\ of\ NP \times N_A} \qquad \text{Equation A2}$$

where N_A is the Avogadro's number (6.02×10^{23}).

The number of atoms per particle can thus be calculated:

$$\boldsymbol{Atoms\ per\ particle = moles\ of\ Ag\ per\ particle \times N_A} \qquad \text{Equation A3}$$

from which the particle density (particle/L) can be obtained from the Ag^+ concentration used during the synthesis:

$$\boldsymbol{partical\ density} = \frac{[Ag]\times N_A}{\boldsymbol{Atoms\ per\ particle}} \qquad \text{Equation A4}$$

therefore the surface atoms (mol/L) is obtained:

$$\boldsymbol{Surface\ atoms} = \frac{4(\boldsymbol{Atoms\ per\ particle})^{2/3}\times(\boldsymbol{Particle\ density})}{N_A} \qquad \text{Equation A5}$$

From which $M_{monolayer}$ can be calculated:

$$\boldsymbol{M_{monolayer}} = \frac{\boldsymbol{Surface\ atoms}}{\boldsymbol{Surface\ atomic\ coverage\ of\ Analyte}} \qquad \text{Equation A6}$$

where the surface atomic coverage of analyte for R6G and MGO is approximately 5.96 and for TP its approximately 4.47. The monolayer coverage on the different sized nanoparticles used is plotted in Figure 5-5